DAMAGE AND FAILURE ANALYSIS OF CO-CURED FIBER-REINFORCED COMPOSITE JOINTS

A Dissertation
Presented to
The Academic Faculty

by

Caihua Cao

In Partial Fulfillment
of the Requirements for the Degree
Doctor of Philosophy in Aerospace Engineering

Georgia Institute of Technology
November 2003

DAMAGE AND FAILURE ANALYSIS OF CO-CURED FIBER-REINFORCED COMPOSITE JOINTS

Approved:

Dr. D. Stefan Dancila, Chairman

Dr. Massimo Ruzzene

Dr. Erian A. Armanios

Dr. Jennifer E. Michaels

Dr. W. Steven Johnson

Dr. Thomas E. Michaels

Date Approved: November 25, 2003

To my father in heaven

To my mom, brother and sisters for their unconditional love and support

ACKNOWLEDGEMENTS

It is time to recall the past, the people who have been in my life over these years and to whom I should express my heartfelt appreciations for their contributions in bringing me to this stage. Sometimes, when I am immersed in both happy and painful memories, it is very difficult for me to express my feelings in words. The years as a Ph.D. student at Georgia Tech had really taught me a lot, not only in the technical field, but also in helping me know more about myself and regaining my dignity and confidence which are the most important ingredients for my future life.

Among those contributors to today's achievement, my academic advisor, Dr. D. Stefan Dancila, deserves my deepest gratitude for his support, guidance, patience, encouragement, and for shaping me not only as an engineer but also as an artist. Many times after discussing the research work, we talked about our common interests in photography. His inspiring thoughts had enriched me and also made my study life more colorful.

I owe a lot to Dr. E. A. Armanios for unique valuable discussions and also for the help he provided even when on a busy schedule. His wisdom, professionalism and the ability to grasp the essence behind any phenomenon deserve my admiration.

Dr. W. S. Johnson, Director of the Composites Education and Research Center of GT, is a witty professor with a very attractive personality. Taking his course of Fracture Mechanics was a joyful experience. His well-organized and well-prepared lectures

influenced me not only in the course itself but also taught me how to plan and arrange time efficiently for life-long learning. Whenever I met him on campus or at a seminar, he always expressed warm greetings. His consistent care and concern were very important to me, especially at a time when I was at a low point of my life.

My thanks should also go to Dr. M. Ruzzene, Dr. J. E. Michaels and Dr. T. E. Michaels as my Ph.D. thesis defense committee members. I really appreciate their input, which was essential in improving the quality of my dissertation.

I would like to thank Dr. J. Jagoda, Associate Chair for Graduate Studies and Research in the School of Aerospace Engineering, who facilitated the use of the Machine Shop resources for my work. His unspoken help was very valuable and had contributed much to my achievement.

During these years at GT I have made many friends not only among students, but among professors as well. Professor Dr. Jianmin Qu has been my teacher, friend and mentor since I joined GT. His wisdom, patience and kindness help me gradually step out of some dark days of my life and also gave me the courage to face the challenge and embrace a new life. Dr. C. P. Wong, a Regents' Professor in the School of Materials Science & Engineering, has been a friend and mentor as well during these years. I would always remember his help during my most difficult time at GT. His offer of support provided security and encouragement and allowed me to identify other opportunities.

Special thanks go to Ms. Lorreta Carroll in the Administrative Office of Aerospace Engineering for her sharing and understanding of my situation based on our similar experience and the same gender. Her philosophical words are etched in my heart. I should also thank Mr. Harry Rudd for his perfect and unparalleled machining work on

my specimens. My consistent testing results would have been impossible without his precise effort. Mr. Howard Simpson also assisted me a lot in many aspects which deserve my appreciation.

Many people, whom I did not know before coming to the U.S., have been in my life during these years. Their being by my side had made me feel the love and care which I needed to go through any rough time. I am grateful to Mr. Samer A. Tawfik, Ms. Xin-Yuan Tan and Mr. Kwangtae Ha as my colleagues in the Structures Group of Aerospace Engineering for their care and help. Thanks go to Dr. Jon Wallace, Mr. Li Shengyuan and Ms. Song Xiaoyan for their friendship and consistent support which I still need for the future life. Dr. Liu Yuxian, a medical doctor in acupuncture, is one of my closest friends and has given me so valuable advice in taking care of my health which was so critical for going through these tough years. Mr. Abe Wong and Mrs. Margie Wong, who treated me as their family member and tried to help criticize my thesis during their precious leisure time, deserve my special gratitude. Mr. and Mrs. Hightower are the kindest people I have ever met and they behave as a model of Christian life and always regard me as a daughter for whom they showed a lot of love.

A special word of recognition should go to my eldest sister Ms. Cao Yifan (Cao Caiyun), who contributed so much on my achievement today. Her sparing no effort in support of all my pursuits, including the Ph.D. degree, made my dream come true today. I still remember those days in chilly winter when she rode a bicycle and I ran along with her to train me during the years of being an athlete. Without her support and sacrifice for my family, I would not have been able to study here without any worries. My elder sister Cao Caiping plays the role of correspondent between me and my family. The

opportunity to call her anytime made me feel that the family link is always connected and I felt recharged every time.

Finally, but most importantly, I would like to thank my mom Mrs. Xie Cunzhu for her unconditional and consistent love and support, especially when I was at the most difficult time. Though she did not receive any formal education, she acts as an educator with the quality of honesty, endurance, persistence and sacrifice. Her wisdom, strength and positive attitude in facing and handling the challenges and difficulties of life, especially after my father's passing away, had influenced me a lot and taught me to be strong.

TABLE OF CONTENTS

LIST OF TABLES

LIST OF FIGURES

LIST OF SYMBOLS

AE Acoustic Emission

SNO Single Nested Overlap

U Zero-Degree Unidirectional Lay-up

Q Quasi-Isotropic Lay-up

SQ Straight Laminate with Quasi-Isotropic Lay-up

SU Straight Laminate with Unidirectional Lay-up

LQ Single Lap Joint with Quasi-Isotropic Lay-up

LU Single Lap Joint with Unidirectional Lay-up

NQ Single Nested Overlap Joint with Quasi-Isotropic Lay-up

NU Single Nested Overlap Joint with Unidirectional Lay-up

Designation of manufactured specimens

Design Configuration	Unidirectional	Quasi-isotropic
Straight Laminate	SU	SQ
Single Lap Joint	LU	LQ
Single Nested Overlap	NU	NQ

SUMMARY

Joints represent a design challenge, especially for composite structures. Among the available joining methods, co-curing is an efficient way to integrate parts for some applications. Coates and Armanios have proposed a Single Nested Overlap (SNO) co-cured joint configuration, obtained from a single lap joint through the overlap/interleafing of the adjoining top/bottom adherend plies, respectively. Through a comparative investigation, they have demonstrated joint strength and fatigue life improvements over the single lap joint counterparts for unidirectional and quasi-isotropic adherend lay-ups.

This research extends the comparative investigation of Coates and Armanios by focusing upon characterizing and differentiating the damage initiation and progression mechanisms under quasi-static loading. Six specimen configurations are manufactured and tested. It is confirmed that single nested overlap joints show 29.2% and 27.4% average improvement in strength over single lap counterparts for zero-degree unidirectional and quasi-isotropic lay-ups, respectively.

Several nondestructive evaluation techniques are used to observe and analyze damage initiation, damage progression and failure modes of the studied specimens and to monitor their mechanical response. Using X-ray Radiography and Optical Microscopy techniques during quasi-static loading, a physical characterization of damage and failure

mechanisms is obtained. The acoustic emission data acquired during monotonic loading could reveal the overall picture of AE activities produced by the damage initiation, development and accumulation mechanisms within the specimen via parametric analysis. Further AE analysis by a selected supervised clustering method is carried out and shown successful in differentiating and clustering the AE data. Correlation with physical observations from other techniques suggests that the resulting clusters may be associated to specific damage modes and failure mechanisms.

CHAPTER 1

INTRODUCTION

1.1 Background

A joint is a structural connection of two or more members for the purpose of load transfer. A joint member is typically referred to as an adherend. In this study the main focus is placed on joints of two composite adherends. Fiber-reinforced composite materials have superior qualities (high specific stiffness, high specific strength) compared to metal materials and are particularly useful in spacecraft, aircraft, automobile and the sports industries.

Most structures contain one or more joints. For example, there are thousands of parts/components in a typical airplane, which need to be connected and/or assembled to form the complete aircraft structure. Joints are necessary for a number of reasons, some of which are discussed in this chapter.

Parts/components need to satisfy manufacturing, handling and transport size limitations, and therefore a large structure can in general only be obtained by the assembly of smaller components. Additionally, different parts of a structure may be designed and manufactured using different materials. Furthermore, for some structures a

requirement for inspection disassembly may exist. Lastly, structural maintenance and damage repair may require the presence of a joint.

Joining methods for composite materials include mechanical fastening, adhesive bonding, combined mechanical fastening and adhesive bonding, co-curing and fusion bonding (for thermoplastic composites only). A large volume of research has been published for the first three joining methods but comparatively less for co-cured joints.

Joints represent one of the greatest challenges in the design of structures in general and in composite structures in particular since they entail discontinuities in the geometry of the structure and/or material properties, and introduce high local stress concentrations (MIL-HDBK-17-3E, 1997). Therefore, the overall structural strength may be determined by the joints and not by the basic adherend structure.

Successful joint design relies on knowledge and understanding of potential failure modes. Failure modes depend on joint type, joint geometry and laminate lay-up for a given composite material system. Obviously, failure modes for mechanically fastened joints and adhesively bonded joints can be very different, while failure modes for adhesively bonded joints and co-cured joints with the same configuration, for example, single lap joint, may be similar. Co-cured joining methods may be an alternative to adhesively bonded joints, without the presence of the foreign adhesive involved.

Even among co-cured joints, different joint configurations may have very different damage mechanisms and failure modes. Coates and Armanios (2000) and Coates (2001) investigated experimentally several types of co-cured composite joint designs and proposed two new joint designs, the Single Nested Overlap (SNO) joint, and the transverse layer joint, and showed their higher quasi-static and fatigue strength compared

to the baseline single lap joint, the simplest joint concept. The failure modes of single nested overlap joints appeared different from those of the baseline single lap joints. The specific damage mechanisms and failure modes that are behind the improvements of strength and fatigue life observed have, however, not been established. They recommended such investigation be pursued in order to isolate parameters responsible for strength enhancement and as a result gain better understanding and ultimately control over the failure mechanisms.

1.2 Objectives

This study focuses on a comparative investigation of damage and failure mechanisms in co-cured fiber-reinforced composite single nested overlap (SNO) and baseline single lap joints. Specimens of these two types of joints with two different lay-ups, manufactured from the same material system using an autoclave cuing method, are tested under quasi-static loading on an MTS machine. During loading, the joint specimens are monitored and examined by several nondestructive evaluation (NDE) methods such as Acoustic Emission, Optical Microscopy and X-ray Radiography. The effort in correlating those damage and failure mechanisms with the acquired acoustic emission data is also made. The specific objectives of this study are the following:

1. To comparatively characterize damage initiation, damage progression , and failure modes and to differentiate these damage and failure mechanisms using Acoustic Emission and other NDE techniques;
2. To understand and identify the sources for the reported improvements of quasi-static joint strength of SNO joints.

CHAPTER 2

LITERATURE SURVEY

A broad literature review of relevant research on damage mechanisms, failure modes and failure analysis for straight composite laminates, mechanically fastened composite joints, adhesively bonded composite joints and co-cured hybrid and composite joints is presented in this chapter to build a solid foundation for the proposed work and also for reference convenience.

The applications of NDE to composite materials in general, and joints in particular, are also reviewed. The failure analysis tools covered are basically experimental and non-destructive, such as Acoustic Emission, Ultrasonics, X-ray Radiography, and Optical Microscopy. Emphasis is placed on the less well represented studies of co-cured composite joints.

At the end of the chapter, the main advantages and disadvantages of adhesively bonded composite joints, mechanically fastened composite joints, and co-cured composite joints are listed for comparison.

2.1 Straight Composite Laminates

Fiber reinforced laminated composites can offer directional strength and stiffness which make the optimum design of a wide range of load bearing structures possible. However, composite materials exhibit complex damage and failure mechanisms. One of the current major issues in the use of composites is the understanding and prediction of damage modes and failure mechanisms. A thorough knowledge of the failure mechanisms is bound to lead to the design of efficient and durable structures (Sriram and Armanios, 1993).

For straight laminated composites, the common damage modes include matrix cracking, fiber/matrix debonding, interlaminar failure and fiber breakage. Matrix cracks, the earliest damage mode of composite laminates with off-axis plies, usually occur through the thickness within laminates where fibers run at an angle to the primary load direction. The existence of matrix cracks usually causes stiffness reductions and thus affects performance. Many authors (Hashin (1986); Hart-Smith (1993); Sriram and Armanios (1993); Gao (1996); Kellas *et al.* (1993); Highsmith and Reifsnider (1982); to name just a few) have investigated material property changes induced by matrix cracks.

Delamination is another type of damage mode. This damage usually initiates along free edges or locally within laminates between two neighboring plies due to interlaminar tensile or shear stress. Delamination growth redistributes the stresses in the plies of a laminate and may influence residual stiffness, residual strength and fatigue life (O'Brien (1982, 1985 & 1988); Harris and Morris (1985); Armanios *et al.* (1991); Masters (1989); Barsoum (1989); Wang (1989); and Lagace (1992)).

Fatigue of fiber reinforced laminated composites is also a very important issue for a reliable and durable design. Since the load level threshold at which composites become sensitive to cyclic loading is a very high fraction of their static failure load, composite structures are considered not fatigue critical (McCarty, 1987). However, composite components with holes, cutouts, impact damage, or geometry discontinuity (joint) are more susceptible to fatigue due to the brittle character of fiber reinforced composites. Fatigue damage in composite materials consists of various combinations of matrix cracking, fiber-matrix debonding, delamination, void growth and local fiber breakage. The mechanism, type and distribution of damage depend upon the material system (combination of fiber and matrix materials), stacking sequence, fabrication techniques, geometry of the component, stress state and the loading history. Furthermore, the mechanisms are sensitive to a number of other parameters including hole-size, type of loading, frequency of cyclic loading, and temperature and moisture (Stinchcomb and Reifsnider, 1979). Significant contributions to this topic have been made by Rotem and Hashin (1976), Hashin (1981), O'Brien and Reifsnider (1977), Reifsnider *et al.* (1983), Talreja (1985 & 1987), Highsmith and Reifsnider (1986), and Whitworth (1990).

2.2 Mechanically Fastened Joints

Bolted and/or riveted joints form the category of mechanically fastened joints, representing one of the most frequently used joining methods for composite structures, especially for thick composite adherends, for the assembly of heavily loaded components, for easy disassembly for damage inspection (periodic maintenance) and repair, for out-of-plane load carrying members, or for the case where access (equipment access) is required.

Bolted joints in composite structures are among the most challenging problems an engineering mechanics specialist has to deal with (Oplinger, 1996). It is well known that the response of composite materials is brittle and that there are severe stress concentrations developed around fastener holes or cutouts. Composite materials will not smooth out the stress peaks around holes or cutouts by yielding, as metals typically do. Therefore, a good composite bolted joint design requires a more accurate knowledge of damage mechanisms and failure modes.

There are six typical modes of failure for bolted joints in advanced composites (Figure 2.1):

1. Tension failure;
2. Shear-out failure;
3. Bolt pulling through laminate;
4. Cleavage-tension failure;
5. Bearing failure;
6. Bolt failure.

Preferably, the designed failure mode is bearing failure in order to prevent catastrophic failure (Hart-Smith, 1987). Oplinger (1996) reviewed the progress in the analysis and design of bolted joints in composite structures since the advent of advanced composite materials in the mid 1960s. The review included the contact problem and stress concentration, two-dimensional stress analysis and failure prediction and the effort in three-dimensional stress analysis and the need for 3-D stress analysis.

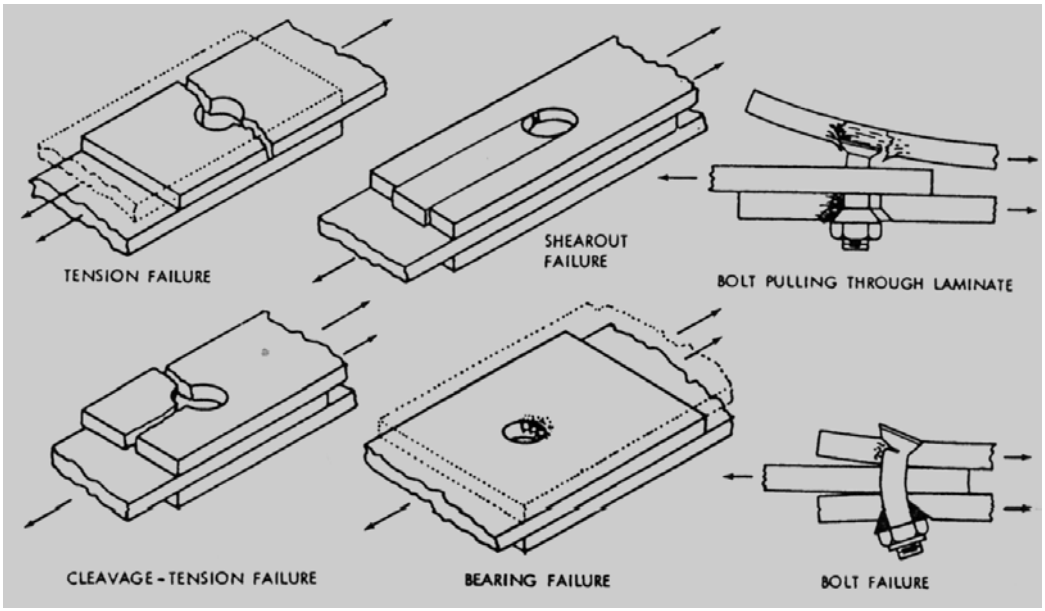

Figure 2.1 Modes of failure for bolted joints in advanced composites.
(From Hart-Smith, 1987)

Soni (1981) conducted stress analysis of composite laminates with a single through-the-thickness circular hole under uniaxial tensile load and the ultimate failure strength and modes of failure were predicted via the finite element technique, classical lamination plate theory and a stress tensor polynomial failure criterion.

Fiber-reinforced composites could be weakened by drilling holes, by stress concentrations in the region of the holes due to brittle response (no plastic yielding) and by anisotropy. Herrera-Franco and Cloud (1992) had conducted an experimental study on relieving stress concentrations around bolt or rivet holes using strain-relief inserts for composite fasteners. An insert (hard or soft) in the form of a thin bushing of isotropic

material was adopted and glued into the hole. Through this, the local stress concentration could be accommodated by ductility or other mechanisms of compliance, and then the efficiency of the joint or joint strength would increase.

It is well known that the stress field in the vicinity of a bolt hole in a composite is three-dimensional and interlaminar stresses are always present at free edges; while most studies on bolted joints were based on two-dimensional analysis due to its simplicity. The limitations of a 2-D study are obvious: it can not model countersink holes and delaminations cannot be explicitly considered in the failure analysis (Ireman, 1998). Ireman developed a 3-D finite element model of a bolted single-lap composite joint to determine non-uniform stress distributions through the thickness of composite laminates in the vicinity of a bolt hole. Also, an experimental program was conducted to validate the numerical model. In his numerical and experimental study, a number of important parameters/features were considered such as laminate stacking sequence, laminate thickness, bolt diameter, bolt type, clamping force, contact, friction, etc.

For reliable joint strength evaluation and failure prediction, an analytical study of bolted single- and double-lap composite joints under mechanical and thermal loading was presented by Kradinov *et al.* (2001). The contact phenomenon, bolt-hole clearance and interaction among the bolts were considered. The contact stress, contact region around bolt holes and bolt load distribution were solved from the coupled equations simultaneously using the complex potential theory and the variational formulation.

Relatively little work has been done in the area of fatigue strength with loaded holes of bolted joints. Crews (1981) investigated both the static and fatigue strength of a graphite/epoxy laminate considering a range of bolt clamp-up torques and several test

conditions. It was found that the simple pin-bearing case had the lowest joint strength and the bolt clamp-up torque not only affected the static strength and fatigue limit but also the failure modes and the bolt-hole elongation. The higher the clamp-up torque, the higher the strength. An ultrasonic C-scan technique was employed to show the delamination damage around the hole at some intervals of fatigue testing. The effect of water exposure upon the joint static bearing strength was slight; however, it reduced the fatigue limit by up to 40%.

2.3 Adhesively Bonded Joints

In the case of an adhesively bonded joint, the adherends are joined by a suitable adhesive. The advantages of this configuration include design flexibility, relatively uniform stress distribution compared to mechanically fastened joints, little or no weight penalty (no additional weight from bolt or rivets), etc. The limitations of using adhesive joints lie in the difficulty to measure the bond integrity after assembly and also the difficulty in verifying the quality and performance of a bonded joint during service, since the bond is easily affected by environmental conditions or by service induced damage (Youssef *et al.*, 1992).

There are several important parameters that need to be considered to assure a good quality adhesive joint: joint configuration (single lap, double lap, step lap, scarf joint, etc., Figure 2.2); adherend thickness; adherend tapering; adherend surface treatment; selection of adhesive; and curing of the adhesive.

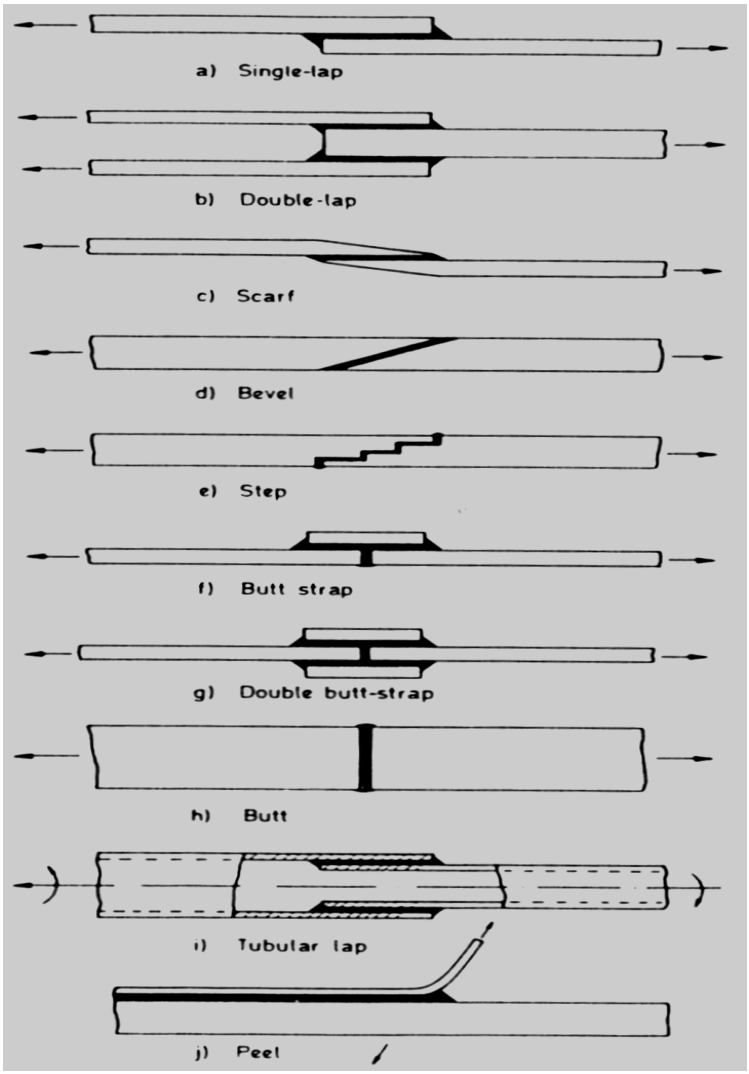

Figure 2.2 Adhesively bonded joint types.
(From Adams and Wake, 1984)

In general, there are three types of defects in adhesive bonds (Youssef *et al.*, 1992):

1. *Physical discontinuities* such as voids, porosity, inclusions, contaminations and unbonded areas which may be introduced in the bond during fabrication or debonds and cracks that can occur in service;

2. *Weak adhesive* which can be caused by adhesive aging, fabrication problems or environmental degradation;

3. *Poor adhesion* which can result from ineffective surface preparation or contamination of adherends.

In comparison with mechanically fastened joints, the typical failure modes of adhesively bonded joints are as follows:

1. Failure within adherend;
2. Adhesive failure (between adhesive and adherend interface);
3. Cohesive failure (within bond);
4. Mixed cohesive/adhesive failure.

Adhesively bonded joints are more widely used for lightly loaded parts due to the limitation of adherend thickness. It is preferable that failure occurs within the adherend rather than within the bond region, i.e., the strength of joint should surpass that of the adherend.

The lack of reliable inspection methods that can assure the bond quality, i.e., having adequate load transfer capability, makes a good design practice necessary in order to ensure that the load is transferred in shear and to minimize any direct or induced peel stress (Hart-Smith, 1987).

To ensure a safe and durable joint, its design must be based on stress analysis plus prototype testing and full scale component/structure testing. Although numerical analyses could provide fast evaluation and reference for design, analytical stress methods are more effective for identifying key parameters. Tsai *et al.* (1998) conducted improved theoretical analyses of adhesively bonded single-and double-lap joints. The solutions

were improved by including the shear deformation of the composite adherends. The study concluded that the classical solutions which neglected the adherend shear deformations over-estimated the non-uniformity of the adhesive shear distribution and the maximum adhesive shear stress (strain). The shear stiffness, overlap length and thickness of adherend were considered as the key parameters which determined whether adherend shear deformation should be included or not in the theoretical stress analysis.

For adhesively bonded stepped-lap joints and doublers, Hart-Smith (1981) studied the effects of non-uniform adhesive properties on their behavior based on his previous work considering a uniform adhesive throughout. Several aspects were investigated for the non-uniformity of adhesive throughout the bond such as load redistribution around flaws and porosity, effects of variation in thickness of the adhesive layer and non-equilibrium absorption of moisture to change the adhesive properties.

Other than using plain resin adhesive, two types of fiber pre-impregnated (prepreg) composites were used as fiber-reinforced adhesives to bond single lap composite joints (Li *et al.*, 2001). The results from testing showed that the prepreg bonded joints had a higher loading capacity compared to those bonded by plain resins. The fiber orientation and stacking sequence of the prepreg adhesive had a significant effect on the load bearing capacity of joints. Environmental conditioning such as UV radiation attack and sea water reduced the load bearing capacity of joints. Finite element analysis explained that the reduced peel stress and interfacial shear stress in the joints with unidirectional prepreg adhesive resulted in better performance of those joints.

The application of adhesively bonded joints in the automotive industry was studied by many researchers. For example, the critical component for a rear wheel drive vehicle is

the propeller shaft, used to transmit power from the engine to the differential gear, which should be designed to satisfy the requirements of torque transmission capability, fundamental natural bending frequency and torsional buckling resistance. Kim *et al.* (2001) substituted a one-piece composite shaft for a conventional metal shaft and adhesively bonded it to the steel or aluminum yoke of a universal joint. It was shown that through optimum design of the composite shaft and the adhesive bonding to the yoke, the above requirements were easily satisfied while achieving a weight reduction of approximately 40% as well as reduction of noise and vibration compared to a two-piece steel shaft.

The fatigue behavior of adhesively bonded joints was also investigated. Johnson and Mall (1985) undertook both experimental and analytical studies to determine whether the adhesive debond initiation stress could be predicted for arbitrary joint geometries. Two types of adhesive systems were used to join the adherends and a fracture mechanics approach was presented to predict the maximum cyclic stress that an adhesive joint could sustain without debonding. The conclusions derived were that the total strain energy release rate G_T might be the governing factor for debond initiation and cyclic debonding in tough structural adhesives; that debond initiation and growth could take place without peel stresses; and that the analytical predictions of the loads required to initiate debonds in tapered-adherend cracked-lap-shear specimens agreed well with experimental results.

Few results on the long-term durability characteristics of bonded joints in warm/moist conditions and few quantitative predictions of life-time performance are available. The effect of the environment on the fatigue of bonded composite joints was investigated by Ashcroft *et al.* (2001). It was found that the failure modes in the lap-strap joints studied

were heavily dependent on environmental conditions, especially temperature. As temperature changed from -50^{o}C to +90^{o}C, the dominant fracture path transferred from interlaminar failure of the composite adherend to cohesive failure of the adhesive. Also the glass transition temperature T_g of the adhesive was very important for the fatigue performance of joints. Briskham and Smith (2000) employed the cyclic stress durability testing of lap shear joints of different adhesive-pretreatment combinations exposed to hot-wet conditions compared to unstressed or static stress durability testing.

2.4 Co-Cured Hybrid/Composite Joints

A co-cured joint, whose curing and bonding processes are achieved simultaneously, can be regarded as an adhesively bonded joint (at least an evolution from an adhesive joint), for which the adhesive is the excess resin extracted from the composite materials during consolidation. This configuration makes the design and analysis of a co-cured joint simpler (Shin *et al.*, 2000a). No additional adhesive and no surface treatment of the composite adherends are needed.

The co-cured composite joint concept was investigated both experimentally and numerically in designing composite spar-wing skin joints (Cope and Pipes, 1982). The thick skin and thin spar sections of four joint configurations were cured together and then tested by applying out-of-plane loading. Crack initiation and propagation was noted by visual inspection and it was concluded that the crack initiation from insert debonding was not simultaneous with catastrophic failure but did initiate the failure process. A finite element modeling was also accomplished to predict the joint strength through the

application of the Tsai-Wu, the maximum stress and the maximum shear failure criteria. It was found that the numerical results provided bounds to most experimental data.

An important concern in the co-curing of large structures is the minimization of the coefficient of thermal expansion mismatch between tooling and the parts to be co-cured. Co-cured structures require tooling that should not apply unnecessary stresses to the assembly during heating or cooling. An integrally co-cured wing/fuel box was manufactured and showed that this process can be utilized for manufacturing a variety of aircraft structural elements such as an entire wing, horizontal stabilizer, fuselage, rudder or elevator (Oliva, 1991).

A strength model for co-cured stepped-lap composite joints under tensile static and fatigue loading was developed and the shear mode was found to be the most important parameter for this type of joint under tensile loads. The Tsai failure index calculated using the stress distributions from finite element analysis and compared to the experiment contributed to the conclusion that the design accuracy was low by just considering the linear elastic properties of the resin on the joining interfaces in finite element analysis (Kim *et al.*, 1995).

An investigation of hybrid co-cured joints consisting of a composite adherend and a metal adherend has been reported by some researchers. This joint concept can be applied to hybrid structures such as golf clubs and automotive composite propeller shafts which have a conventional adhesively bonded joint by epoxy adhesives with fillers between a carbon/epoxy shaft and a metal shaft (Lee and Cho, 2000). Lee *et al.* (1997) have studied co-cured steel-composite tubular single lap joints under torsional or axial loading. Static and dynamic torque characteristics for this type of joint were studied both experimentally

and numerically and compared to those of the conventional adhesively bonded joints. Several bonding parameters such as surface roughness, bonding length and stacking sequence of the composite adherend were investigated in detail. Also, the nonlinear shear behavior of the epoxy resin was incorporated into the finite element torsional analysis for more accurate calculation of static torque capacity. It was concluded that both the static and fatigue strengths of the co-cured joints were larger than those of the conventional adhesively bonded joints. Cho and Lee (2000) proposed a further optimized design method for the co-cured steel-composite tubular single lap joint by suggesting a failure model which incorporated the non-linear mechanical behavior of the steel adherend and the failure mode of joints, such as steel adherend failure and composite adherend failure. Four design parameters (the thickness ratio of the steel adherend to the composite adherend, the residual thermal stresses, the stacking sequence of the composite adherend, and the effect of a scarf in the steel adherend) were considered in the optimum design to maximize the joint strength under axial loading. Also, the fracture surface was examined in order to assist the optimum design. The failure mode of a co-cured joint with a $[0]_{8T}$ composite adherend was observed to begin with the delamination of the outer seven plies of the composite from the inner ply, followed by the failure of the last ply along the circumference of the steel adherend. The conclusion drawn was that the axial load-bearing capability of the co-cured joint had a maximum value when both the steel adherend and composite adherend failed simultaneously.

Another published study is related to the tensile load carrying capability of co-cured steel-composite single lap joints or double lap joints. Shin *et al.* (2000) investigated experimentally the shear lap strength of a co-cured steel-composite single lap joint under

tensile loading. Different bonding parameters were investigated such as bond length, surface roughness and stacking sequence of the composite adherend and the failure mechanisms of this specific co-cured single lap joint were defined and classified into four types:

1. Interfacial failure (between the steel adherend and the thin resin layer);
2. Interlaminar delamination failure (between the plies of the composite adherend);
3. Cohesive failure (within the thin resin layer or within the first ply of the composite laminate);
4. Adherend failure (within steel or composite adherend).

The most desirable failure for this co-cured joint is cohesive failure, which occurs either within the thin resin layer or within the first ply of the composite laminate, in order to reach the maximum strength of the material in a co-cured single lap joint and the question about improper surface preparation before bonding or an improper bonding process is excluded. Based upon the examination of the fracture surfaces, the operating failure mode was actually a partial cohesive failure (interfacial failure plus cohesive failure within the first ply of the composite adherend) for this co-cured single lap joint. In addition, the lap shear strength was maximum for a $\{[+45/-45]_{4S}\}_S$ stacking sequence and an optimum stiffness difference between the composite laminate and the steel was required for the optimum lap shear strength of a co-cured single lap joint. Shin and Lee (2000a) then conducted stress analysis by using the finite element method and investigated the stress distributions in a co-cured steel-composite single lap joint subjected to tensile load including the residual thermal stresses resulting from the curing

process. From the previous study (Shin *et al.*, 2000), the operating failure mode for this joint was partial cohesive failure other than the desired purely cohesive failure. Shin and Lee found that the interfacial tensile and shear stresses at the joint base were the primary factors causing interfacial failure between steel and composite adherends

Similarly, Shin and Lee (2000b) investigated both experimentally and numerically the tensile load-bearing capacity of co-cured steel-composite double lap joints. The operating failure mechanism was found to be cohesive failure by delamination at the first ply of the composite laminate. The tensile load capacity of the co-cured double lap joints was calculated by the three-dimensional Tsai-Wu failure criterion using stress distributions obtained from finite element analysis.

For fiber-reinforced composite materials, thermally induced stresses may occur at the micromechanics level that are the results of the mismatch in the coefficients of thermal expansion (CTE) between the fiber and matrix, or at the layer level that are a result of the mismatch in coefficients of expansion between layers with different fiber orientations (Hyer, 1998). CTE mismatch also exists for a hybrid co-cured joint, for example, with a composite adherend and an aluminum adherend and this will introduce residual thermal stress in the joint after cure. Lee and Cho (2000) studied experimentally the tensile load capabilities of co-cured steel-composite tubular single lap joints with respect to environmental temperature and stacking sequence of the composite adherend. The stress distribution in the co-cured joint was calculated by finite element analysis considering both the influence of the residual thermal stresses after cure and the thermal degradation of the composite at elevated environmental temperatures. The conclusions of this study included that the accurate failure index might be obtained and the calculated tensile load

capabilities agreed fairly well with the experimental values only when the residual thermal stresses and the thermal degradation of the composite were considered.

Cho *et al.* (1997) manufactured by co-curing a hybrid one-piece drive shaft and initiated a way to reduce the fabrication thermal residual stresses from the mismatch of CTE between carbon-fiber composite and aluminum by applying a compressive preload to the aluminum tube before the co-curing operation.

Practical joint design in both composite and metallic structures needs new design concepts for lower cost, higher joint efficiency and better performance. An interesting study was carried out by Lagace and Allen (1985) for alternative manufacturing methods for bonding graphite/epoxy composites either by single lap joint or double lap joint type. Altogether six manufacturing methods were investigated which cured one or co-cured both adherends during the bonding process using either film adhesive or the excess resin within the composite materials as the bonding agent. They found that there were no advantages obtained by curing only one of the adherends; the adhesive film should be used in all bonding operations to have maximum strength and the joint strength was controlled by the weak surface, i.e., weak link. For the co-cured single lap joint without additional adhesive, it failed in the thin bond line between the adherends and its strength could be improved by co-curing film adhesive between adherends.

Coates and Armanios (2000; 2001) proposed a new joint concept for strength enhancement for co-cured composite joints from a single lap joint to a Single Nested Overlap (SNO) joint (Figure 2.3). It was found that both the static and fatigue strengths improved for the new concept. The failure mode of co-cured single lap joints appeared different from that of co-cured SNO joints. An Acoustic Emission monitoring technique

was used to monitor the damage initiation, propagation and accumulation during loading of the joint and the stage of damage initiation, the damage accumulation rate and the amount of damage accumulation were characterized as different for these two types of joints. The measured acoustic emission was lower for co-cured single lap composite joints; the damage developed earlier and more intensely in SNO joints during loading to failure, and the damage accumulation rate for SNO joint during the final 30-40% of loading was much higher than that of the single lap joint. However, that study did not explain the damage and failure mechanisms which contributed to the strength and fatigue life enhancements of SNO joint over single lap joint and the dominant damage mechanisms were not identified for these two types of joints either.

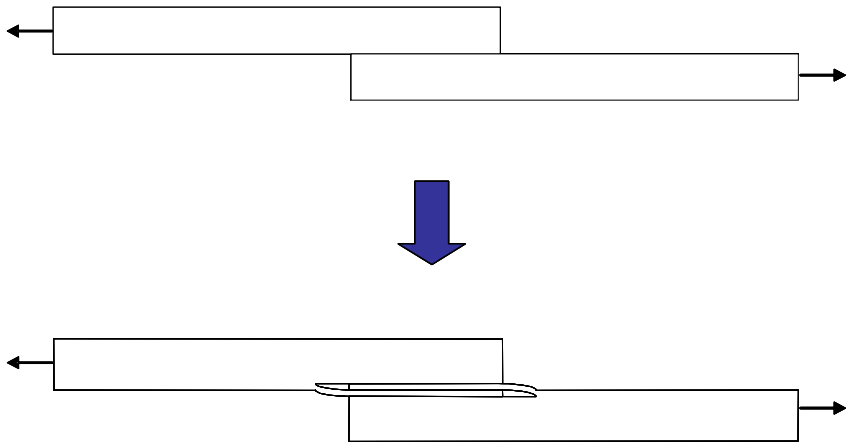

Figure 2.3 Joint design concepts evolving from a single lap joint to an SNO joint.

2.5 Comparisons of Composite Joining Methods

Various joining methods have their own advantages and disadvantages/limitations. A detailed comparison is provided by Schwartz (1994), Messler, Jr. (1993), and Shin *et al.*, (2000) for three general methods for joining composite members or at least one composite adherend (mechanically fastened joints, adhesively bonded joints and co-cured joints) and summarized in Tables 2.1-2.3.

2.6 NDE Tools

2.6.1 Review of Major NDE Methods

Nondestructive Evaluation/Inspection NDE/NDI is a necessity for both manufacturing quality control and in-service performance monitoring for maintenance purpose. With the advent of composite materials and their wider applications in the aerospace industry, etc., an increasing need for fast, reliable and economical NDE techniques to inspect composite components which have uniquely complex damage/failure modes and responses is evident.

One of the design goals of modern aircraft structure consists of higher fatigue life (endurance), damage tolerance capability and corrosion resistance in order to minimize the maintenance costs and also comply with operator requirements and enhanced airworthiness requirements. Non-destructive evaluations (NDE) are essential, although time-consuming and expensive, to fulfill the above requirements and for the assessment of widespread fatigue damage and existing repairs (Schmidt *et al.* 2000).

The existing major non-destructive inspection/evaluation methods include the following seven techniques:

1. Tapping Technique
2. Thermography
3. X-ray Radiography
4. Eddy Current
5. Acoustic Emission
6. Ultrasonic Techniques
7. Laser Based Technology (LBT)

Tapping Technique

The original tapping technique, which was qualitative, used a coin or hammer to lightly tap various bodies to gain information about unseen structural details and it relied exclusively on the ability and experience of an inspector to "hear" the difference between an acceptable and an unacceptable bond or delamination. Thus it is limited in scope and can only be used to detect gross debonds. A quantitative tapping test with the assistance of a miniature force transducer was studied to improve the flaw characterization especially for the detection of edge defects in laminated plates (Kenner *et al.* 1985).

Thermography

Infrared thermography is one of the NDI methods, which is based on very simple theoretical principles. In-service incidents such as impact may cause local fiber breakage and delamination at the point of incidence and in adjacent composite structure. This damage characteristic reduces the nominal thermal conductivity at the damaged site. In a suitably oriented heat flow field, the damage site will reduce the flow of heat, causing a

thermal gradient to appear on the inspection surface which can be readily observed using commercially available thermographic cameras. This method is non-contact and thus avoids the application of couplants or other surface preparations. It is very useful to detect in-service damage such as impact and lightning damage whose superficial visual appearances often belie the full extent of their underlying damage (Hillman and Hillman, 1985). More recently a new thermography method called Lock-in Thermography has been developed. This method is a combination of infrared thermography and the thermal wave technique and thus is more sensitive and has higher detection capability compared to the conventional reflection and through transmission techniques (Bai and Wong, 2000).

X-ray Radiography

X-ray Radiography is a well-recognized and documented evaluation method with a wide range of industrial applications. However, the conventional low-kV X-ray Radiography can only be used for imaging flaws like resin-rich areas, fiber-rich areas, voids, inclusions and folds in the material. For impact induced damage or in-service damage such as delaminations in composite materials, Penetrant-Enhanced X-ray Radiography (PEXR) is used to obtain good contrast radiographs and thus evaluate more accurately the damage state of composite structures. When combined with stereo-imaging, PEXR can image the impact damage in three-dimensions (Birt, 2000).

Eddy Current

Nondestructive testing of aging aircraft structures is essential for flight safety and low cost maintenance. Among many NDE methods being used in aircraft maintenance, Eddy

Current testing with inductive sensors is a well established technique especially for layered structures. However, for Eddy Current (EC) testing, a fundamental requirement is that a distribution of currents has to be induced in the examined material which must be electrically conductive. The existence of damage such as cracking makes the magnetic field in the material inhomogeneous, and this inhomogeneity can be detected by gradiometer sensor. A newly developed system with Superconducting Quantum Interference Devices (SQUID) gradiometer was employed for aircraft wheel and fuselage testing. Result showed that this advanced system performed better than the conventional Eddy Current testing method in finding smaller cracks without disassembly and with higher separation resolutions (the separation of the crack signal from the underlying signals from the structure) (Krause *et al.* 2000).

Acoustic Emission

Acoustic Emission is a technique based on monitoring elastic stress waves that are generated by rapid local redistributions of stress which accompany the operation of many damage mechanisms. Stress waves that travel to the piezoelectric transducer attached on the material surface are then converted into electrical signals from which the Acoustic Emission system can measure and produce data displays. The signals are then filtered, amplified and analyzed to extract their acoustic parameters and recorded for analysis. The operator could evaluate the state and behavior of the structure/material under stress from these acoustic parameter plots when using conventional acoustic emission analysis. Using multiple sensors mounted across the surface of material or structure, it is able to locate the damage source by the location capability of the AE technique; damage severity

around those critical locations could be evaluated by direct AE analysis or by combining other NDE techniques such as Ultrasonics, Eddy Current, X-ray radiography, etc. With the advent of advanced computer technology and data processing techniques, acoustic emission systems can record the waveform information about each hit signal. Pattern recognition and waveform analysis based on the recorded AE parameter data and waveform information can provide additional knowledge about the activities inside the material or structure and their characteristics. The severity of those events, material quality or structural integrity could then be evaluated based on these analyses.

Acoustic Emission is a very useful tool in detecting elastic stress waves and correlating them with the responsible source mechanisms because of its high sensitivity, real-time capability and volume-monitoring character. The Acoustic Emission technique has its promising applications in many areas, including material characterization, manufacturing quality control and in-service damage detection and monitoring of structures. A large volume of research work has been done related to qualitative and quantitative evaluations of composite components and structures using the acoustic emission technique. It is well known that composite materials are very noisy under load particularly during quasi-static tensile testing or tension-tension cyclic fatigue loading. Awerbuch *et al.* (1985) monitored Acoustic Emission during quasi-static loading-unloading cycles of filament-wound graphite-epoxy laminate coupons and assessed the validity of the Kaiser and Felicity effects. They concluded that the Felicity ratio could be an indicator of damage severity and/or material quality, and ultimately used as an acceptance/rejection criterion. Hamstad (1986) reviewed several applications of Acoustic Emission as a tool for composite materials studies such as correlating AE with other

measures of damage, applications to time-dependent studies, impact studies, cure studies, etc. Komai *et al.* (1991) investigated the relationships between several AE parameters and AE original sources and discussed fracture mechanisms of carbon fiber reinforced plastics (CFRP) in terms of observations of fracture surfaces and internal damages of the laminates by a scanning electronic microscope (SEM) and a scanning acoustic microscope (SAM), respectively. It concluded that the unidirectional reinforced carbon/epoxy composites went through fiber/matrix interface debonding and fiber breakage.

Bakuckas, Jr. *et al.* (1994) first used model specimens of titanium matrix composite system exhibiting dominant failure mechanisms and established correlations between the observed damage mechanisms and the AE amplitude. These correlations were then used to monitor the damage growth process in titanium matrix composite laminates exhibiting multiple modes of damage. Prosser *et al.* (1995) used an advanced waveform-based acoustic emission system to study the initiation of transverse matrix cracking in cross-ply graphite/epoxy composites. It found that transverse matrix cracks initiated at the specimen edge rather than within the interior of the specimen for cross-ply laminates; the stress required to initiate cracking was a function of the thickness of 90 degree layer in the middle of a cross-ply composite. They also brought an important outcome of these tests that the same source mechanism in a composite such as transverse matrix cracking produced a wide range of signal amplitudes depending on the thickness of the middle 90 degree layer and also the length of propagation of the crack across the width of the specimen. Tsamtsakis *et al.* (1996) investigated the behavior of quasi-isotropic carbon fiber reinforced epoxy laminates under monotonic tensile loading using several

nondestructive techniques such as acoustic emission, X-ray radiography, the edge replica technique and optical microscopy techniques. They concluded that lower amplitude events were produced when the crack propagation occurred in a stable way and delamination covered the medium range of amplitudes. Wevers (1997) mentioned that the acoustic emission (AE) technique is the only nondestructive test technique possibly capable of detecting the different damage types in composites, though the distinction between the AE signals coming from different damage types is not straightforward. But it is possible to distinguish between AE signals attributed to different damage types by cooperatively using other techniques such as replica, light microscopy, penetrant enhanced radiography, etc. Mizutani *et al.* (2003) conducted four-channel acoustic emission monitoring for both the ambient and cryogenic tests of unlined filament-wound CFRP tank. They evaluated the soundness of the tank by using traditional AE parameter analysis and conducted waveform-based detailed source location analysis near the leak point. Acoustic Emission is the only possible way to undergo those tests - including ambient temperature tests, cryogenic temperature tests and cryogenic pressurization test - without disintegrating the tank structure.

Acoustic Emission has also been used to study fatigue behaviors of composites. Awerbuch *et al.* (1984) monitored fatigue damage progression and accumulation through acoustic emission during low cycle tension-tension fatigue loading. The major goal of their work was to determine the potential of the acoustic emission technique as an on-line nondestructive test procedure for monitoring damage initiation and progression during fatigue loading. Attempts were made to qualitatively distinguish between emission generated by friction and that generated by actual fatigue damage progression. Gustafson

and Selden (1985) performed tension-tension fatigue tests on quasi-isotropic graphite/epoxy specimens and monitored nondestructively damage initiation and growth using both acoustic emission and X-ray radiography. The stages and characteristics of transverse cracking, onset and growth of delamination were described. The distinction between emission generated by friction and emission by crack propagation was not made due to lacking of a definite correlation between AE event amplitude and energy characteristics and type of damage growth. Research in structural health monitoring for a wide range of applications now attracts a lot of scientists. Embedding optical fibers in the material or structure is one of the techniques to monitor live in-service behavior. Acoustic Emission proves to be also useful in this related research. Surgeon and Wevers (1998) quantified the damage state of quasi-isotropic CFRP with embedded optical fibers during fatigue testing using acoustic emission and microfocus radiography. They concluded that separation of some of the active damage phenomena with different amplitudes based on AE results was possible. Tsamtsakis *et al.* (1998) investigated the fatigue behavior of quasi-isotropic carbon fiber reinforced epoxy laminates under tension-tension cyclic loading and used acoustic emission to monitor the different damage mechanisms activated throughout the fatigue life. They concluded that after filtering out the friction related events, AE technique could be used efficiently to evaluate the fatigue damage process in terms of cumulative AE counts during the different stages of the fatigue life. Tsamtsakis and Wevers (1999) continued the research on quantifying the fatigue damage development in quasi-isotropic CFRP and a model based on AE data was formulated. It was found that fatigue damage grew with cyclic loading and its accumulation was a nonlinear function of cycles and stress.

Ultrasonic Techniques

The ultrasonic technique is also based on wave theory. However, mechanical waves are first converted from electrical pulses by a piezoelectric transducer and then emitted into a couplant such as water. The intensity of wave reflection or transmission through the material under inspection which is immersed in the water tank is measured by a receiving transducer. A portion of ultrasonic wave energy is reflected by defects, damage and interfaces and the energy transmitted through the material is reduced due to reflection and attenuation. Therefore, both reflection and transmission of energy can be used for ultrasonic inspection. A map/image of the intensity of reflection/transmission which provides a measure of the discontinuities in the material is called a C-scan. C-scans are now used routinely to assess the integrity of materials and structures (Herakovich, 1998). Ultrasonic NDE, which has proven to be a reliable and reasonably priced approach that can reveal most critical defects such as porosity, contaminations, delamination, fiber- or matrix-rich areas and impact damage, will enable the inspector not only to locate the anomalies within a structure but also to determine the type of defect that has been found (Steiner, 1992). The necessity of a couplant may limit, however, its on-site, large area inspection capability.

Laser Based Technology (LBT)

Laser based technology (LBT) is used to inspect and analyze fatigue critical components, such as engine components while on-the-wing, for microscopic fatigue damage. The basic principle behind LBT is to direct a laser beam on the component and analyze the spatial-temporal characteristics of the light scattered off the component

surface. The proposed concept is based on the assumption that cyclic fatigue manifests itself in localized modifications of the object surface. The application of this technology will lead to the ultimate goal of using condition based maintenance to replace the time-on-the-wing maintenance which in the end will reduce the maintenance cost and increase aircraft readiness and safety (Moffatt and Markov, 2002).

2.6.2 NDE for Composite Joints

NDE techniques are mostly necessary for adhesively bonded composite joints and co-cured composite joints in order to ensure their structural integrity and performance and also meet design and service requirements.

Not much work has been published in nondestructive inspection/evaluation/testing of composite joints. For adhesively bonded composite joints, the ultimate goal is to be able to predict the bond strength using nondestructive techniques. However, limited breakthrough has so far been achieved. Frequently used NDE methods for adhesively bonded composite joints are Ultrasonics and Acousto-Ultrasonics, Acoustic Emission, Radiography, and Thermography (Guyott, *et al.* 1986; Bar-Cohen and Mal, 1987; Tanary, *et al.* 1992; Prassianakis, 2000). For co-cured composite joints, the research and development of NDE techniques on this type of joints do not match the increasing application trend of the co-curing joining method. Georgeson (2000) investigated the Ultrasonics method such as Through-Transmission Ultrasonics (TTU) and Pulse-Echo Ultrasonics (PEU) to evaluate co-cured composite structures and co-cured curved joints. Co-curing allows potential geometric complexity, such as curved-shaped spar-wing skin

joints. However, this imposes additional inspection requirement to fulfill the orientation-dependent detection of defects inside the curved joints.

In this study, Penetrant-Enhanced X-ray Radiography, Acoustic Emission and Optical Microscopy will be used to investigate the damage initiation, damage progression and failure modes of co-cured composite joints with two joint configurations and two types of lay-ups.

Table 2.1 Mechanically fastened composite joints

Advantages	**Disadvantages**
Permit disassembly without destruction of the substrate;	Weaken the materials by drilling holes and machining;
Require no surface preparation;	Cause stress concentrations around holes;
Generally are not affected by thermal or humidity cycling ;	Add weight and bulk to joint that reduces the joint efficiency;
Are readily inspected for joint quality;	Have corrosion problems around fasteners;
Can undertake heavy load for thick-adherend joint;	Cause possible leaks through open joints or fastener holes;
Have less critical mating or fit-up requirements.	Have complex stress profiles and possible multiple failure mechanisms.

Table 2.2 Adhesively bonded composite joints

Advantages	Disadvantages
Eliminate the need for drilled holes that weaken the members;	Do not permit disassembly without destruction;
Distribute load over a large area;	Require special surface preparation or treatment and curing of adhesive;
Add minimum weight to structure;	Can degrade in service from temperature and humidity cycling;
Minimize corrosion problems;	Have the difficulty in inspecting bond integrity;
Have low cost potential;	Require design to minimize peeling stress;
Have superior life under conditions of cyclic stress;	Apply usually for thin adherends only;
Smooth external surfaces at the joint to improve aerodynamic flow.	Require accurate mating for adherends.

Table 2.3 Co-cured composite/hybrid joints

Advantages	**Disadvantages**
Need no adhesive;	Have thin bond line;
Need no surface treatment of composite adherend;	Have CTE mismatch between different adherends causing residual thermal stress;
Have integrated design philosophy & manufacturing simplicity;	Need high requirements on tooling for complex co-cured joints/structures;
Have simpler analysis and design of a co-cured joint;	Have few research, practice and application database.
Apply for high temperature service condition;	
Others are similar to adhesively bonded joints.	

CHAPTER 3

MATERIAL SYSTEM AND PROPERTIES

3.1 Material System

A Hexcel Corporation IM7/8551-7 composite material system is used for this research. 8551-7 is an amine-cured, toughened epoxy resin system and IM7 is a continuous graphite filament used as reinforcement. IM7/8551-7 is a damage-resistant system, recommended for structural applications requiring high strength, stiffness and damage tolerance. The material is available in refrigerated unidirectional prepreg form.

3.2 Manufacturing

The cure cycles from the manufacturer of the material system defined by the variation of temperature and pressure with respect to time are used for fabricating the composite laminates or co-curing composite joints (Figures 3.1 and 3.2). Figure 3.3 shows the autoclave used for the fabrication of all composite specimens for this study.

Composite laminate panels with three different lay-ups: $[0]_8$, $[90]_{16}$ and $[+45/-45]_{6S}$ have been manufactured for the measurement of in-plane material elastic properties. Some composite laminate specimens cut from respective $[0]_8$ and $[90]_{16}$ panels are shown in Figures 3.4 and 3.5.

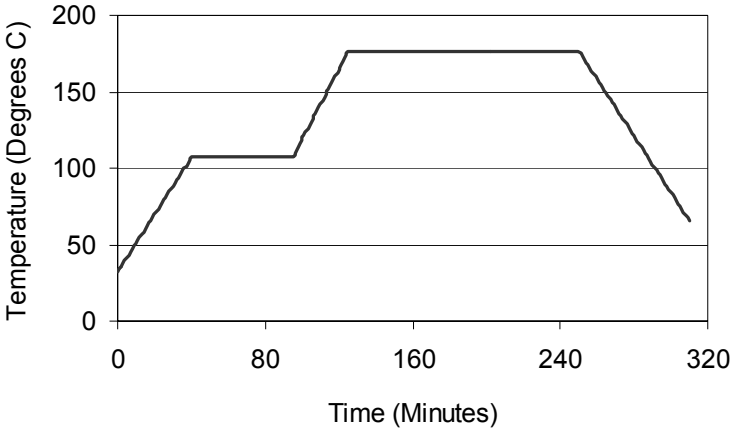

Figure 3.1 Temperature profile for a two-stage autoclave curing process.

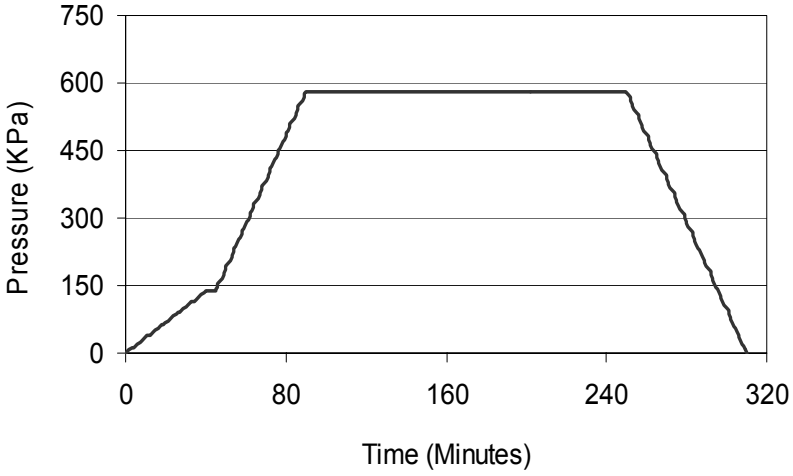

Figure 3.2 Pressure profile for a two-stage autoclave curing process.

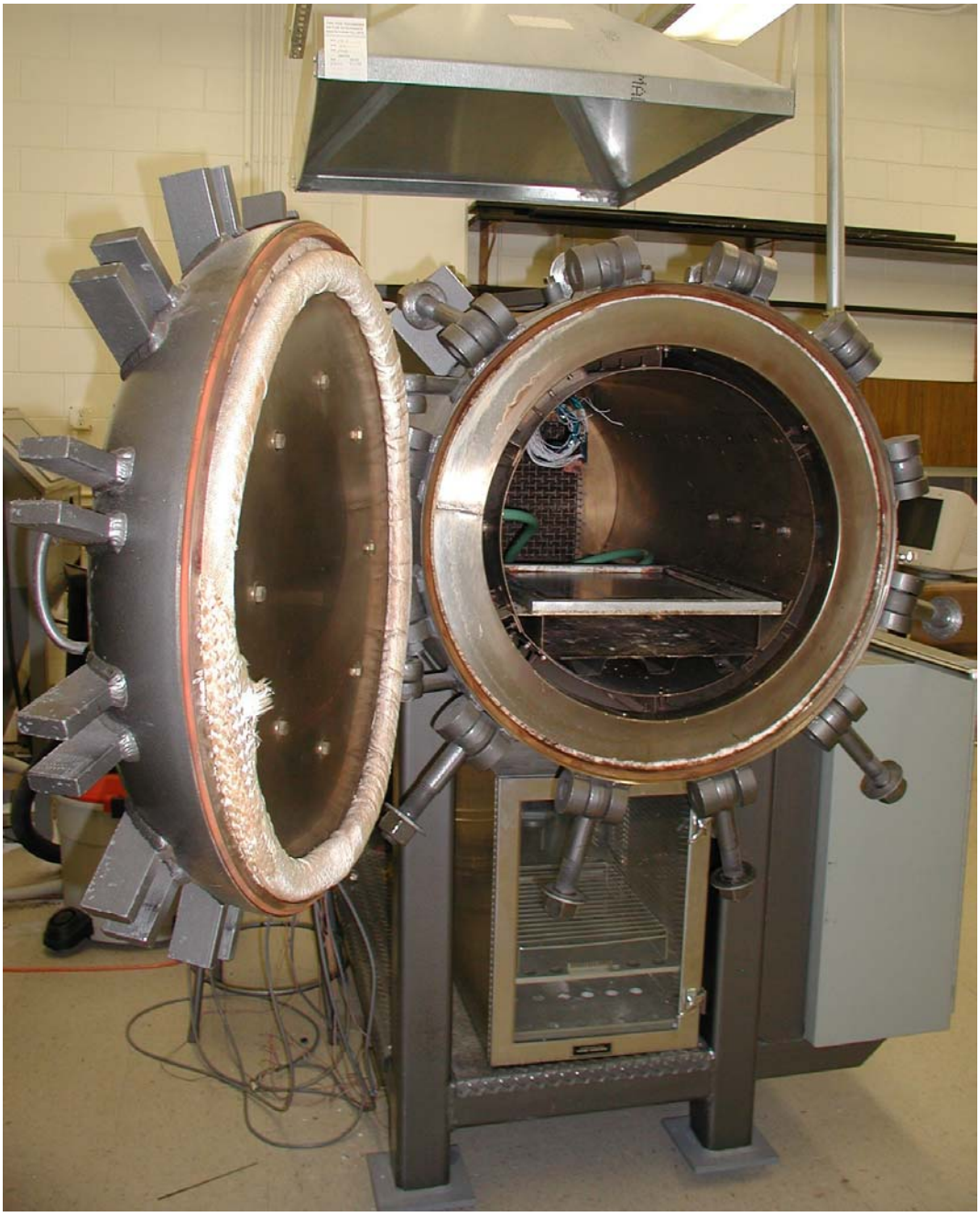

Figure 3.3 The autoclave used for fabricating composite laminates and co-cured composite joints.

.

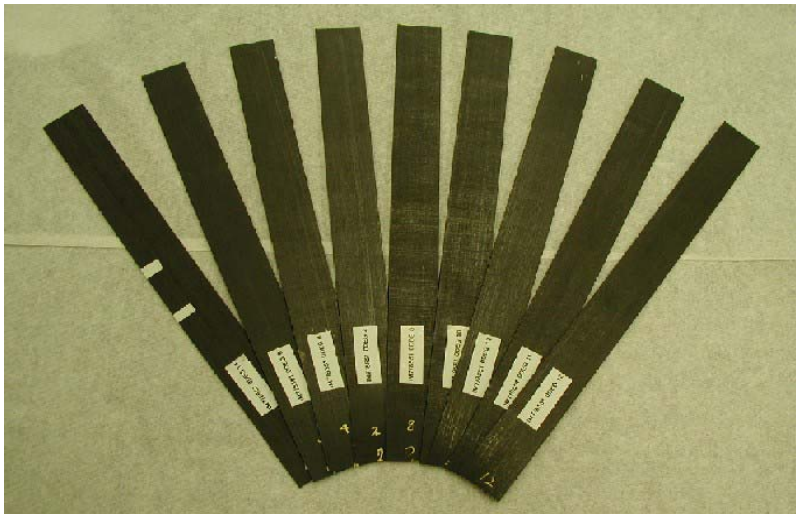

Figure 3.4 Fabricated composite laminate specimens of $[0]_8$.

Figure 3.5 Fabricated composite laminate specimens of $[90]_{16}$.

3.3 In-Plane Tensile Testing

The in-plane tensile properties of unidirectional graphite/epoxy composite have been determined through testing. The test follows the ASTM Standard Test Method for Tensile Properties of Polymer Matrix Composite Materials D3039/D3039M-00. In Figure 3.6, it shows four prepared specimens with strain gages and wiring for obtaining the strain values during tensile testing.

3.4 In-Plane Shear Testing

The in-plane shear modulus of elasticity has also been characterized in this study. Uni-axial tension tests of laminates $[+45/-45]_{6S}$ are performed for in-plane shear properties. The test follows the ASTM Standard Test Method for In-Plane Shear Response of Polymer Matrix Composite Materials D3518/D3518M-94.

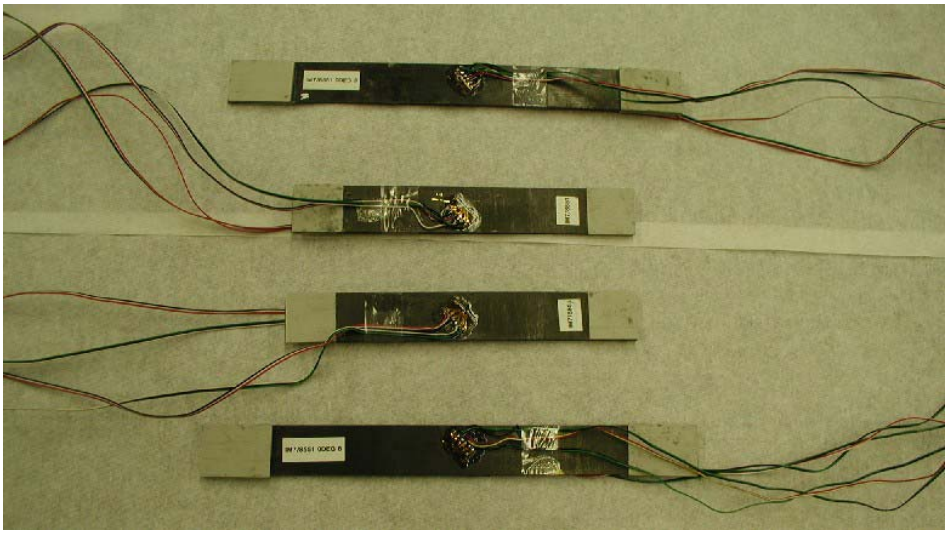

Figure 3.6 Composite laminate specimens prepared with strain gages and wiring.

3.5 Testing Results

The averaged in-plane elastic material properties for the unidirectional IM7/8551-7 lamina are listed in Table 3.1 and the complete testing data of material properties, including statistics, is presented in Table 3.2.

Table 3.1 In-plane material properties of unidirectional lamina (IM7/8551-7)

E_{11} (GPa)	142
E_{22} (GPa)	8.2
ν_{12}	0.35
ν_{21}	0.024
G_{12} (GPa)	3.95

Table 3.2 Complete testing data of in-plane material elastic properties

Specimen	0° Unidirectional		90° Unidirectional		$\pm45^{\circ}$ Angle-ply
	E_{11} (GPa)	ν_{12}	E_{22} (GPa)	ν_{21}	G_{12} (GPa)
1	146.52	0.323	8.621	0.01332	4.61
2	141.86	0.33	8.142	0.04474	4.023
3	142.11	0.357	8.171	0.01625	3.953
4	145.91	0.368	8.195	0.01692	3.918
5	139.01	0.338	8.288	0.01951	3.913
Average	143.08	0.343	8.2834	0.02215	4.083
Average w/o #1	142	0.35	8.20	0.024	3.95
STDEV	2.4526	0.0150	0.0547	0.0118	0.0439
CV	1.725	4.319	0.667	48.582	1.112

CHAPTER 4

DAMAGE AND FAILURE ANALYSIS TOOLS

In this study, damage and failure mechanism in composite laminates and co-cured composite joints will be characterized and recorded using several nondestructive testing tools and techniques including Visual Observation, Optical Microscopy, X-Radiography and Acoustic Emission. These techniques have distinct advantages over each other in detecting damage and failure modes in composite materials and it is necessary for a better analysis by combining their results observed.

4.1 Visual Observation

Specimens are visually inspected either by naked eye or by visual aids such as a digital camera before and after testing to asses the manufacturing quality, machining quality, failure modes, and fracture surfaces of laminates and joints. An Olympus C-3030ZOOM digital camera is used to record and document the results of visual inspection. Digital cameras use a charged coupled device (CCD) as the means of capturing images. The camera used for examination consists of 3,340,000-pixel CCD and Olympus high-resolution optical lens that could deliver a high picture quality.

4.2 Optical Microscopy

An Olympus Microscope is used to provide enhanced, detailed observations of specimen edges and surfaces, including the fracture surface. This microscope is mostly used for reflected light observation purpose and usually consists of a BH2-UMA Universal Vertical Illuminator, a detachable revolving nosepiece, an observation tube, a swing-out Nomarski prism, eyepieces, a light source, and square stage with drive controls (left and right, back and forth). There are four prisms on the detachable revolving nosepiece which supply simultaneous mounting of the full magnification range of 5x, 10x, 20x and 50x Universal Optics. A digital camera can be connected to the microscope observation tube and allows high-resolution color image recording.

The composite specimen with polished edge is mounted on the square stage and observed under the microscope using low to high magnifications. Damage states such as initiation and progression of matrix cracks in the angle-plies, matrix crack density evolutions along the specimen length, and delaminations between two groups of plies with different orientations can be observed.

4.3 X-Radiography

X-rays are a form of electromagnetic radiation, of the same physical nature as visible light, radio waves, etc., but which have a wavelength that allows them to penetrate all materials with partial absorption during transmission. A radiograph is a photographic image produced by a beam of penetrating ionizing radiation after passing through a specimen.

A Hewlett-Packard Faxitron X-ray Radiographic System with self-contained, radiation-shielded cabinet, designed to give high-resolution radiographs of small to medium sized objects, is used to obtain radiographs of composite joints/laminate specimens. A fluid called "penetrant", which consists of zinc iodide, water, isopropyl alcohol and Kodak 'Photo-Flo 600', is used to fill, through capillarity, the cracks and delaminations that develop in the composite specimen and thereby allows a visual identification of internal damage in radiographic images. This penetrant-enhanced X-radiography (PEXR) could supply good contrast radiographs especially for delaminations and better serves the damage characterization goal.

4.4 Acoustic Emission

When materials are loaded to a certain stress level, elastic waves emitted from the sudden deformation caused by damage or defect growth travel to the transducers/sensors attached on the material. The sensors then convert these waves into electrical signals which the Acoustic Emission instrumentation can record, store and process. From this, the operator could monitor and evaluate the behavior and state of the structure/material under stress. A SPARTAN AT (1992 model) computer controlled acoustic emission system and a DiSP (2002 model) Acoustic Emission Workstation are used for acoustic emission data acquisition. Figure 4.1 shows a schematic setup of the Acoustic Emission Technique.

Acoustic Emission (AE) testing for nondestructive evaluation (NDE) purpose is different from the other traditional NDT techniques, such as Radiography, Ultrasonics, Eddy Current, etc., which detect geometric discontinuities by beaming some form of

energy into the structure under test. AE Testing detects microscopic movements while the material or structure is under loading; for example, crack growth, fracture of inclusions and leakage are among the hundreds of processes that produce their own detectable emissions and can be effectively monitored by this technique. This technique is one of the few NDE methods that allow continuous on-line monitoring.

Acoustic Emission sources in composite materials are multiple and could be matrix cracking, fiber/matrix interfacial debonding, longitudinal splitting, interlaminar failure or delamination and fiber fracture. The AE from each type of source mechanism shows different values of AE parameters and also different waveform information. The most commonly used Acoustic Emission parameters to describe the intensity and characters of emission signals include hits, counts, energy, rise-time, duration and amplitude.

Counts, sometimes called threshold crossing or ringdown counts, represent the number of times the AE signal crosses a given threshold (Figure 4.2). Cumulative counts represent the summation of counts up to certain loading level and are used to compare the total AE activities and damage accumulation rate of different joint configurations and laminates under loading.

Duration is the time from the first to the last threshold crossing within a hit. Amplitude is defined as the peak voltage attained by the AE signal waveform. Usually, a high correlation exists between counts and duration, i.e., higher counts the higher duration. However, from these parameters, it is very hard to distinguish those AE signals from different damage sources or damage mechanisms. More advanced AE analysis technique is recommended. With the modern development in computer technology and data processing, newly produced Acoustic Emission equipment possesses more powerful

functions compared to the older models, such as pattern recognition function. By unsupervised or supervised clustering method, AE data can be clustered into several meaningful groups and possible correlations could be built up between the clustered AE data and those related source mechanisms. Besides, waveform-based AE analysis can be carried out based on the recorded waveform information during testing and a deeper insight into the AE activities and their properties could be achieved.

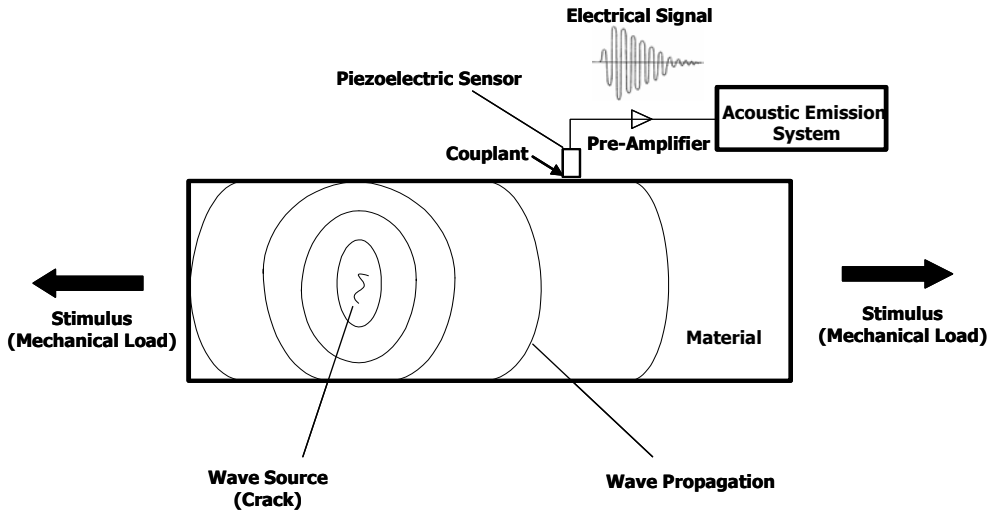

Figure 4.1 A schematic diagram for the setup of the Acoustic Emission Technique.

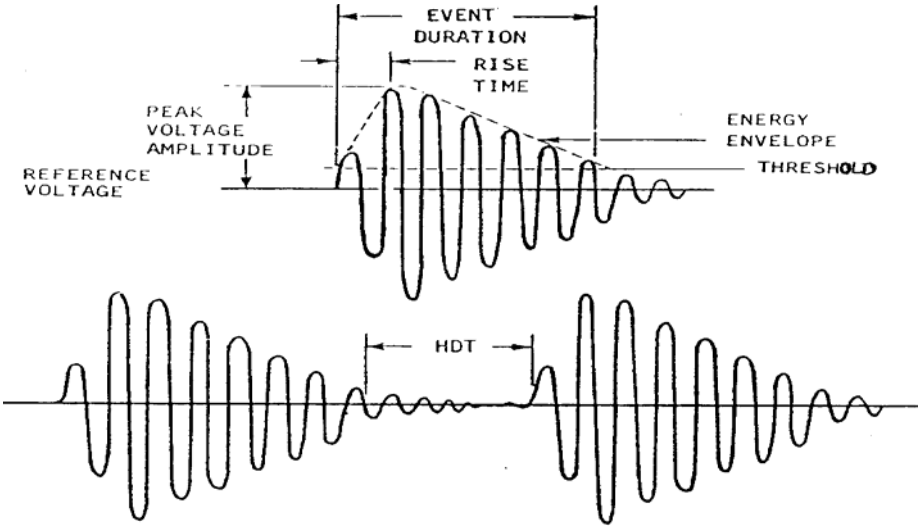

Figure 4.2 Acoustic Emission parameters and waveform of a hit.
(From SPARTAN AT USER'S MANUAL, 1992)

CHAPTER 5

JOINT MANUFACTURING AND EXPERIMENTAL SETUP

Single lap and single nested overlap joints are manufactured from composite prepreg IM7/8551-7 using an autoclave co-curing method. The cure cycles of the material system from the manufacturer presented in the previous chapter are adopted for fabricating all the specimens for this study.

5.1 Joint Geometry

The same specimen geometry is used as that in Coates' work (2001) (Figure 5.1). The composite joint specimens are cut from manufactured joint panels, allowing a more consistent quality and eliminating manufacturing edge effects by discarding those edge specimens. In order to remove the effect of eccentricity of applied load with respect to the joint center axis along the loading direction, fiberglass tabs with two different thicknesses are bonded to the ends of joint specimens using super glue cured at room temperature.

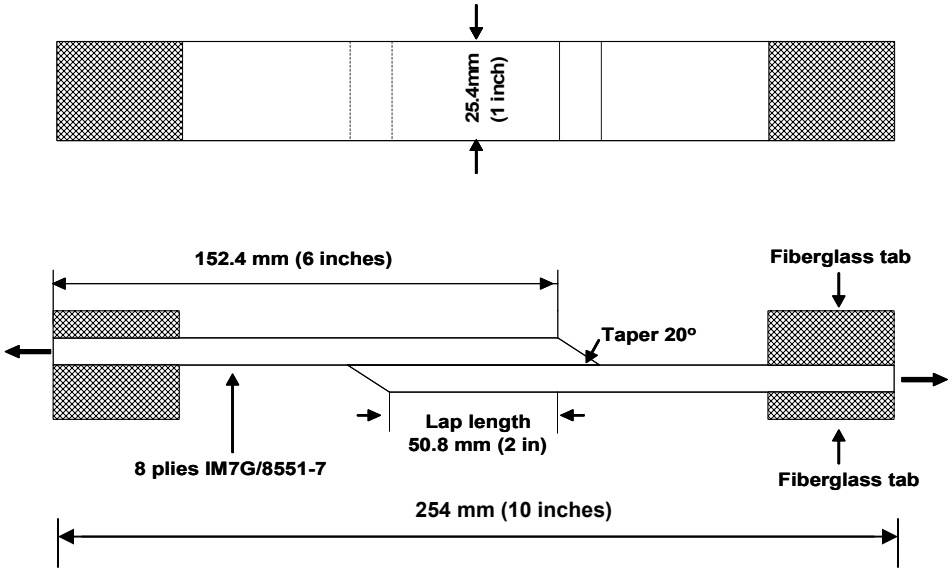

Figure 5.1 Geometry of co-cured composite joints.

5.2 Manufacturing

Joint panels are manufactured by combining two adherend panels laid in advance. Two lay-ups, a unidirectional lay-up $[0]_8$ and a quasi-isotropic lay-up $[0/\pm45/90]_s$, are used for adherends of each type of joint. For single lap joints, two adherend parts are simply laid over each other with an overlap length of 50.8mm (2 inches) within the joint region. All joints are manufactured with a 20^o taper at one end of an adherend in order to reduce the stress concentration. The taper is built by staggering the plies in the ply termination region. The carefully prepared prepreg joint is then placed into an aluminum mold (330mm x 432mm) with two thin shims as ancillary tooling. The mold is vacuum bagged before being placed in the autoclave for curing.

For manufacturing single nested overlap joints, the only difference lies in the fact that the bottom ply of top laminate must be placed in between the top ply of bottom laminate and its adjacent ply, instead of directly overlapping the two adherends.

Two co-cured composite joint panels taken from the autoclave after curing are shown in Figure 5.2. Each panel is then cut into coupons or specimens with the dimensions mentioned above (25.4mm x 254mm or 1”x10”).

For reference purpose, corresponding straight laminates for respective unidirectional and quasi-isotropic lay-up, are also manufactured and prepared for similar testing. These joint and laminate specimens are given a code for easy labeling and documentation according to the scheme demonstrated in Table 5.1. Five sets of specimens prepared with fiberglass tabs are shown in Figure 5.3.

Table 5.1 Designation of specimens manufactured

Design Configuration	Unidirectional	Quasi-isotropic
Straight Laminate	SU	SQ
Single Lap Joint	LU	LQ
Single Nested Overlap	NU	NQ

Figure 5.2 Two fabricated joint panels with some joint specimens.

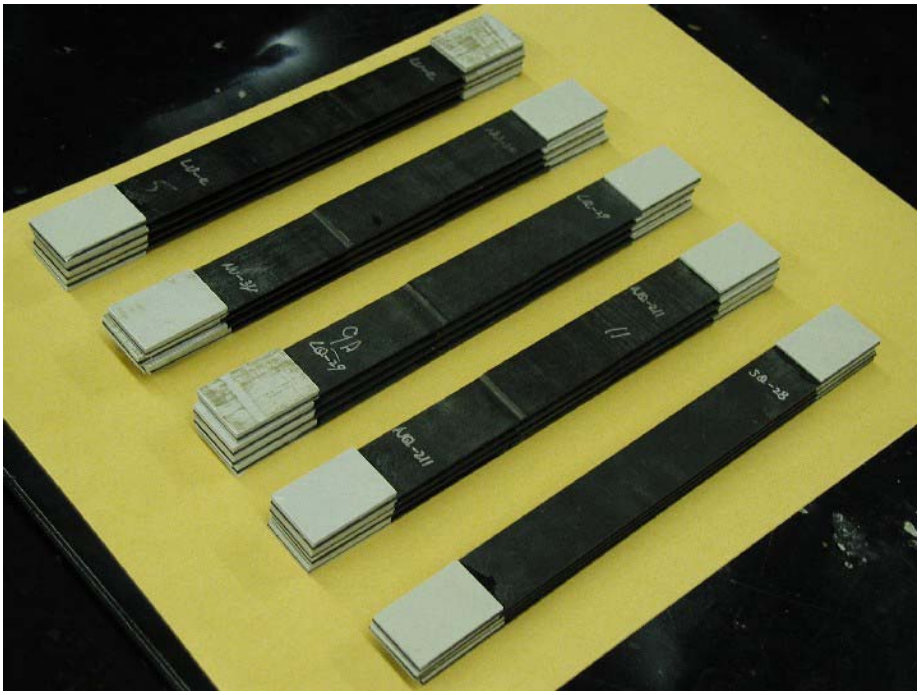

Figure 5.3 Composite specimens prepared with fiberglass tabs.

5.3 Experimental Setup

An MTS testing machine with a 50 kN load-cell capacity is employed to do all mechanical testing, and load-control mode is adopted. The quasi-static loading rate selected is 50 N/second. The joint tensile failure loads and the loading history with respect to time are recorded by the MTS system. Load information is automatically provided by the MTS testing system as a parametric input electrical signal of voltage between 0-10V via a coaxial cable connection for the acoustic emission system. Acoustic emission data is acquired during loading by the acoustic emission system. Two models of acoustic emission systems from Physical Acoustics Corporation (PAC) are used, SPARTAN AT system of 1992 model is used for the work covered in Chapter 6; a new DiSP Acoustic Emission Workstation of 2002 model is for the remaining work covered in Chapter 7. The new device could record the waveform information besides the AE parameter data and will be used for pattern recognition or AE clustering. The test setup is shown in Figure 5.4.

A resonant transducer (Model S-140B, Dunegan Research Corporation) connected to the acoustic emission system is placed against the joint specimen just outside the joint region using a couplant and held in place by using adhesive tape (Figure 5.5). The couplant used here is a white lithium grease which aids the acoustic signal transmission between the surfaces of specimen and transducer. The preamplifier (1220A Acoustic Emission Preamplifier, Physical Acoustic Corporation) is set by selecting input in a single ended mode with 40 dB gains. A threshold of 45 dB is chosen for both SPARTAN AT and DiSP systems. Figure 5.6 shows the acoustic emission signals of a specimen acquired and displayed by SPARTAN AT system.

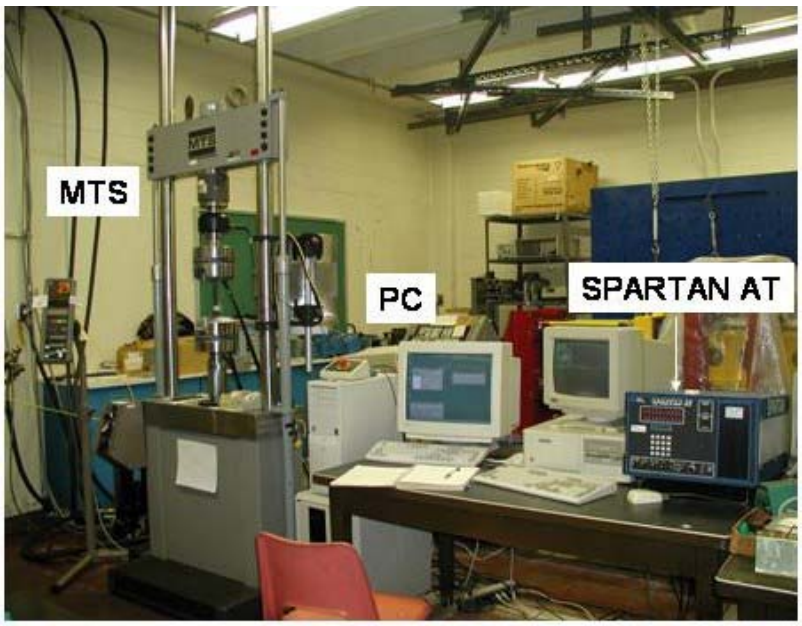

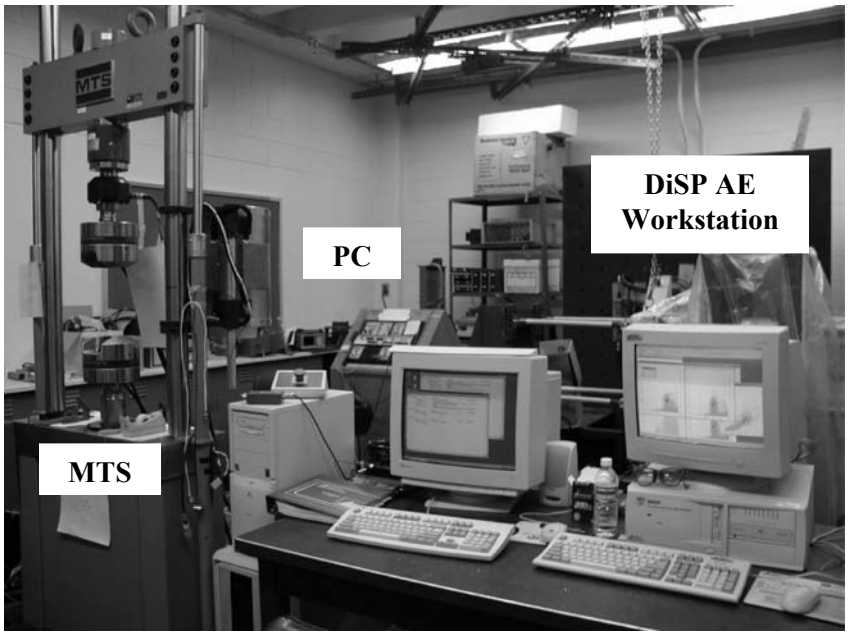

Figure 5.4 Test setup with MTS and Acoustic Emission systems.
(top: SPARTAN AT system; bottom: DiSP AE Workstation)

Figure 5.5 An Acoustic Emission transducer mounted on a specimen during test.

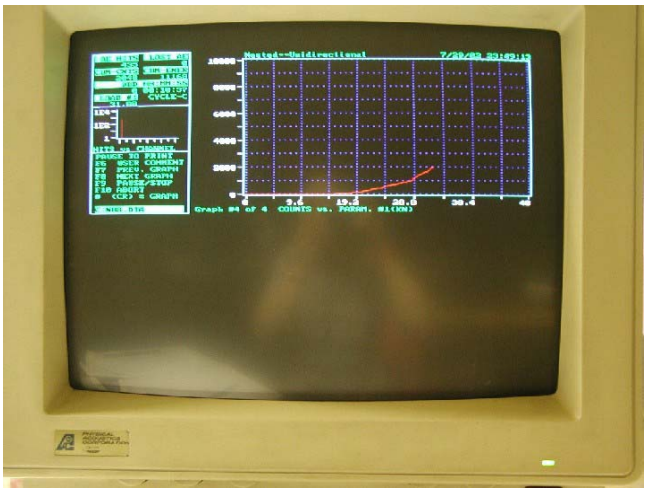

Figure 5.6 Real-time monitoring of acoustic emission using SPARTAN AT system.

CHAPTER 6

DAMAGE AND FAILURE MECHANISMS UNDER QUASI-STATIC, TENSILE LOADING

An investigation of failure mechanisms of straight laminates with zero-degree unidirectional and quasi-isotropic lay-ups, and of their corresponding single lap and single nested overlap co-cured composite joints is presented and the physical characterization of damage and failure mechanisms is the main focus in this chapter. Using the labeling codes introduced in the previous chapter (Table 5.1), those six specimen configurations to be studied can be described as SU, LU, NU; SQ, LQ and NQ. They are also categorized into "U" group and "Q" group respectively.

First, six sets of specimens will be monotonically loaded until failure following the experimental setup in Chapter 5. At least four specimens for each configuration will be tested while the Acoustic Emission technique is used to record the corresponding acoustic emission data. These data are processed and compared within the same group and the overall picture of the AE activities and AE data distribution trends could be obtained.

Second, post-failure fracture surface morphology is analyzed by visual and microscopic methods to gain further insight into the progression of damage and the failure modes.

Finally, Penetrant Enhanced X-ray Radiography and Optical Microscopy are used to characterize the progression of damage and failure at predetermined load intervals during quasi-static loading. The endeavor to correlate this with the recorded acoustic emission data is pursued.

6.1 Monotonic Loading - Acoustic Emission Data

Sets of four/five specimens have been tested for each of the six configurations (SU, LU, NU; SQ, LQ and NQ). Each specimen was loaded monotonically at a loading rate of 50 N/second using a MTS machine with a 50 kN-capacity load cell and its acoustic emissions were monitored and recorded by using SPARTAN AT acoustic emission system (1992 model). Then, every recorded data file (PAC .dta file) was transformed into ASCII format which could be processed in Microsoft Excel. Only one AE parameter COUNTS is selected to correlate to load or stress and to gain an overall impression on the acoustic emission activities and AE data distribution trends. This chapter will mainly focus on the physical characterization of damage and failure mechanisms within co-cured composite joints or straight laminates. The more detailed AE data analysis with more parameters will be covered in Chapter 7.

The failure loads of each specimen are shown in Table 6.1. The small variations of thickness and width from specimen to specimen due to manufacturing and machining cause variations in stress levels for a given specimen load level. The failure stresses, calculated as the failure load of the joint divided by the average cross-sectional area of the adherend part (8 plies), are listed for each specimen in Table 6.2. The acoustic emission data plots of counts vs. load are shown in Figs. 6.1-6.6. The corresponding

combined plots of cumulative counts vs. load are shown in Figs. 6.7-6.8 for unidirectional and quasi-isotropic lay-up, respectively. For comparison, the plots of cumulative counts vs. average stress are also illustrated in Figs. 6.9-6.10.

Table 6.1 Failure loads (kN)

Specimen No#	SU	LU	NU	SQ	LQ	NQ
1	45.02+	28.15	40.9	24.82	18.15	24.05
2	45.04+	30.09	38.85	22.95	20.15	23.3
3	45.06+	29.85	36.3	22.85	17.05	22.38
4	45.05+	30.21	38.7	23.05	19.3	23.15
5					19.2	22.69
Average	45.04+	29.58	38.69	23.42	18.77	23.11

(Note: For SU, the testing is stopped manually before failure due to the limited load-cell capacity of 50 kN.)

Table 6.2 Failure stresses (MPa)

Specimen No#	SU	LU	NU	SQ	LQ	NQ
1	1429+	883	1307	777	566	833
2	1491+	944	1241	761	613	725
3	1508+	941	1136	714	539	702
4	1508+	1064	1267	802	603	738
5					592	717
Average	1484+	958	1238	764	583	743

(Note: For SU, the testing is stopped manually before failure due to the limited load-cell capacity of 50 kN.)

From the data in the above tables, it is apparent that the nested overlap joint improved its joint strength over single lap joint for both U and Q lay-ups. The average joint strength increase for unidirectional lay-up NU over LU is 29.2% and for quasi-isotropic NQ over LQ is 27.4%. Also, it can be observed that the joint strength of NQ is almost the same as that of straight laminate, SQ, which suggests that this joint configuration acts like a perfect joint, for which failure takes place outside the joint region. This observation is supported by fracture surface analysis that shows the failure site is indeed located outside the joint region.

From Figs. 6.1-6.10, different joint design configurations do show different acoustic emission activities and distribution trends. For each set of specimens with the same joint configuration and lay-up a common trend for the acoustic emission signals emerges.

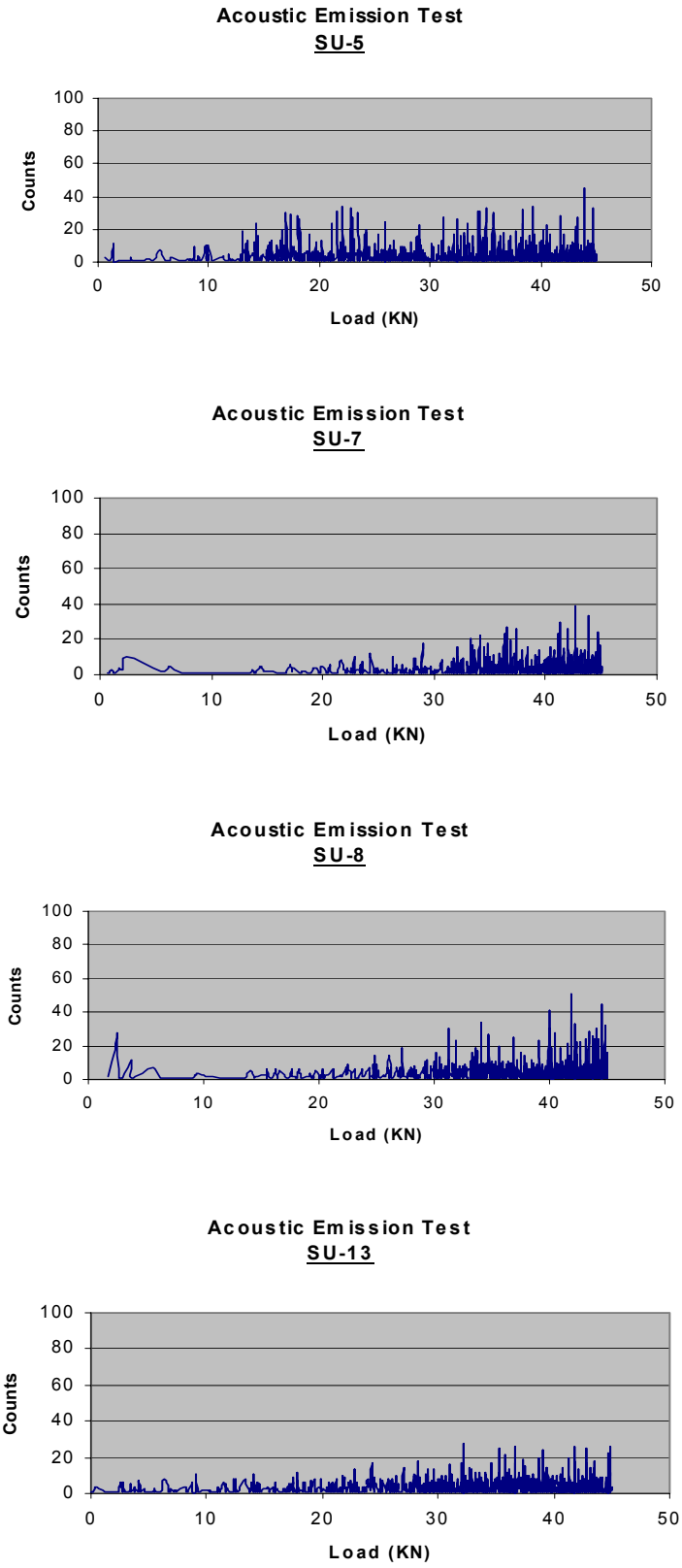

Figure 6.1 AE counts vs. load for SU specimens.

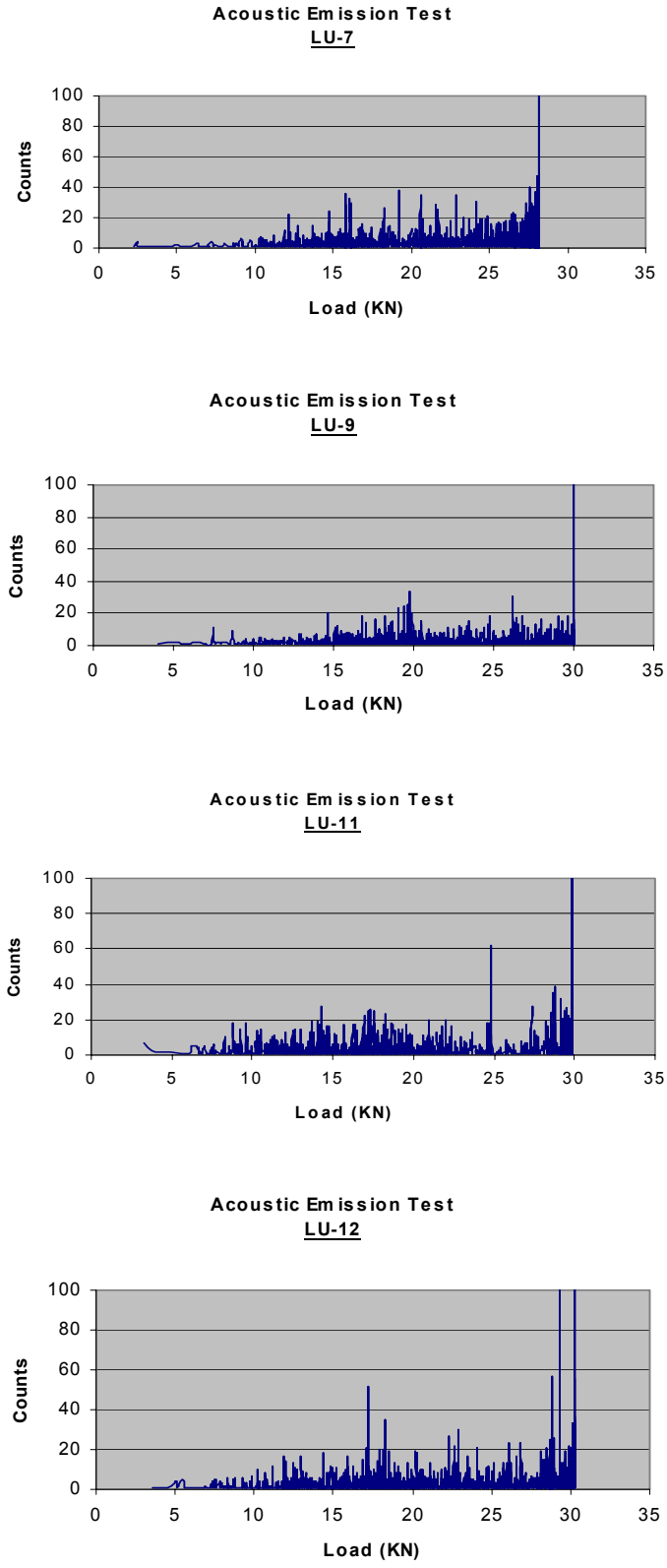

Figure 6.2 AE counts vs. load for LU joint specimens.

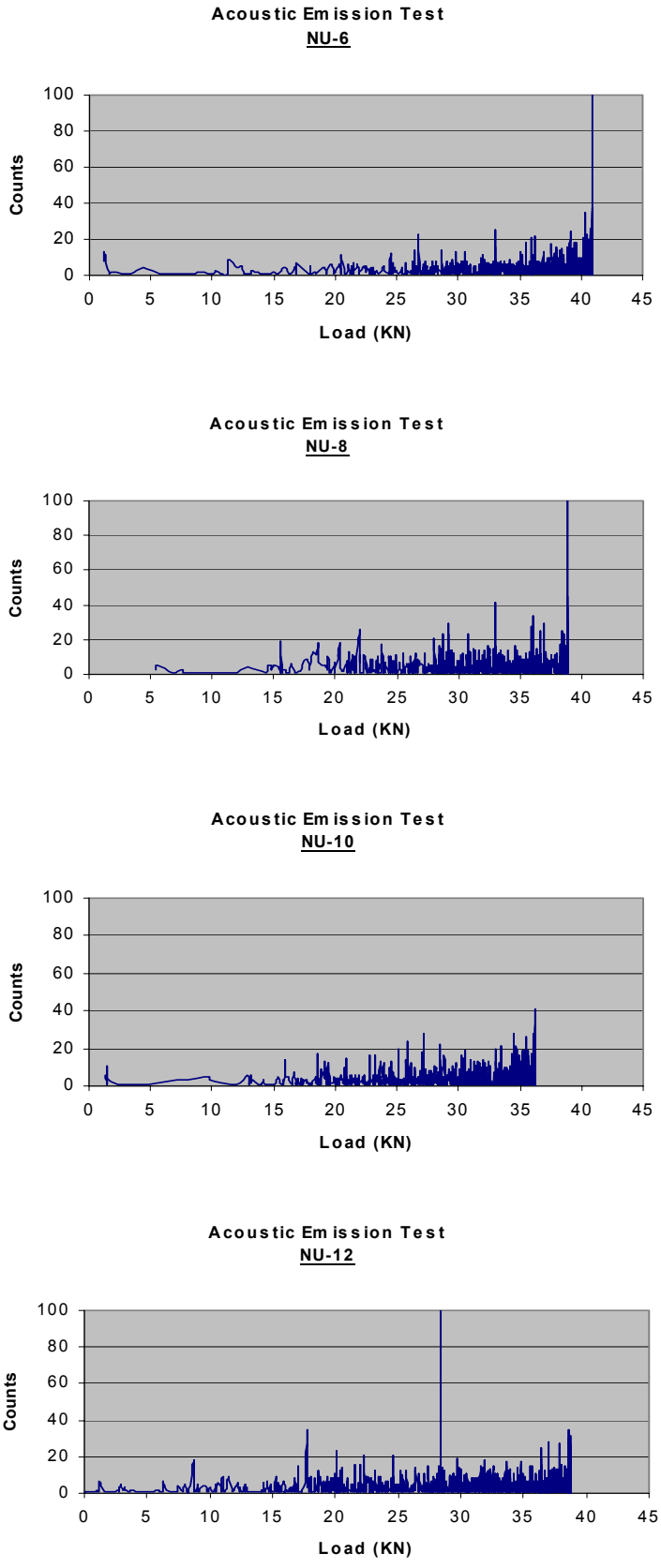

Figure 6.3 AE counts vs. load for NU joint specimens.

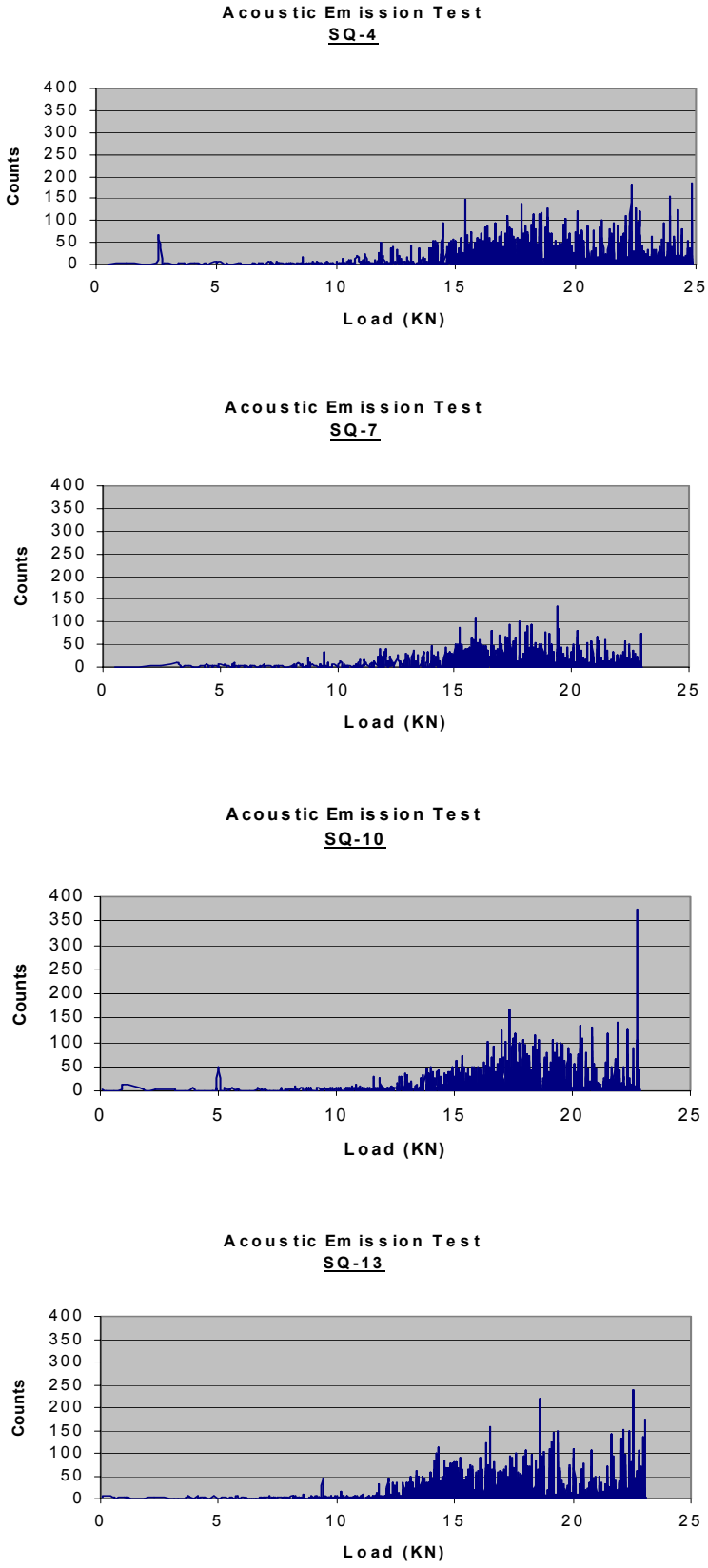

Figure 6.4 AE counts vs. load for SQ specimens.

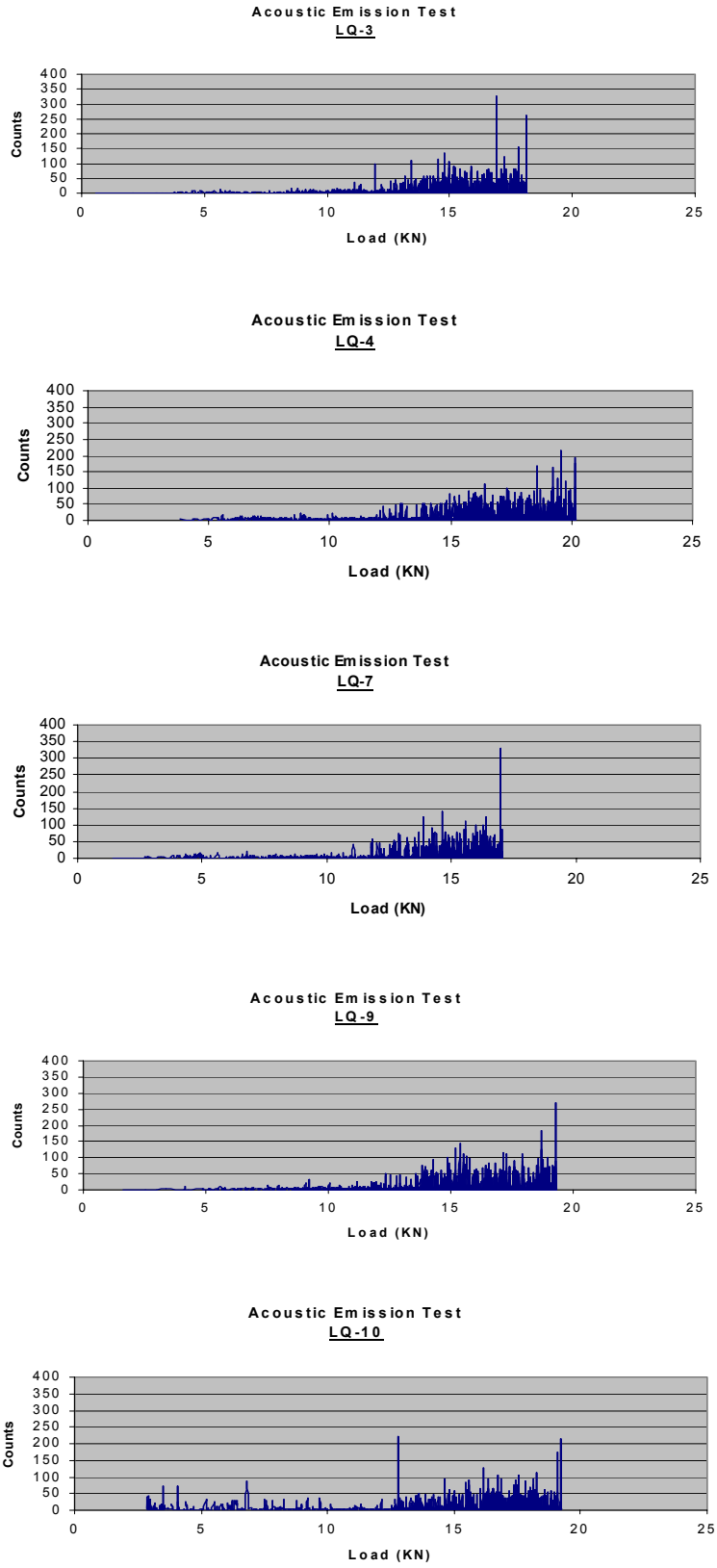

Figure 6.5 AE counts vs. load for LQ joint specimens.

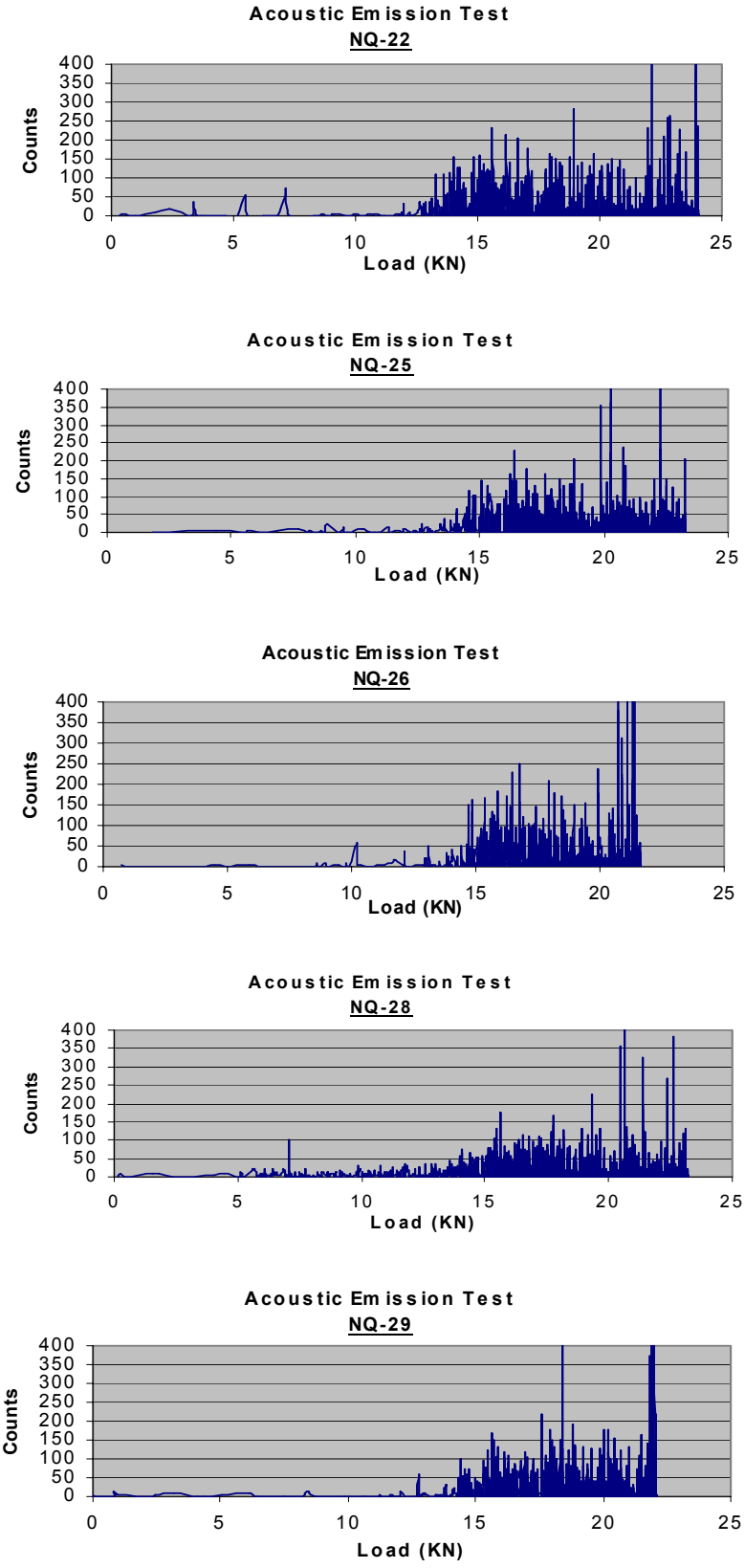

Figure 6.6 AE counts vs. load for NQ joint specimens.

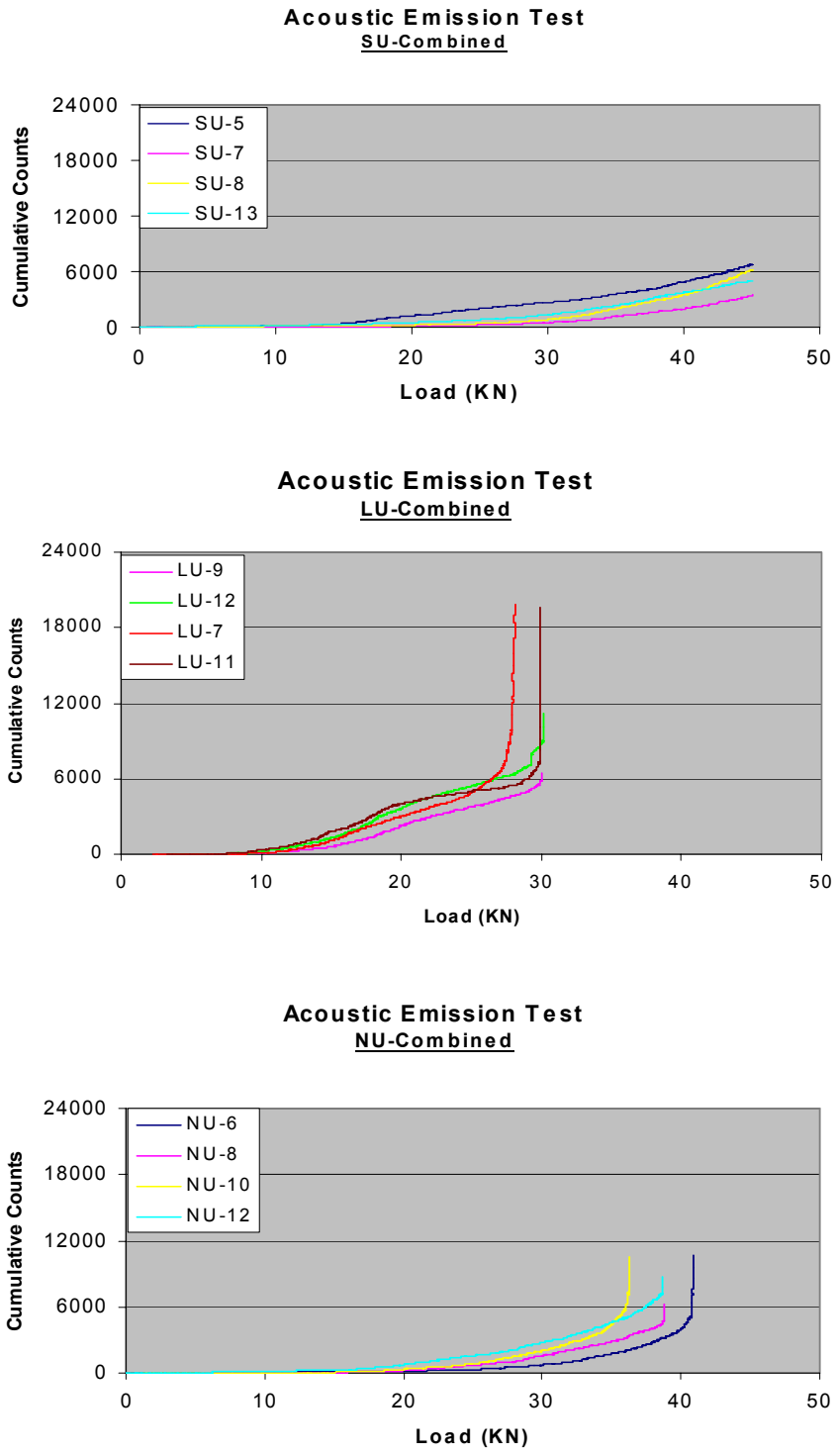

Figure 6.7 Comparison of cumulative counts vs. load for U specimens.

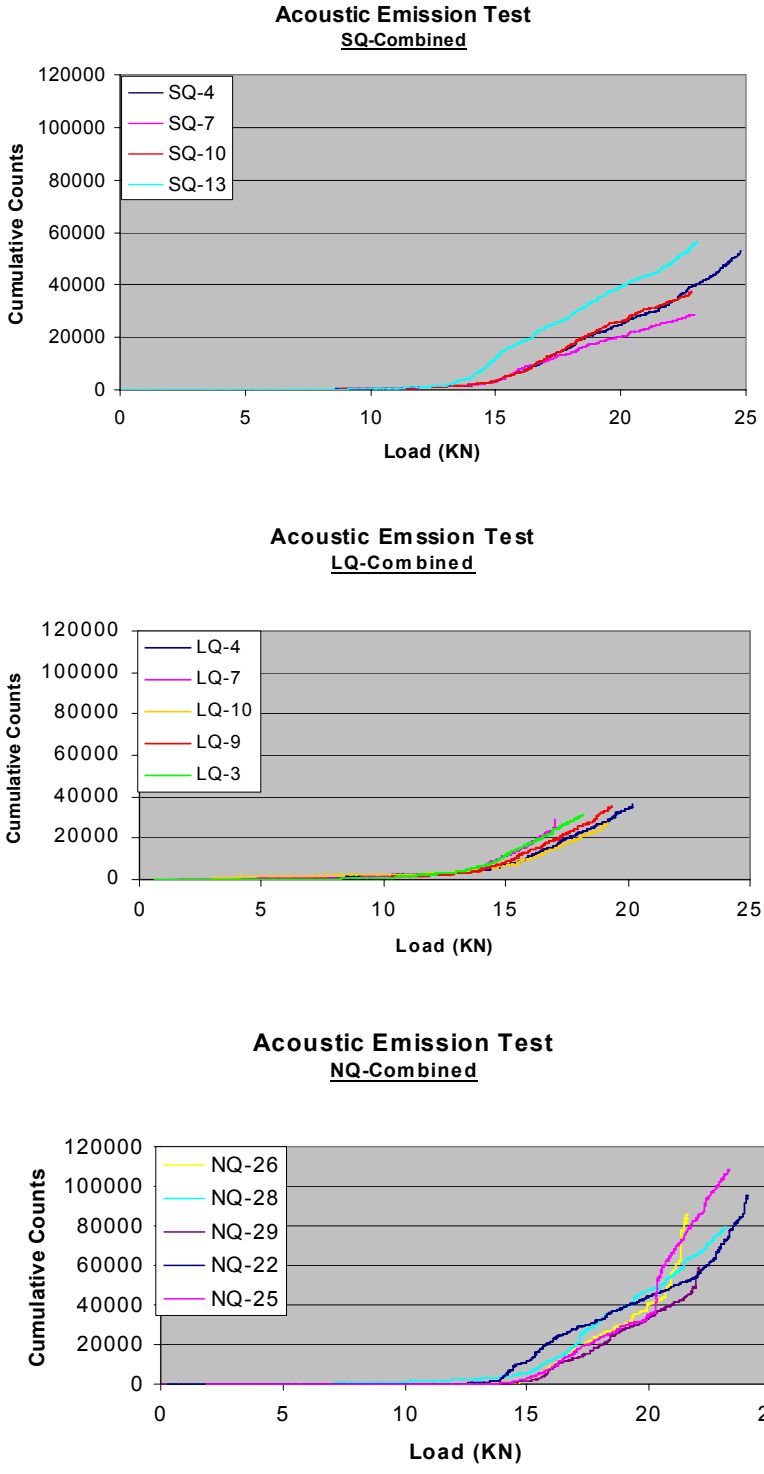

Figure 6.8 Comparison of cumulative counts vs. load for Q specimens.

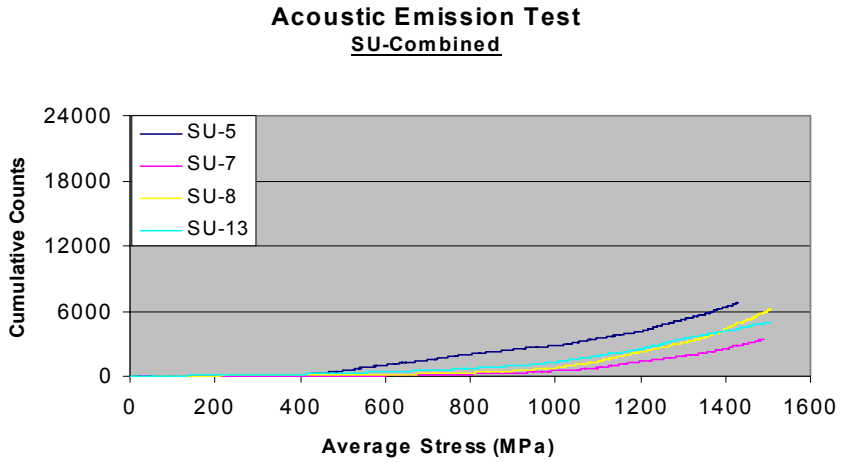

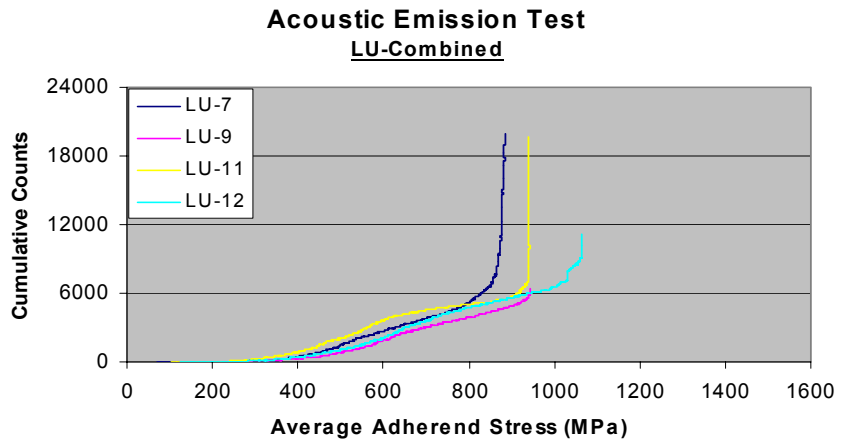

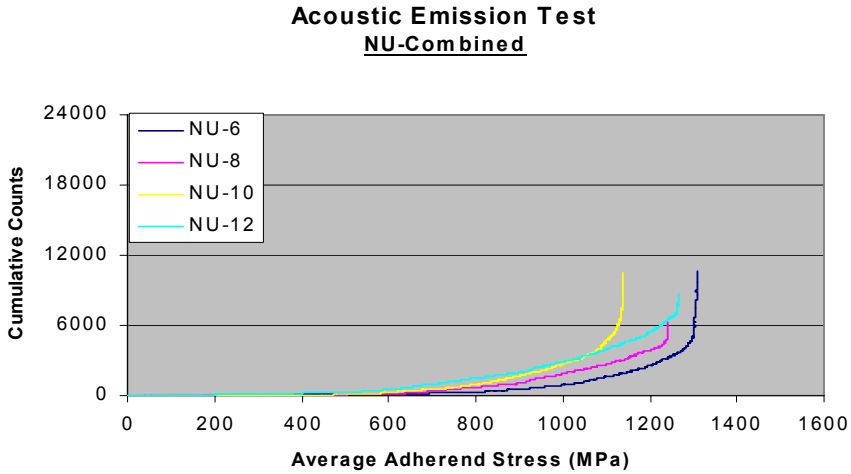

Figure 6.9 Comparison of cumulative counts vs. average stress for U specimens.

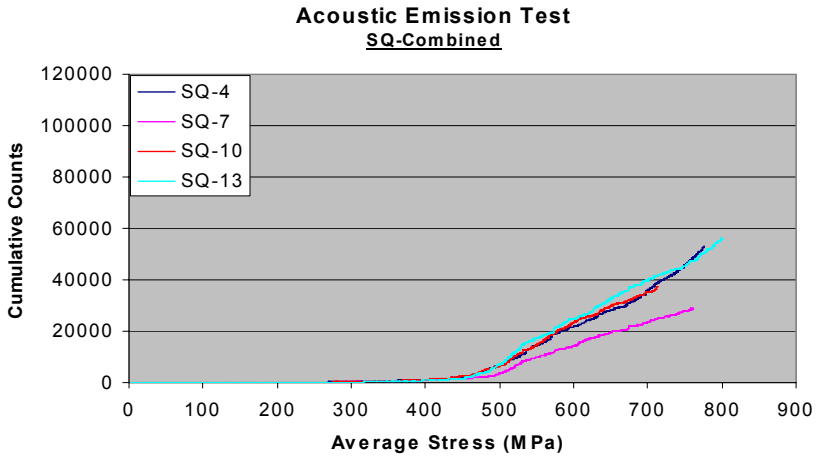

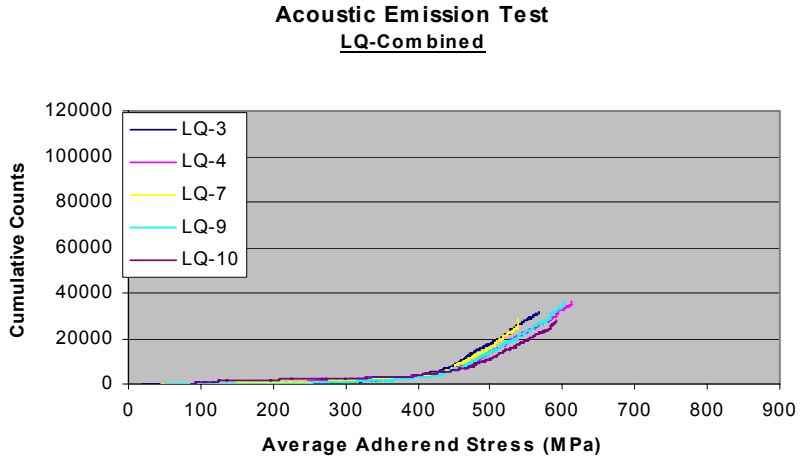

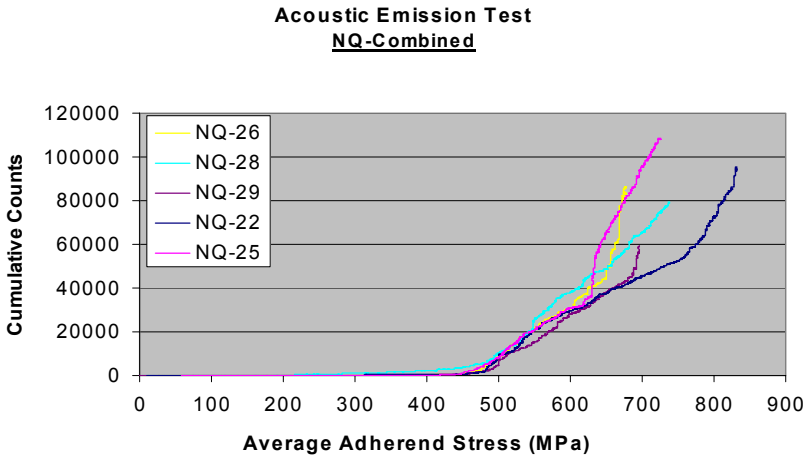

Figure 6.10 Comparison of cumulative counts vs. average stress for Q specimens.

The U laminate and joints are quieter from the point of absolute counts number and the AE counts are more uniformly distributed. The cumulative counts grow smoothly from the beginning to the end of loading, but the failure of U lay-up is more abrupt compared to that of Q lay-up (Figs. 6.1-6.3 and 6.4-6.6).

For Q laminates and joints, a knee in the cumulative counts vs. stress plots, which is assumed to relate to the onset of a distinct damage mechanism, is observed at a stress level between 420~480 MPa (between 13~15 kN). After this knee, the counts accumulation rate is higher, which suggests that damage develops and propagates more intensely (Figure 6.10).

6.2 Monotonic Loading - Visual Observations

Failed specimens are visually observed and the fracture surfaces and failure modes are recorded by using a digital camera (Figs. 6.11-6.16).

Figure 6.11 shows SU laminates after loaded up to 45 kN. Due to the high strength of these specimens and the limitation of the load-cell capacity of the MTS machine used, the test was interrupted manually before the specimens failed. These specimens maintain an intact appearance after testing.

Figure 6.12 shows clearly the fracture surfaces of failed LU joints. The surfaces have a very clean, smooth appearance. The two adherends separated from each other at the co-cured bond surfaces. This failure mode appears to be mostly due to shear failure since the eccentricity of loading was reduced by mounting glass-fiber tabs of different thickness at both joint ends. It is interestingly observed that the fracture surfaces show partial reflection areas within joint region on both joint parts, which might suggest the

joint failure started from the separation of the taper end and its propagation with a non-symmetric fashion; only part of the joint surface kept bonded while the remaining joint strength could not resist the asserted load level, then joint failure happened.

Figure 6.13 depicts the failure surfaces of NU joints, which show more than one failure mechanism at work. Besides the shearing separation between surfaces, longitudinal splitting, fiber or ply pull-out and fiber fracture are also observed within and outside joint region. By close observation with the naked eye, it is found that a lot of damage occurred due to the existence of two nested-overlap plies between two adherends. Nested-overlap ply portions from one adherend are fractured and left in the other adherend completely or partially; some portion of nested-overlap ply just pulled out from the nested-overlap region; some portion of the outer ply peeled off from the joint end. Overall, the existence of nested-overlap plies induced more damage mechanisms and hence the complex fracture surfaces which are at different thickness levels of the joint.

Figure 6.14 records the failed pattern of SQ laminates. The fractured pieces show a +45 or -45^{o} angle with respect to loading direction at the breaking ends which represent the typical failure mode of this type of laminate.

Figure 6.15 is the photograph for the failure surfaces of LQ joints. This case should be similar to that of LU. However, the manufacturing imperfections such as warped neighboring plies of the two adherends (see Figure 6.22 in the next section) resulted in some additional damage in two joint specimens (LQ-10 and LQ-14).

Figure 6.16 shows the failed appearance of NQ joints. It is very interesting to see that the fracture sites are all outside the joint region; all joints failed in three pieces as well. Examining the edge, the joint failure appears to have initiated from the adherend part.

For some of the joints tested, however, a delamination did propagate into the joint area while the final failure site is just outside the joint region or at the taper end, which means that the joint overlap part did not fail first. This configuration represents an example of a good joint design.

Figure 6.11 SU laminates after loaded up to 45 kN.

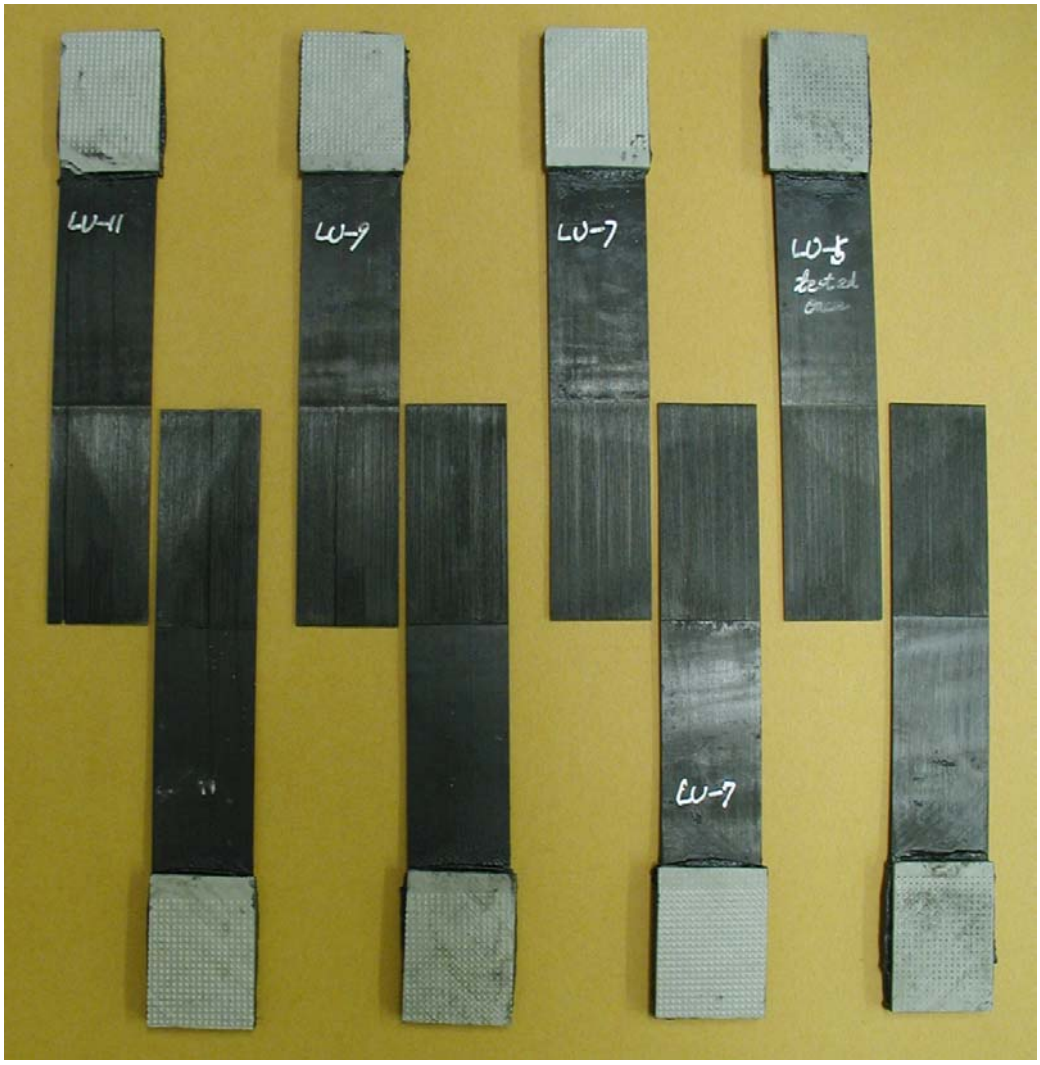

Figure 6.12 Failed LU joint specimens.

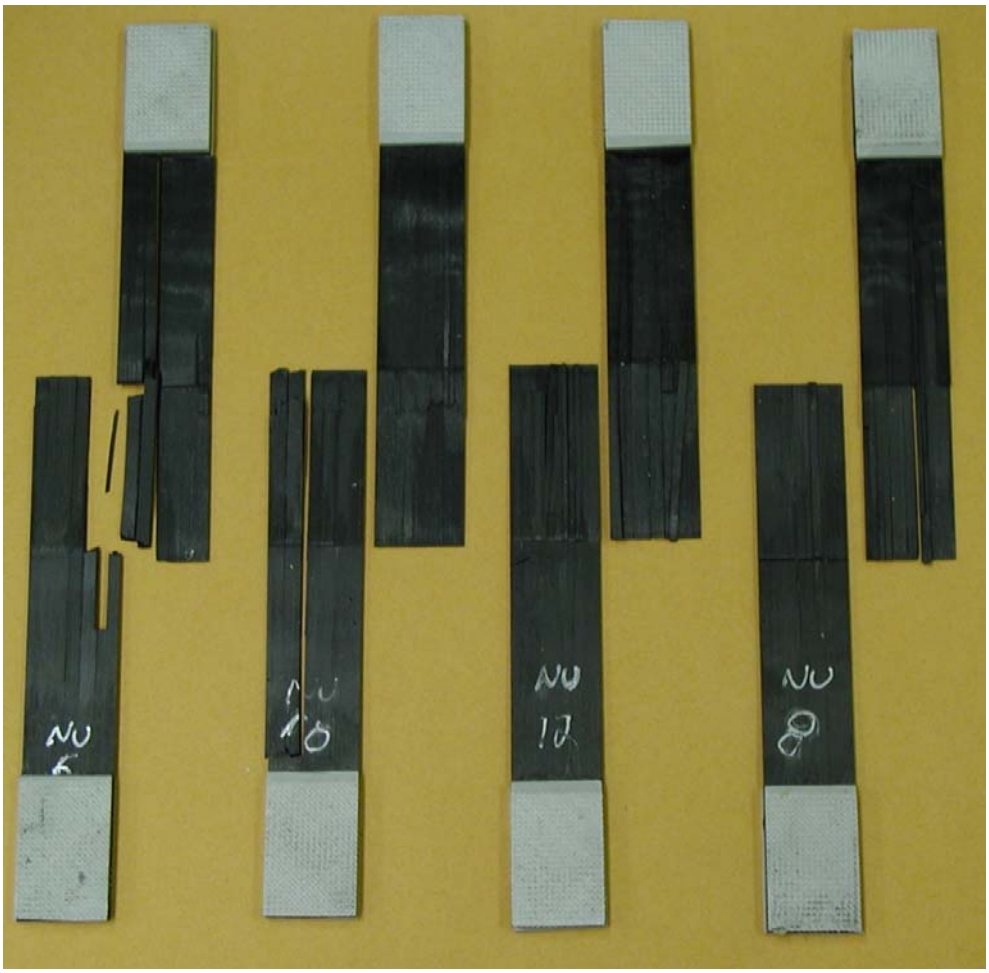

Figure 6.13 Failed NU joint specimens.

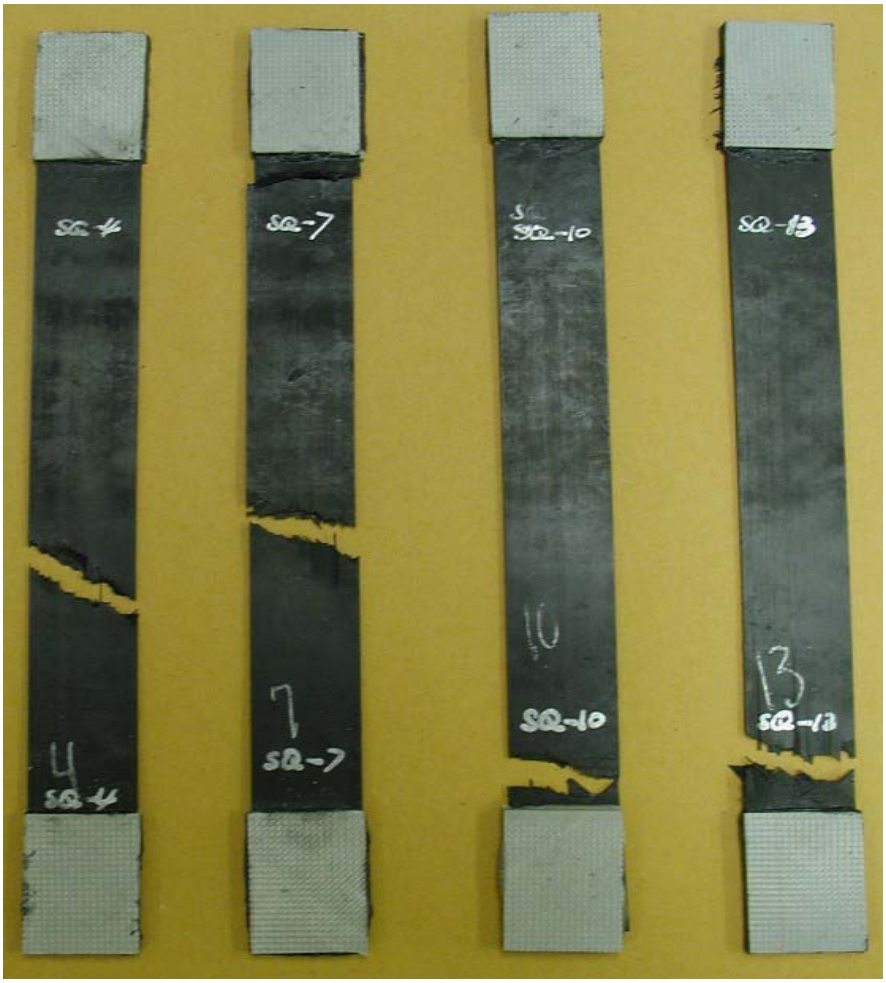

Figure 6.14 Failed SQ specimens.

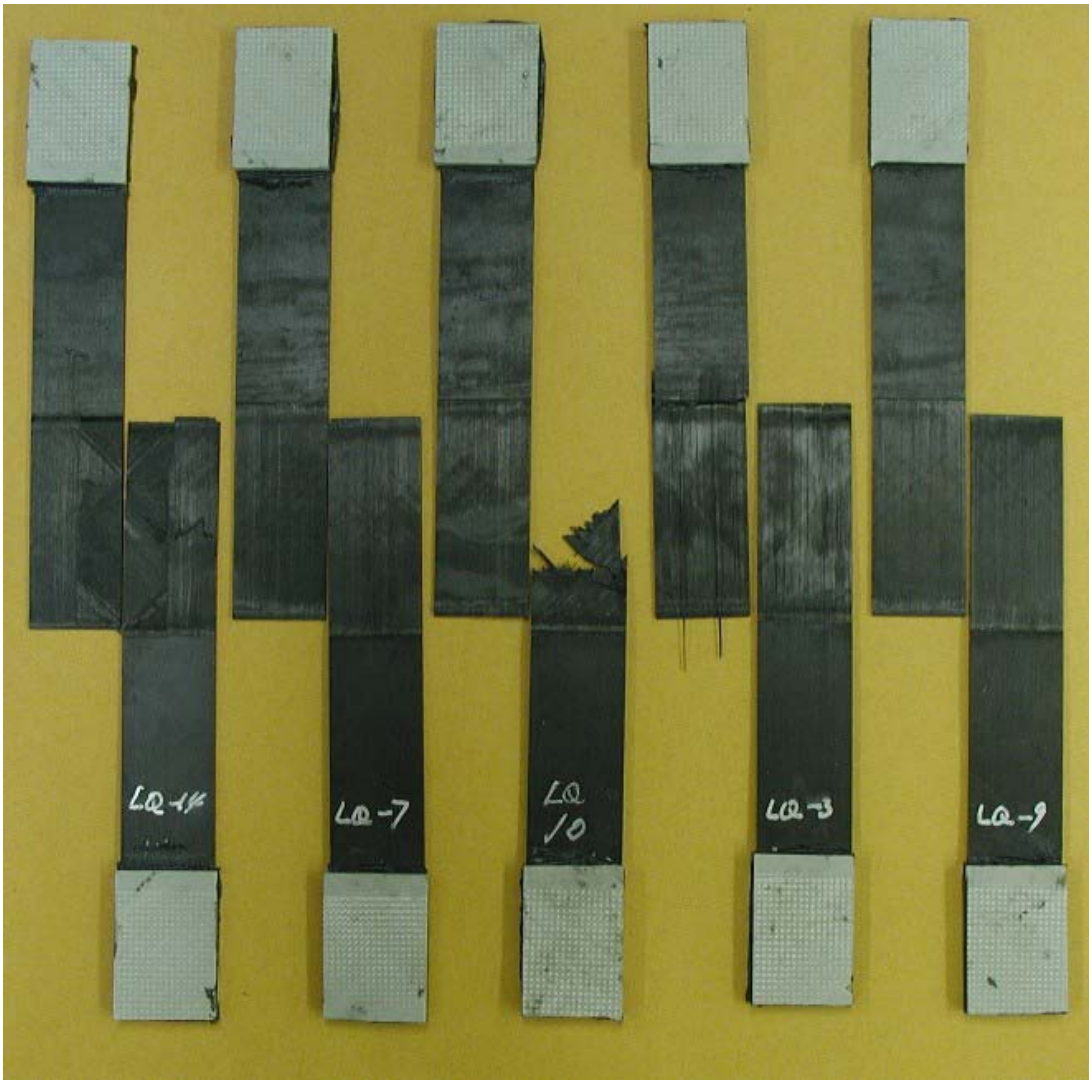

Figure 6.15 Failed LQ joint specimens.

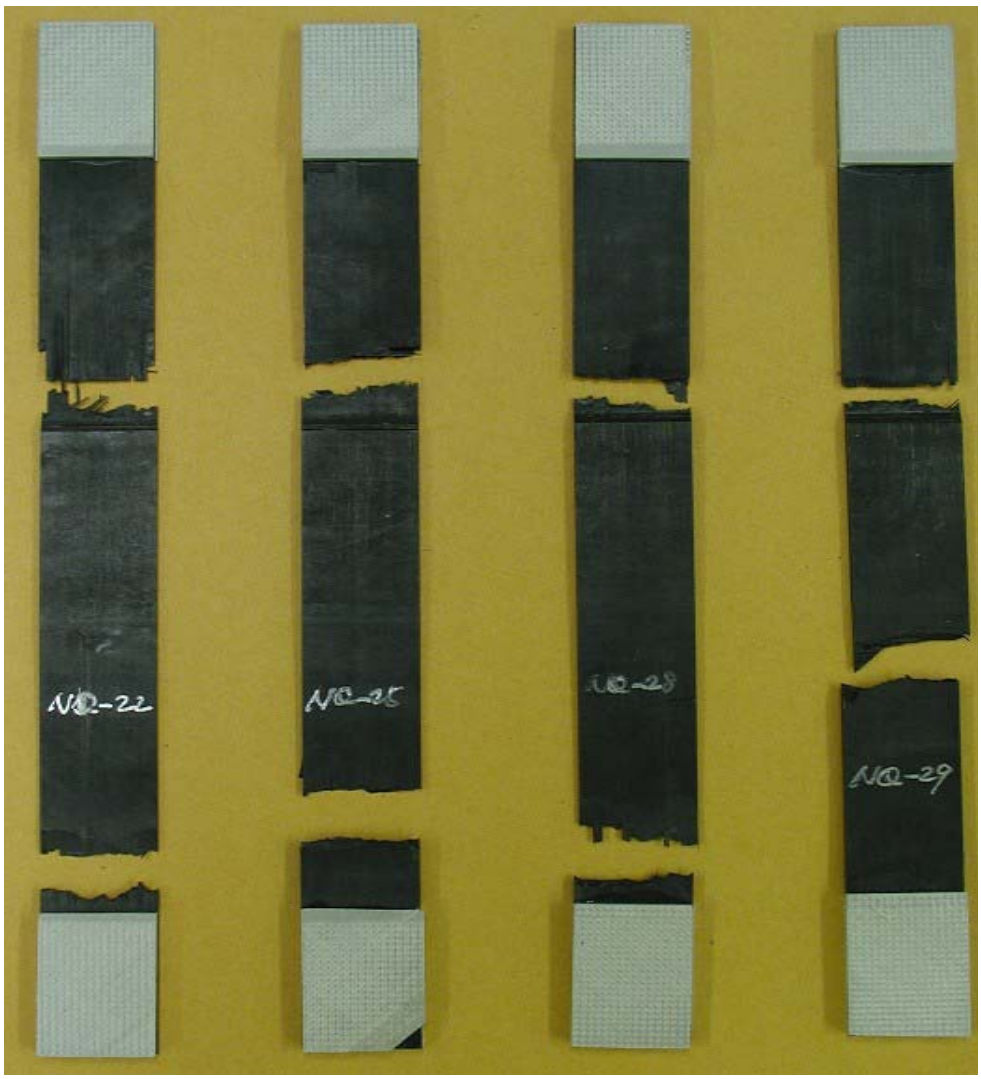

Figure 6.16 Failed NQ joint specimens.

6.3 Quasi-Static Loading - Optical Microscopic Observations

Representative specimen edges have been examined before quasi-static loading using an optical microscope. The edge characteristics of different lay-ups and different joint configurations have been documented for SU, LU, NU; SQ, LQ and NQ specimens respectively (Figures 6.17-6.22).

It is very clear from Figure 6.17 that resin rich areas (dark-looking strips, pointed by arrows) exist between layers. Similarly, the quasi-isotropic laminate with two 0 degree plies as outer surface layers also shows some resin rich areas within the specimen (Figure 6.18).

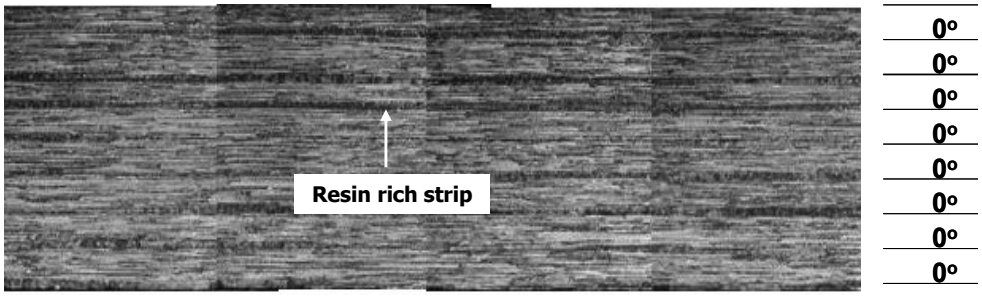

Figure 6.17 Edge view of SU specimen before loading.

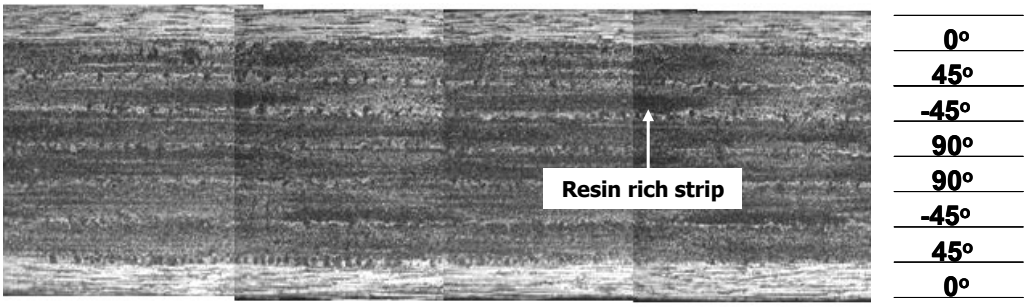

Figure 6.18 Edge view of SQ specimen before loading.

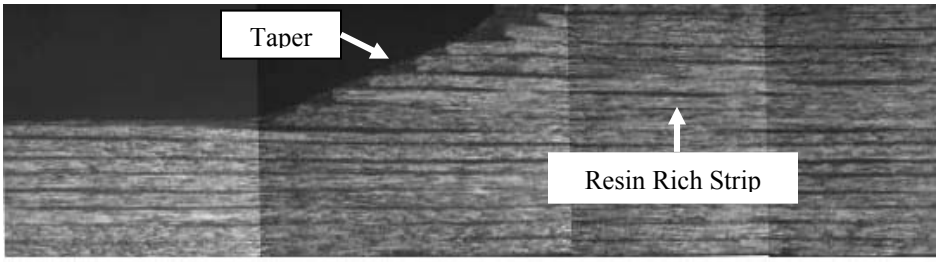

Figure 6.19 Edge view of LU joint specimen joint region before loading.

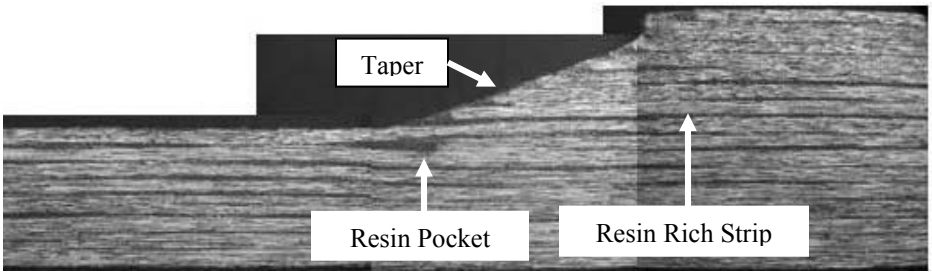

Figure 6.20 Edge view of NU joint specimen joint region before loading.

For joints of U lay-up, there are resin rich strips between plies (Figures 19 and 20). Resin rich spots also exist at the taper where plies terminate. Besides these, for nested-overlap joints, there is a resin pocket where two neighboring plies from each adherend nested and overlapped together.

For joints of Q lay-up, the characteristics of two 0^o neighboring plies are shown in Figures 6.21 and 6.22. For a nested overlap joint, compared to a single lap joint, the top ply of the bottom adherend passes over the bottom ply of the top adherend and forms the

nested-overlap between two adherends rather than staying with its neighboring plies within that adherend.

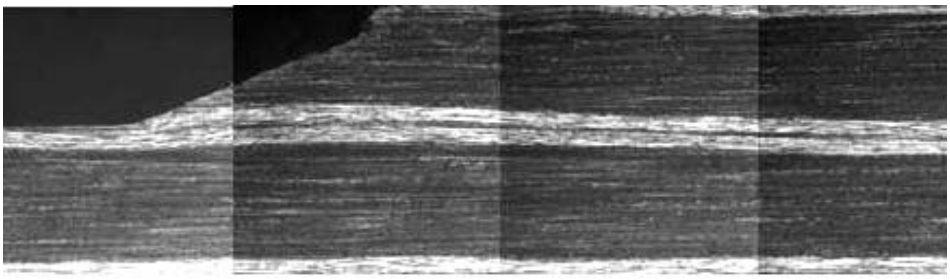

Figure 6.21 Edge view of LQ joint specimen joint region before loading.

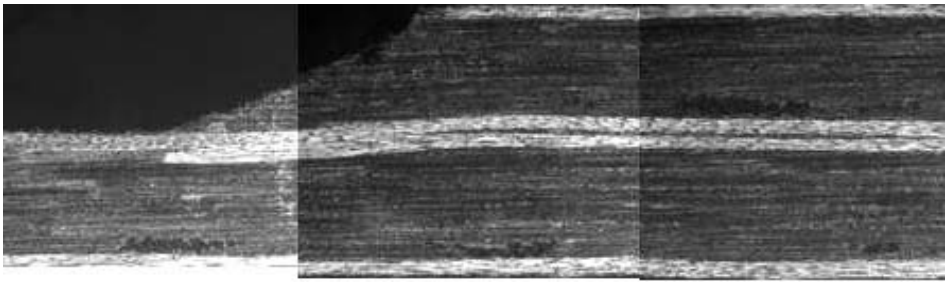

Figure 6.22 Edge view of NQ joint specimen joint region before loading.

6.3.1 Quasi-Isotropic Lay-up

Quasi-isotropic laminate and joint specimens SQ, LQ and NQ are investigated together as a group due to the fact that they share the same stacking sequence. The selected specimen edges to be observed under an optical microscope are polished by different grades of Silicon Carbide Papers (FEPA P #800~4000). For these specimens, loading is interrupted manually at certain predetermined load levels; after unloading specimen is removed from the testing machine and observed through optical microscopy to characterize damage initiation and progression during quasi-static loading from the selected portion of their edges near the joint region.

The interruption load levels are determined by referencing the plots of acoustic emission cumulative counts versus load from the monotonic loading condition. A load level between 13 and 15 kN seems a critical point for the introduction of a new damage mechanism for SQ, LQ and NQ as a transition point or knee is observed on all the plots of cumulative counts vs. load. Loads below 13 kN are also chosen to visualize what happens before that critical point. The selected interval loads include 0 kN, 5 kN, 10 kN, 13 kN, 15 kN, 18 kN, 21 kN and 23 kN or when they could be applied to the studied specimens before failure. The original edge views before loading are documented as reference for other load stages. After being loaded to a specific value mentioned above, the specimen with polished edges was observed under the microscope within the selected region. Microscopic photographs are taken with a digital camera that is connected to the microscope's observation tube. Due to the larger thickness of the joint specimens within the overlap region compared to that of adherend, the mostly used magnification factor is 5X in order to cover the whole thickness of joint for each photo. For monitoring some

cracks' initiation and propagation, a higher magnification is also used to observe these local damage spots (Cao and Dancila, 2003 (b)).

1. SQ Laminate

A 19mm-long edge section of a straight laminate specimen is monitored during this procedure. Matrix cracks are not discovered within the 90^o plies below a load level of 10 kN and this load could be regarded as the manifest of damage initiation in the form of micro matrix cracking. Macro matrix cracking as the new damage mechanism appears at around 13 kN and its progression is proved by the fact that the crack density increases with the load level (Figure 6.23). The crack density (total crack numbers counted divided by 19mm) is calculated for this selected portion of edge (Table 6.3). By referencing the combined plots of cumulative counts vs. load in Figure 6.8, a knee around 14 kN is located. Another damage mechanism called delamination which is initiated from those matrix crack tips show up from about 15 kN (Figure 6.24). Extensive edge delamination thereafter is observed including delaminations between plies of 90^o, 90^o and -45^o, -45^o and $+45^o$ as well as between $+45^o$ and 0^o. This SQ laminate survives the load of 23 kN.

Table 6.3 Matrix crack density evolutions for Q specimens

Load (KN)	SQ (1/mm)	LQ (1/mm)	NQ (1/mm)
Before 10 kN	0	0	0
13	0.49	0	0
15	0.68	0.61	0.65
18	0.84	0.72 (failed)	0.82
21	1.00	-----	0.82

Load = 5 kN

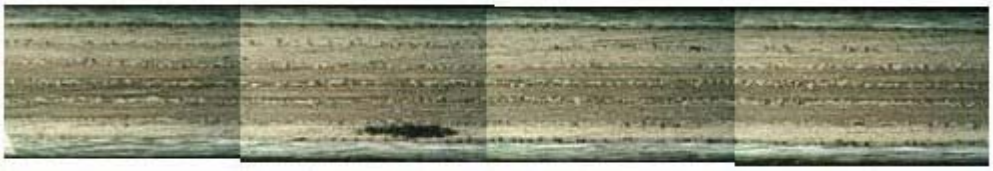

Load = 10 kN

Load = 13 kN

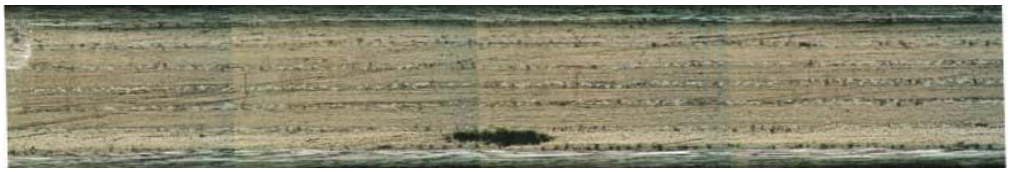

Load = 15 kN

Load = 18 kN

Load = 21 kN

Load = 23 kN (survived)

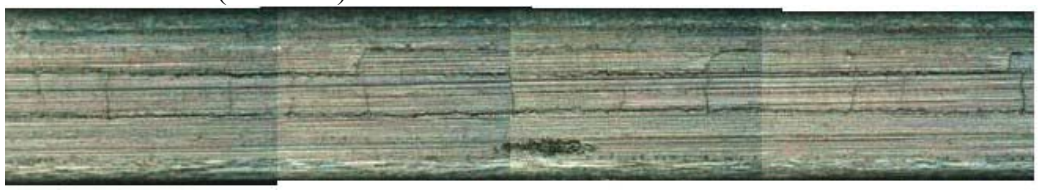

Figure 6.23 Increase of matrix crack density in a SQ specimen.

Load = 10 kN

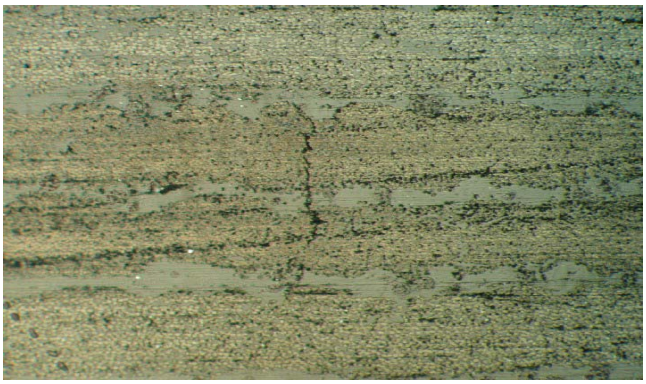

Load = 13 kN

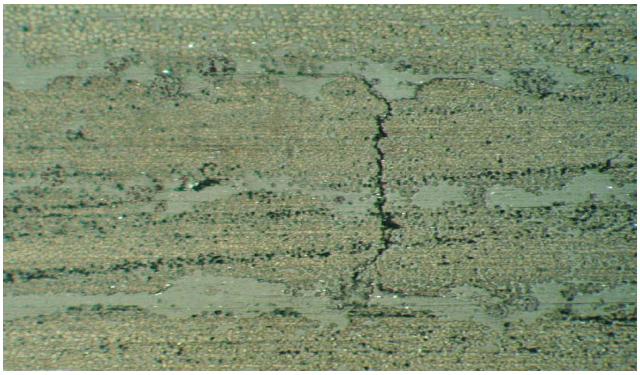

Load = 15 kN

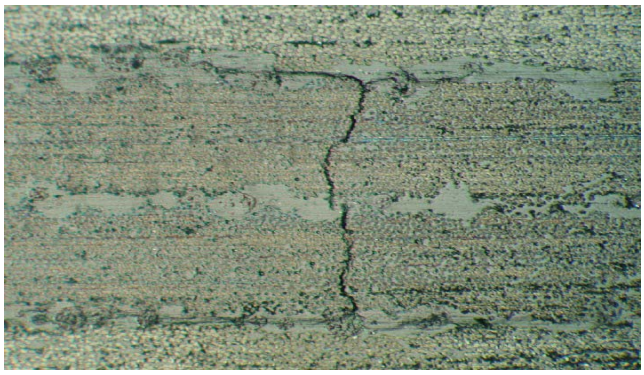

Load = 21 kN

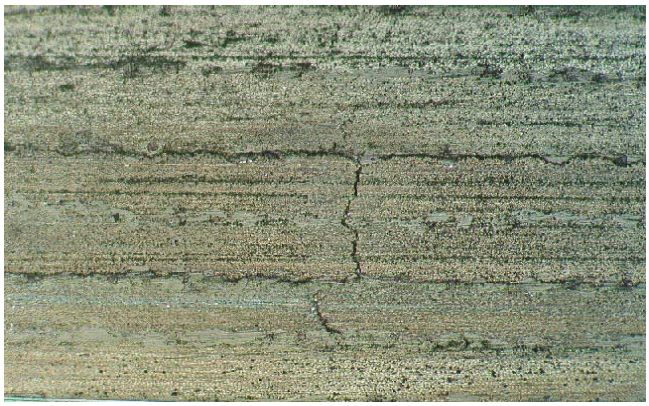

Figure 6.24 Damage evolutions from matrix crack to delamination in a SQ specimen.

2. LQ Joint

Similarly, a LQ joint specimen is loaded and monitored at the same load stages if applies as those for SQ specimen. The selected portion of specimen edge covers both adherend and joint overlap. The matrix cracks within the adherend edge are not found up to the load of 13 kN using optical microscopy; nothing is observed over the joint overlap edge. Matrix cracks seem to occur within the joint adherend and overlap region after 13 kN. This could be confirmed by the knee around 14 kN on the plots of cumulative counts vs. load in Figure 6.8. The matrix crack density over 18mm-long adherend edge within the selected portion could also be found in Table 6.3.

As expected from the previous monotonic failure tests, this specimen failed at 17.87 kN just before the planned load level of 18 kN. This failure load is fairly close to the average failure load of 18.77 kN for LQ. The failed specimen is examined both visually with naked eye and by using a microscope. It is very interesting to note that the fracture occurred not in the form of clean separation between two neighboring 0^o plies from two joint parts, but in the form of partial interlaminar failure and intralaminar failure (Figure 6.25). The left joint end first separated mostly in the form of interlaminar failure from outside, and then the separation became partial intralaminar failure within the 0^o ply of upper adherend. However, the right joint end failed mostly by interlaminar separation between 0^o ply and 45^o ply within the upper adherend. Delamination is also observed between 45^o and -45^o plies near the right joint end, which is initiated from the cracks in the taper.

Load = 5 kN

Load = 13 kN

Load = 15 kN

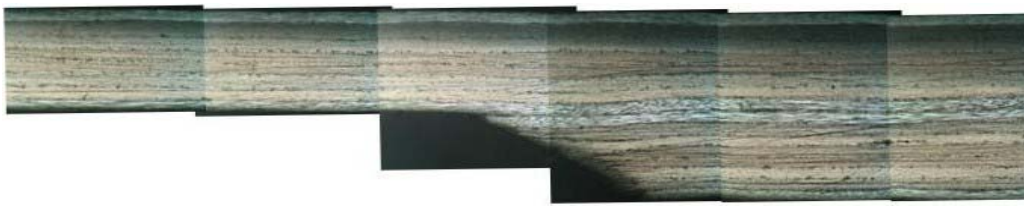

Load = 17.87 kN (Failed) - the left joint end

Load = 17.87 kN (Failed) - the right joint end

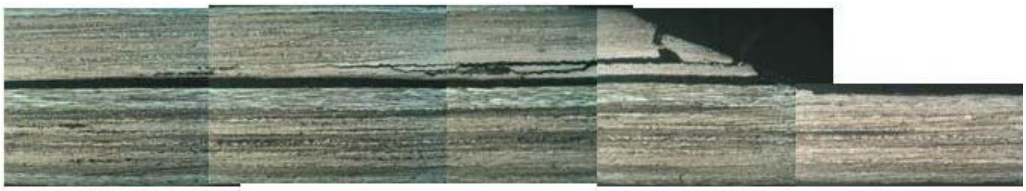

Figure 6.25 Damage progression and failure modes of a LQ joint specimen.

3. NQ Joint

For an NQ joint specimen, the study follows the same procedure as that for SQ and LQ. It is similar to LQ that the matrix cracks are not observed under microscope until a load after 13 kN and nothing is found within the joint overlap region up to this stage. Similarly to SQ and LQ, this could be proved as well by the knee point around 14 kN on the combined plots of AE cumulative counts vs. load in Figure 6.8. The crack density evolution with respect to load level in the adherend portion of 17mm-long is included in Table 6.3. After 18 kN, matrix cracks start to appear within the joint region but nearby the joint taper end. Free edge delamination initiated from matrix crack tips within adherend is then observed nearby joint region at load of 21 kN. Though some delaminations at joint taper are seen, they are not the dominating mechanism for the failure of NQ. The damage modes and their progressions are depicted in Figures 6.26 and 6.27 respectively.

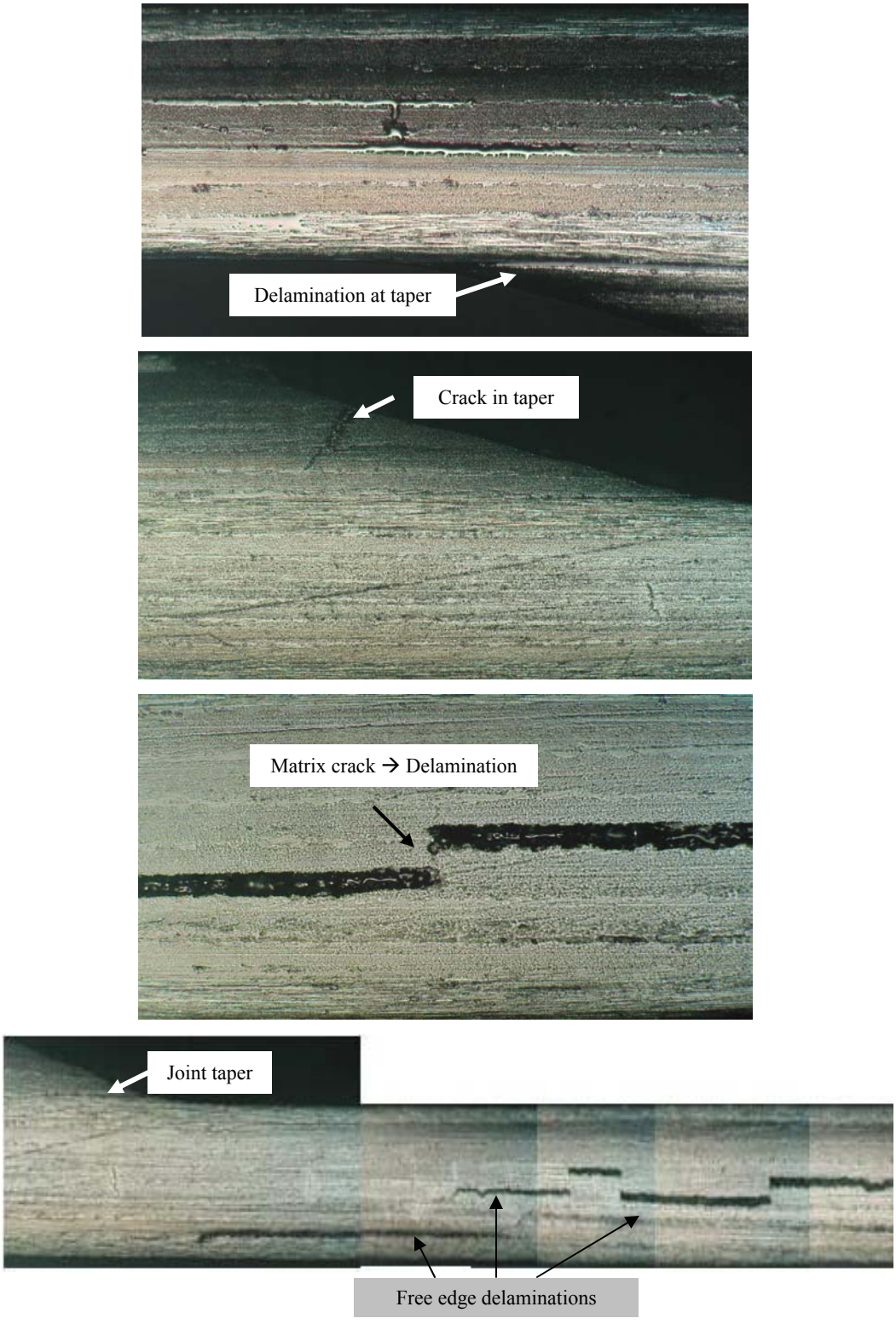

Figure 6.26 Damage mechanisms at load of 21 kN in a NQ joint specimen.

Load = 13kN

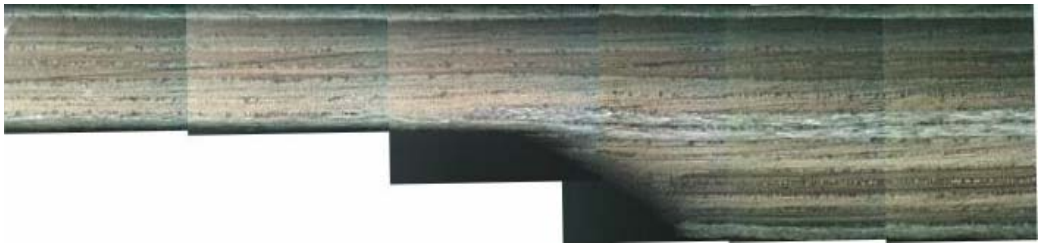

Load = 15 kN

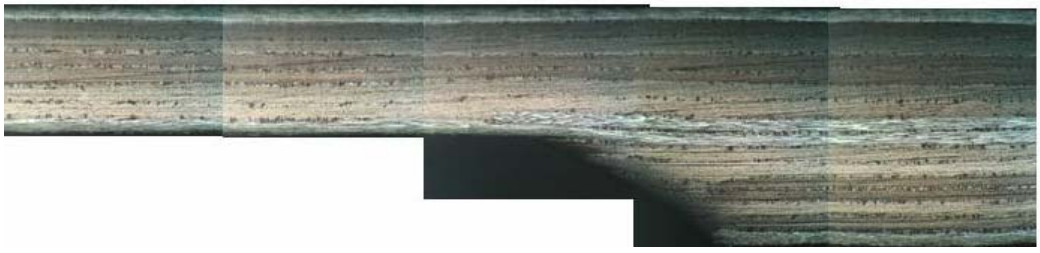

Load = 18 kN

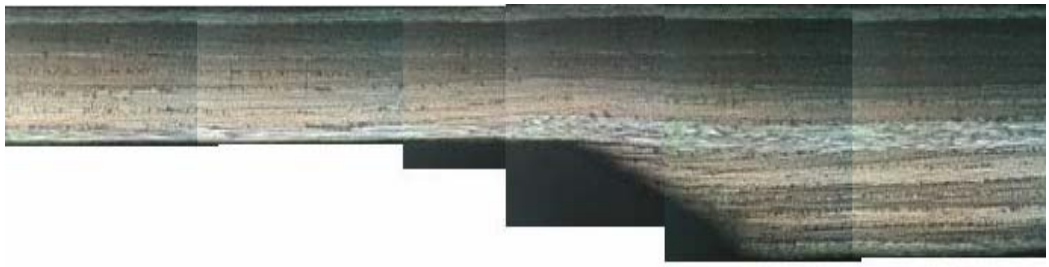

Load =21 kN

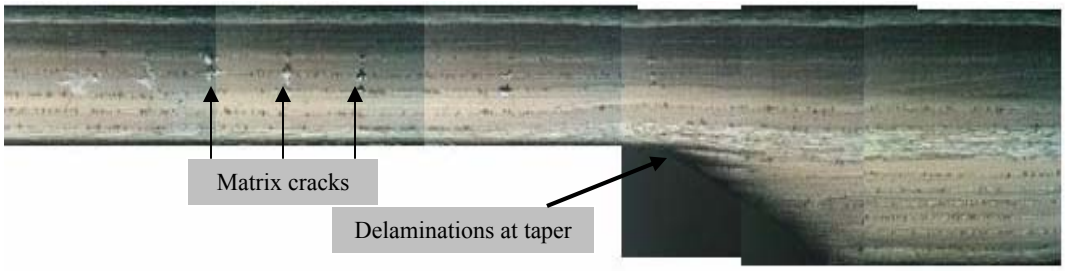

Failed NQ specimen

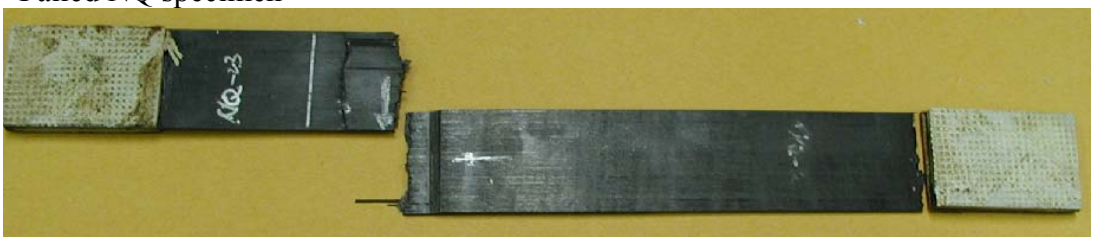

Figure 6.27 Damage progressions in an NQ joint specimen.

6.3.2 Unidirectional Lay-up

Unidirectional specimens, including the straight laminate SU and two joint configurations LU and NU are examined and compared following the similar procedures as for Q specimens using an optical microscope at the selected edge portions to characterize damage initiation and progression.

From the acoustic emission data, there is no obvious knee or transition point on the plots of cumulative counts vs. load for SU and NU though a knee-like point is found for LU at about 10 kN. So, the interval load levels are chosen as follows: 10 kN, 20 kN, and 25 kN, 30 kN and 35 kN. These specimens are loaded quasi-statically up to a certain load level and unloaded before they are observed under the optical microscope for edge damage. For the common load intervals including 10kN, 20kN, and 25kN for SU, LU and NU, there is no damage detected from those edges. A higher load of 35kN is applied for both SU and NU and no damage is observed from their edges either. For a LU specimen, a load of 29 kN which is very close to the average failure load of LU is applied, but no damage is found from the edge under the optical microscope.

Further loading induces the failure of LU and NU at their respective failure load with different fracture surfaces like those shown in Figure 6.28. The failure of LU is very abrupt without much transition process or predictive warning sign (Cao and Dancila, 2003 (a)).

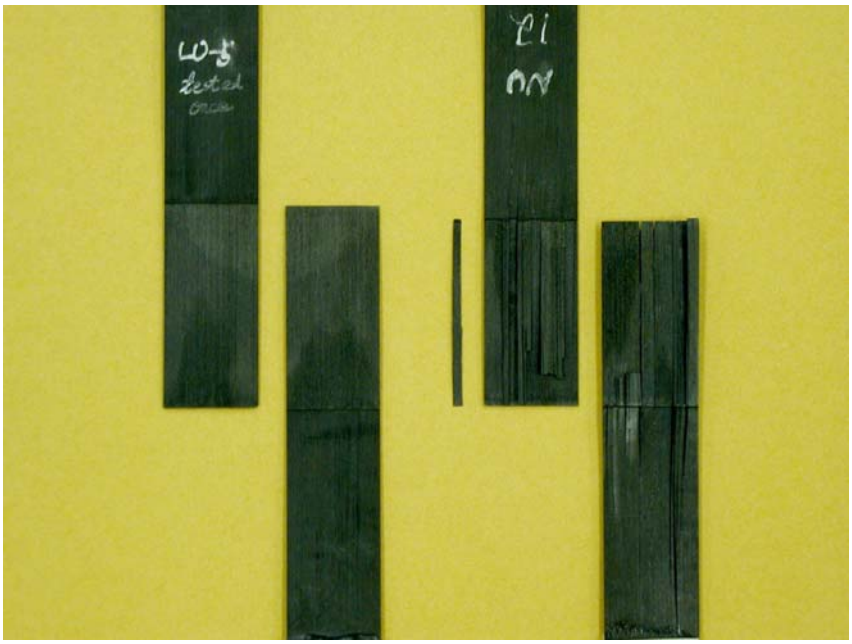

Figure 6.28 Typical fracture surfaces of LU (left) and NU (right) joints.

6.4 Quasi-Static Loading - X-ray Radiographic Examinations

Corresponding to the optical microscopy technique used for the edge damage detection, specimens loaded to different load levels are also examined for internal damage morphology using X-ray Radiography method. Before loading, three types of specimens are examined using X-ray and there is no defect or pre-existing damage found inside. After loading, specimens are prepared with enhanced penetrant and examined in an X-ray cabinet. The produced radiographs are in the form of black and white films. From these films, the internal damages such as the distribution of matrix cracks and delamination across specimen width and along specimen length could be observed.

These morphologies are compared with the corresponding damages observed from the edge.

As mentioned in Section 6.3.1, no matrix cracks are found before 10 kN for both joints of LQ and NQ as well as laminate SQ. This is confirmed by X-ray photos for those early load stages. From a load of 13 kN, matrix cracks start to appear from sparsely to intensively along the specimen length of a laminate or part of adherend of a joint. However, there are no matrix cracks observed up to 15 kN within joint overlap region. This also agrees to the observation by optical microscope technique. Only after the load of 18 kN can some cracks be found within joint overlap but nearby the joint end for NQ. When the nested overlap joint is loaded to 21 kN, free edge delamination (Figures 6.29 and 6.30) initiated from matrix crack tips within adherend propagates along interfaces between 90^o plies or 90^o and -45^o plies and reaches the joint taper.

Similarly for U joints, before loading, SU, LU and NU specimens are examined using X-ray and there is no defect or pre-existing damage found inside. After loaded up to 29 kN for joint LU and 35 kN for both SU and joint NU, the specimens are examined again. No delamination or other type of damage is detected both within joint region and outside joint region. The acoustic emission data recorded from the monotonic loading must come from the damage mechanisms, such as micro matrix cracking between fiber bundles or fiber/matrix debonding along loading direction, that could not be observed either from edge by using Optical Microscopy or from inside using X-ray Radiography technique.

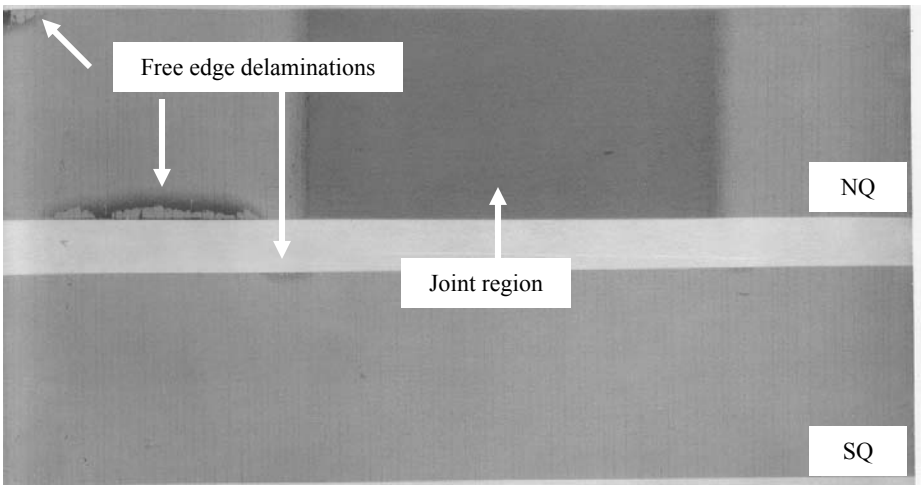

Figure 6.29 X-ray photos of SQ and NQ specimen sections after a load of 21 kN.

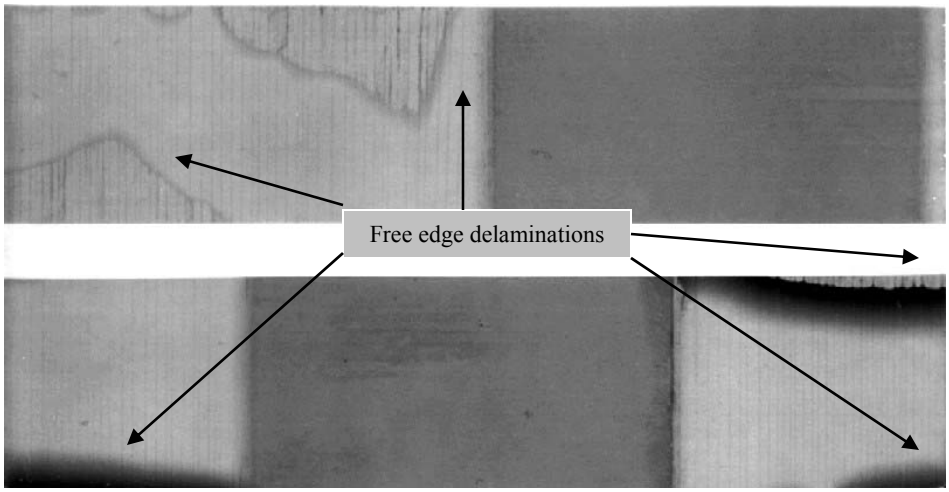

Figure 6.30 X-ray photos (top view) of NQ joint specimens.
(top: after failure; bottom: before failure)

6.5 Interpretations of Data and Results

Under uniaxial tensile loading, the selected six types of specimens of two groups (SU, LU, NU; SQ, LQ and NQ) exhibit different mechanical properties as well as damage and failure characteristics, which could be demonstrated by their failure strengths, related acoustic emission activities and microscopic and X-ray photos.

1. Joint Strengths

Single nested overlap joints NU and NQ show higher joint strength than the respective single lap joints LU and LQ. For 0^o unidirectional lay-up, NU joint specimen shows 29.2% higher average joint strength than LU. For quasi-isotropic lay-up, this increase percentage of NQ over LQ is 27.4%. The improvement of joint strengths confirms the conclusions drawn by Coates and Armanios (2000) and Coates (2001) for this single nested overlap joint configuration over the conventional single lap joint.

2. Damage Mechanisms and Failure Modes

The failure of single lap joints is relatively straightforward, primarily a shear type separation between the two adherends. For LU, the damage mechanisms before the final failure stage are micro matrix cracking and fiber/matrix debonding which produce low-counts acoustic emissions during monotonic loading. It fails catastrophically by shear separation between two joint parts accompanied by longitudinal splitting. The strength of fibers is not sufficiently utilized as fiber breakage is not the dominating damage mechanism. In other words, joint strength is far below adherend strength and fibers do not have the chance to play a leading role for this joint design. For LQ with quasi-

isotropic lay-up, several distinct damage mechanisms are observed such as macro matrix cracking within angle plies and delaminations between plies of different orientations.

In contrast, the failure of single nested overlap (SNO) joint tells a more complicated story. For NU, due to the existence of a nested overlap between two joints parts, there are more types of damage/failure mechanisms including fiber breakage, fiber pull-out, and mixed interlaminar/intralaminar shear failures within the joint overlap region. Since more material is involved during the loading process and a certain amount of load-carrying capability of fibers is also brought into play, this nested overlap joint shows higher joint strength than LU. In addition, two more interfaces are introduced from nested overlap manipulation, which enhances the load transfer between the two joint parts and thus makes this link stronger.

As for NQ, with the similar damage mechanisms mentioned above for LQ, it shows more progressive damage growth. Matrix cracking density is higher than for LQ for the same loading stage; more extensive delamination propagation is observed within the joint part, which is not observed in LQ. When these delaminations reach the joint taper region, the integrity of the base material (joint part) decreases; the geometric discontinuity between joint part and overlap region thus becomes even worse and finally it causes the failure of joint. In this case, the strength of the joint is higher than that of the base material (8-ply quasi-isotropic laminate).

SQ, as a reference for both LQ and NQ, helps understand the damage and failure mechanisms of a perfect joint. This piece of uniform material under monotonic loading demonstrates the whole development process of the damage mechanisms involved including micro matrix cracking, macro matrix cracking, delamination initiation and

propagation, and fiber breakage. The physical characterization of these mechanisms is well documented in Figures 6.23-6.24. It should be mentioned here that some of these damage mechanisms may occur and develop simultaneously, such as matrix crack evolution together with delamination initiation and propagation for "Q" group specimens.

3. Acoustic Emission Tests

From Acoustic Emission tests, it is found that the specimens of quasi-isotropic lay-up are noisier during loading to failure compared to the 0^o unidirectional lay-up counterparts. At low load levels of up to 13 kN, Acoustic Emission counts are relatively low for Q specimens, which suggest low damage occurrence and progression. Above about 13 kN, the AE counts become more intensive and higher, and a knee is observed in the cumulative counts vs. load plots, which may correspond to the introduction of a macro damage mechanism. This coincides with the observation of matrix crack density increase after 13 kN by using Optical Microscopy and X-ray Radiography techniques. For U specimens, the failure is more sudden, with lower counts and slower counts accumulation rate before failure. A critical point, such as a knee, is not obviously observed for U specimens.

4. Optical Microscopic Observations

At different load levels, the specimens are examined from the edge of the selected portion of specimens. Matrix cracks in the 90^o plies are the damage initiation mechanism for Q lay-up. With increasing load, the matrix crack density in the adherend portion also increases, especially after 15 kN. However, within the joint overlap region, very few

matrix cracks and no internal delamination are found even at 18 kN load, except for some small delaminations at joint taper. For a LQ specimen, matrix cracks are the major damage mechanisms before failure. The sudden failure of LQ specimens is due to shear failure partially between two neighboring 0^o plies, or within one 0^o ply at the joint interface, or between 0^o and -45^o plies. For an NQ joint, up to some load level, delamination is induced from the 90^o matrix crack tip within the adherend portion and propagates towards the joint region either along the interfaces between 90^o and -45^o plies, between two 90^o plies, between $+45^o$ and -45^o plies or between 0^o and $+45^o$ plies. For NQ joints, it is the extensive delamination propagating from the adherend part to nearby joint taper end that causes the failure of NQ joint. The joint overlap part survives which is desirable for good joint design.

5. X-ray Examinations

X-ray Radiography is used as a complementary technique to detect internal damage within the specimens. The resulting radiographic morphology is used to characterize the damage mechanism and damage progression at different load stages. The damage that could be easily detected and characterized by X-ray is delamination. Before the appearance of delamination, the distribution of matrix cracks could also be detected, although the image contrast is less satisfactory than that for delaminations. This is the reason that the X-ray photos of Q specimens for the early-stage loading are not included due to the poor quality of the pictures after scanning.

CHAPTER 7

DIFFERENTIATION OF DAMAGE AND FAILURE MECHANISMS USING ACOUSTIC EMISSION

As discussed in the chapters covering the literature survey and the damage and failure analysis tools, the acoustic emission technique has shown a promising capability in detecting and differentiating failure mechanisms via analysis of the recorded acoustic emission (AE) data. Two approaches to acoustic emission analysis typically used include parametric AE analysis and transient AE analysis. There are a number of acoustic emission signal parameters that define the waveform and its characteristics such as ringdown counts, amplitude, duration, risetime, frequency, etc. Typically, parametric AE analysis is used to evaluate overall damage development and accumulation in composites. This approach is also employed by some researchers to identify the sources of AE signals. However, due to the complexity of failure mechanisms and the overlap of AE parameters resulting from wave propagation processes, it is difficult to precisely discriminate damage mechanisms in composites merely through parametric AE analysis. The transient AE analysis is an alternate for that goal and is based on the full waveform analysis of the recorded waveforms. It is assumed that a specific failure mechanism has its own characteristic waveform with a typical frequency spectrum. Signature waveforms

are extracted from thousands of AE signals and used to correlate them to failure mechanisms observed by using alternate techniques (Dzenis and Qian, 2001).

This chapter is focused on the differentiation of damage and failure mechanisms in the studied co-cured composite joints of two joint configurations with two different lay-ups. Only the case of monotonic loading will be considered, since tremendous amounts of data are generated from long-cycle fatigue tests, extraneous signals from friction of matrix cracks and/or delamination interfaces as well as from possible tab-grip friction during cyclic loading. The effort in discriminating fatigue failure mechanisms using this experimental procedure may become prohibitive.

Two lay-ups are considered for co-cured composite joints in this study: i) zero-degree unidirectional $[0]_8$, and ii) quasi-isotropic $[0/+45/-45/90]_s$. As shown in the previous chapters, significantly different damage mechanisms are occurring in these two types of joints. Zero-degree unidirectional lay-up joints including single lap joint LU and single nested overlap joint NU will be studied and compared in "U" group. Quasi-isotropic lay-up straight laminates SQ and joints including single lap joint LQ and single nested overlap joint NQ will be studied together in "Q" group. SQ is included as a reference for "Q" group, particularly for the NQ joint since its joint strength is close to the strength of SQ and they also show the similar damage initiation and progression mechanisms at some common stages. Altogether, five cases are studied in this part including LU, NU; LQ, NQ and SQ.

To investigate the repeatability of test results, four specimens of each case from the same batch manufactured by the author in the composite lab are tested under monotonic loading and those important AE parameters mentioned above as well as the frequency

information of waveforms are recorded using a DiSP-2002 Acoustic Emission Workstation. Every recorded data file (PAC .dta file) which includes all important pre-selected AE parameters was transformed by built-in software in the DiSP-2002 Acoustic Emission Workstation to ASCII format that could be processed in Microsoft Excel. Then, the overall AE histories in terms of counts vs. load of all specimens in each case can be created and compared and AE parametric distributions and correlations be generated and studied via parametric AE analysis. From this analysis, the AE history and damage development and accumulation processes are evaluated, which gives the overall picture of the AE response from the beginning of loading to the final failure of a joint or laminate. Also, relations could be inferred among those highly correlated AE parameters. By using the commercial software package NOESIS v3.3, AE data (PAC .dta file) of a typical specimen acquired during monotonic testing could be clustered into several groups according to the characteristics carried by those recorded AE parameters. In conjunction with the previously acquired observations regarding damage and failure mechanisms by using Optical Microscopy and X-ray Radiography techniques, each clustered group is assumed to correlate with a specific failure mechanism. The detailed test setup is covered in Chapter 5.

7.1 Parametric Acoustic Emission Analysis

7.1.1 Overall Acoustic Emission Histories

Single lap joints and single nested overlap joints of the same stacking sequence or lay-up are investigated together in order to compare the differences in their acoustic emission activities and AE data distribution trend with respect to the load history. This will give an overall picture of damage development and accumulation in the studied specimens. As mentioned above, for each case, four specimens are tested to ensure repeatability of test results and all AE data are recorded using DiSP-2002 Acoustic Emission Workstation. To show the overall AE histories, four plots of the ringdown counts vs. load and two combined plots of the cumulative counts vs. load or average stress are shown together for all specimens for each case. The average stress shown on the abscissa is calculated from the measured load divided by the average cross-sectional area of the joint part of each specimen which consists of 8 plies (not the cross-sectional area of 16-ply overlap region).

Figures 7.1 and 7.2 enlists respectively four plots of ringdown counts vs. load and two plots of cumulative counts vs. load or stress for LU specimens. The ringdown counts before the final failure are below 100 and mostly below 20 with some anomalies around 11 kN in joint LU-25. The cumulative curve follows a slowly and smoothly increasing trend until the final steep jump which corresponds to the failure of the joints. From the results of the previous chapter, no macro damage was detected via X-ray Radiography across the specimen and no micro or macro damage was observed either from the polished edge by Optical Microscopy at various loading stages studied. The AE signals on one hand come from some microscopic damage mechanisms which could not be

detected by the techniques adopted such as micro matrix cracking and fiber/matrix debonding as reported by other researchers; on the other hand the AE data near failure come from the final macroscopic failure mechanisms such as longitudinal splitting and shearing separation of joint parts as observed.

Compared to the AE activities of LU joints, NU follows the similar acoustic emission distributions during the whole monotonic loading history (Figures 7.3 and 7.4). A trend of smooth and slow accumulation of AE counts before failure and a burst-type of data distribution at the final moment is also observed like in LU. However, NU has higher distributed counts compared at the same loading stage with LU and thus shows a higher total number of counts. This may explain the improvement of joint strength to a certain depth that NU has more energy for acoustic emission activities through the whole loading history. No obvious transition point or knee could be seen in cumulative counts plots for both LU and NU. The low-counts characteristics of "U" group are determined by their structures of zero-degree unidirectional lay-up and only micro damage such as micro matrix cracking and fiber/matrix debonding is involved before failure, which was studied in the previous chapter.

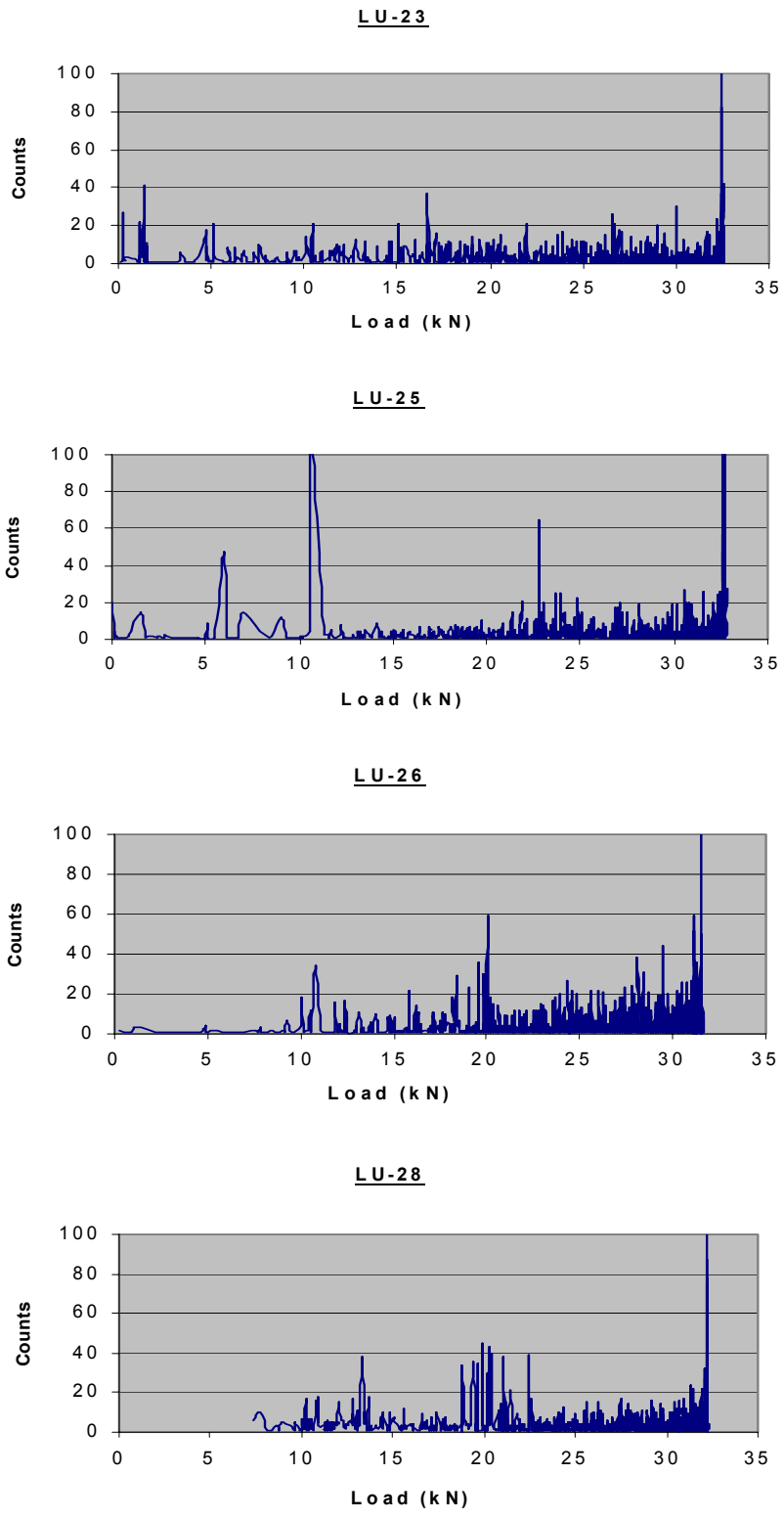

Figure 7.1 Overall AE counts vs. load for LU joint specimens.

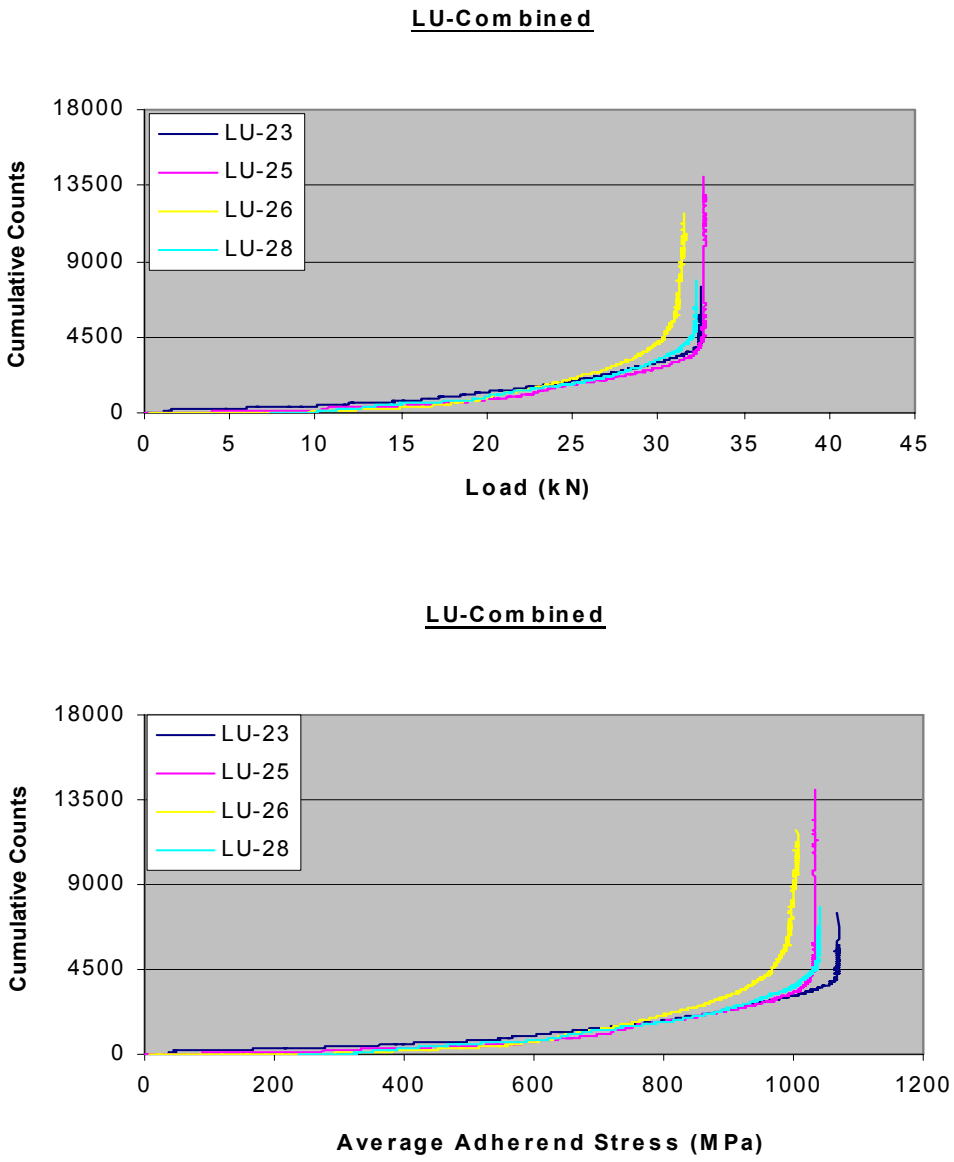

Figure 7.2 Combined cumulative AE counts vs. load or average adherend stress for LU joint specimens.

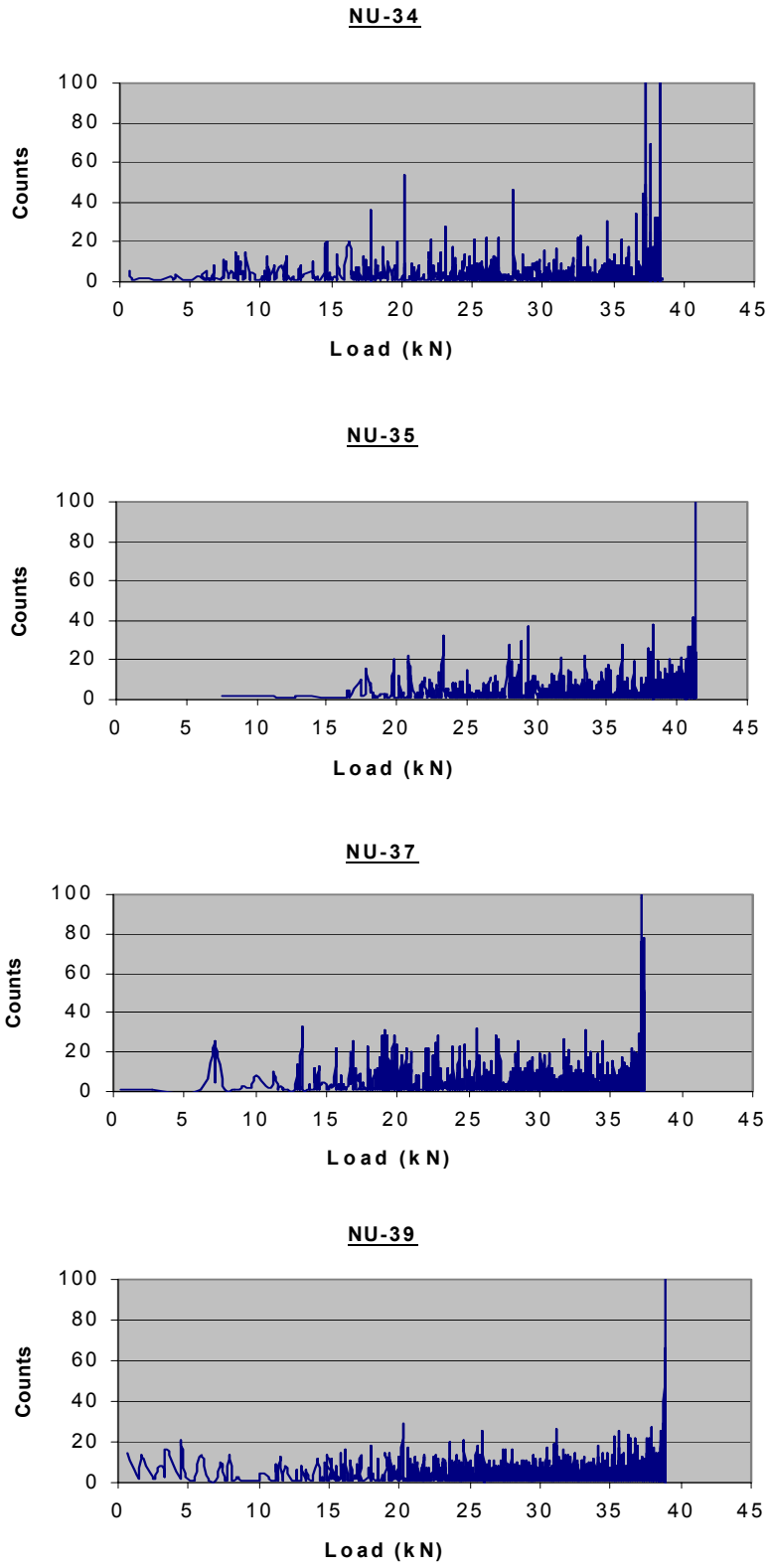

Figure 7.3 Overall AE counts vs. load for NU joint specimens.

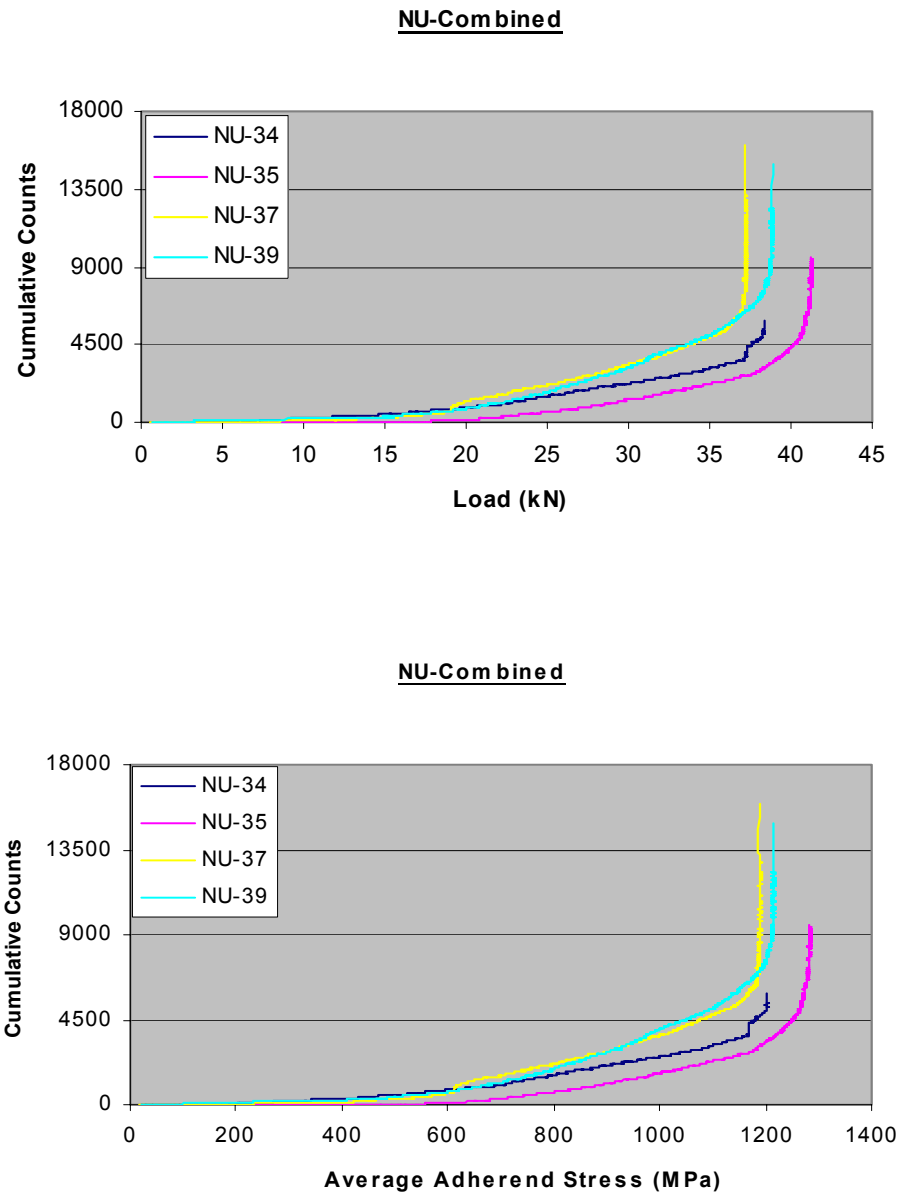

Figure 7.4 Combined cumulative AE counts vs. load or average adherend stress for NU joint specimens.

The overall AE histories of the "Q" group show some differences from those of the "U" group because of different lay-ups. For LQ joints, it behaves similarly as LU but with higher distributed counts especially after ~13 kN and also with higher total cumulative counts (Figures 7.5 and 7.6). This is consistent with the previous observations that before 13 kN no macro matrix cracking was found (Table 6.30 and Figure 6.25) and only those micro damage mechanisms such as micro matrix cracking and fiber/matrix debonding which escaped from the techniques used might have happened before ~13 kN in LQ. From around 14 kN, the continuously emitted AE signals with less than 100 counts dominate the remaining loading process until the final failure. In addition, a knee is observed at about 14 kN in cumulative counts plot. This load could manifest the appearance of macro matrix cracking by comparing the microscopic photographs at 13 kN and 15 kN in Figure 6.25. Table 6.3 also records the macro matrix crack densities from 15 kN and no cracks were found at and before 13 kN. This again confirms macro matrix cracking begins between 13 kN and 15 kN.

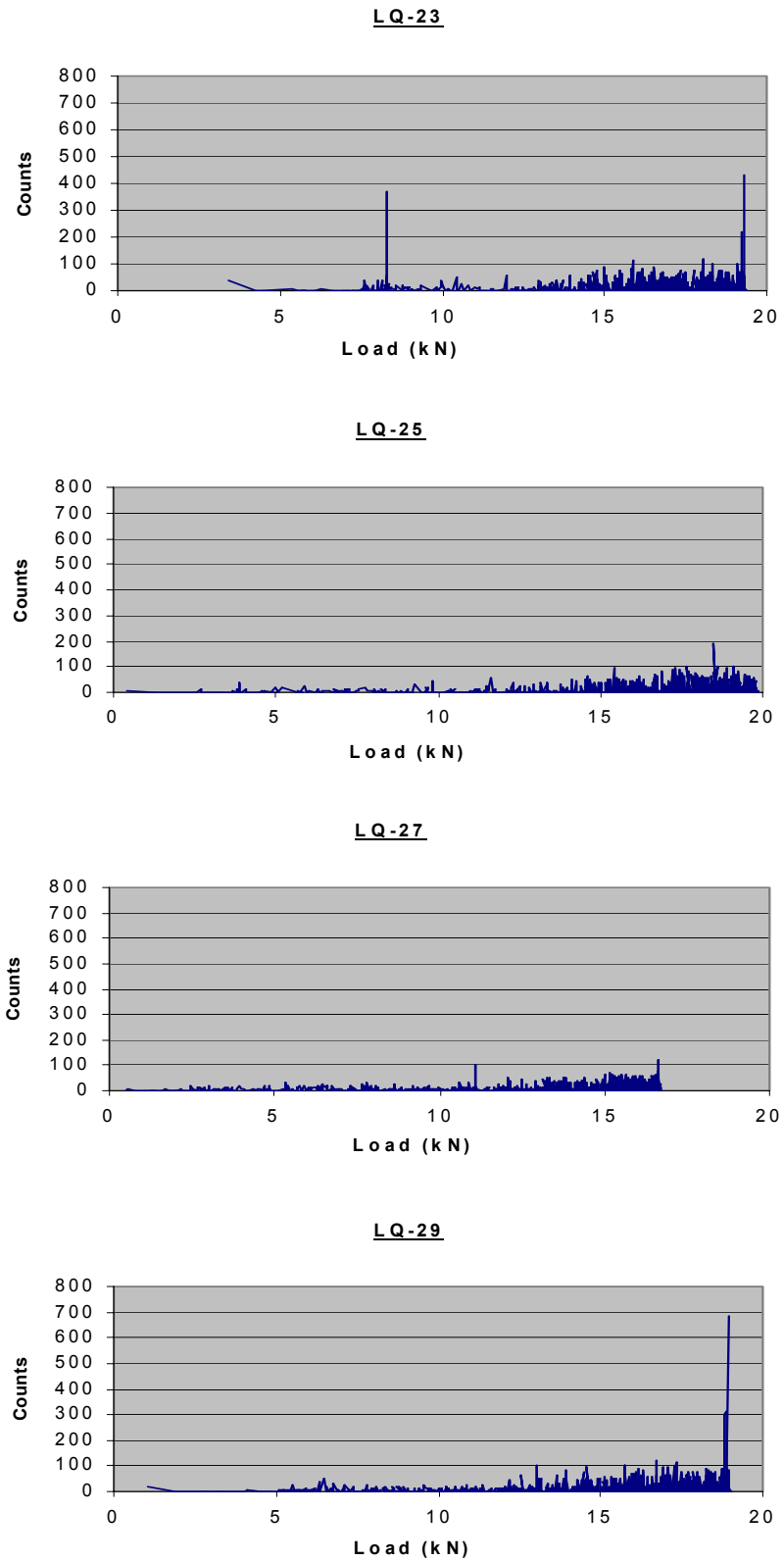

Figure 7.5 Overall AE counts vs. load for LQ joint specimens.

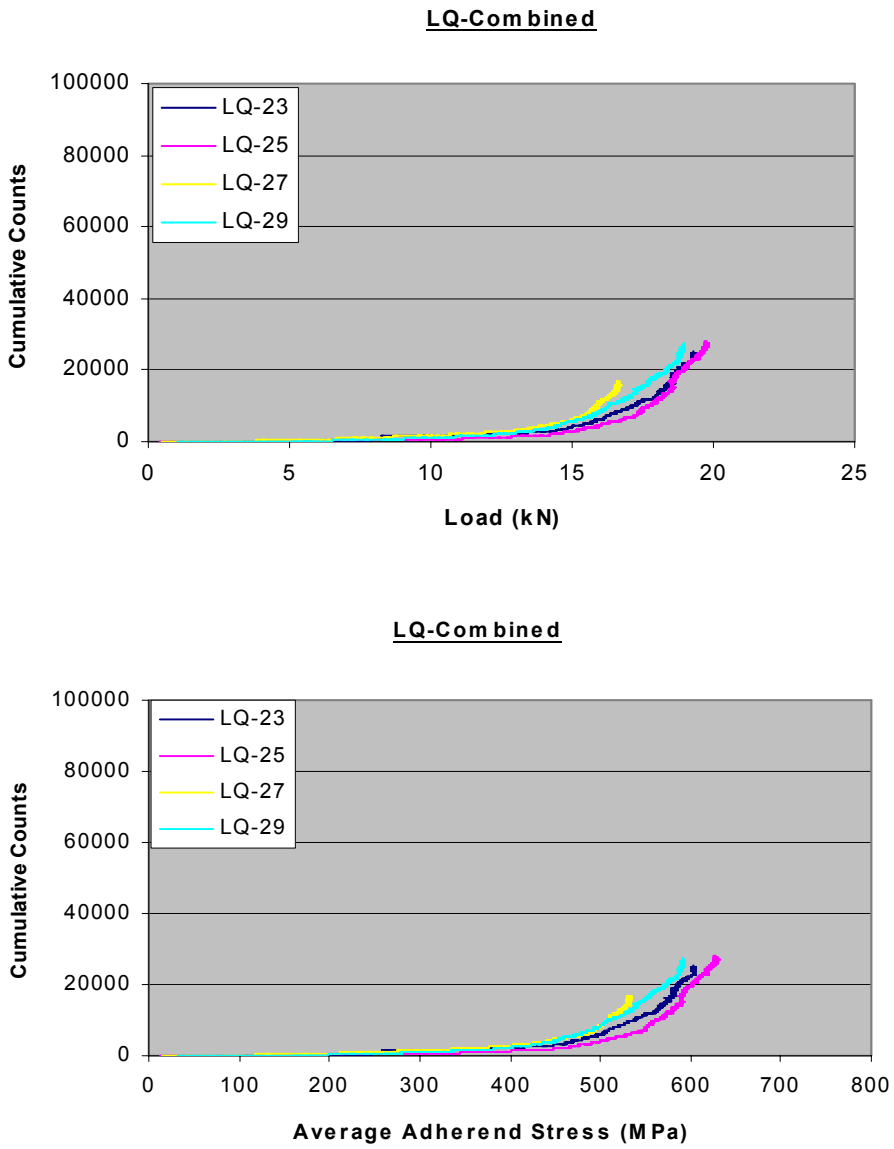

Figure 7.6 Combined cumulative AE counts vs. load or adherend stress for LQ joint specimens.

The NQ joints, with a single nested overlap within the joint region, exhibit even more intensively distributed AE signals (Figures 7.7 and 7.8). Except for the random noises from anomalies before 10 kN, higher AE signals start to occur from a load around 14 kN. Similarly to LQ, this 14 kN is regarded as the load for initiating macro matrix cracking and could be confirmed by referencing Table 6.3 and Figure 6.26. Also, a knee at around 14 kN is a further proof for the appearance of a macro matrix cracking damage mechanism. Those big events with high and intense counts can be seen between 15 kN and 22 kN which could be related to both the evolution of matrix cracking and delamination initiation and propagation as shown in Figure 6.26. Compared to LQ joints, the distributed AE ringdown counts and thus the total counts of NQ joints are much higher which means NQ joints possess more energy for acoustic emission activities. This could at least from one aspect support that NQ has a higher joint strength. The curves of cumulative counts show variations of curvature rather than the relatively flat and smooth shape for LQ, which gives a hint that the complex damage and failure mechanisms that do not happen in LQ joints are involved in this NQ joint structure. Of course, it is already known from analyzing the fractured NQ specimens in the previous chapter, NQ is a good joint design since it fails the material outside joint.

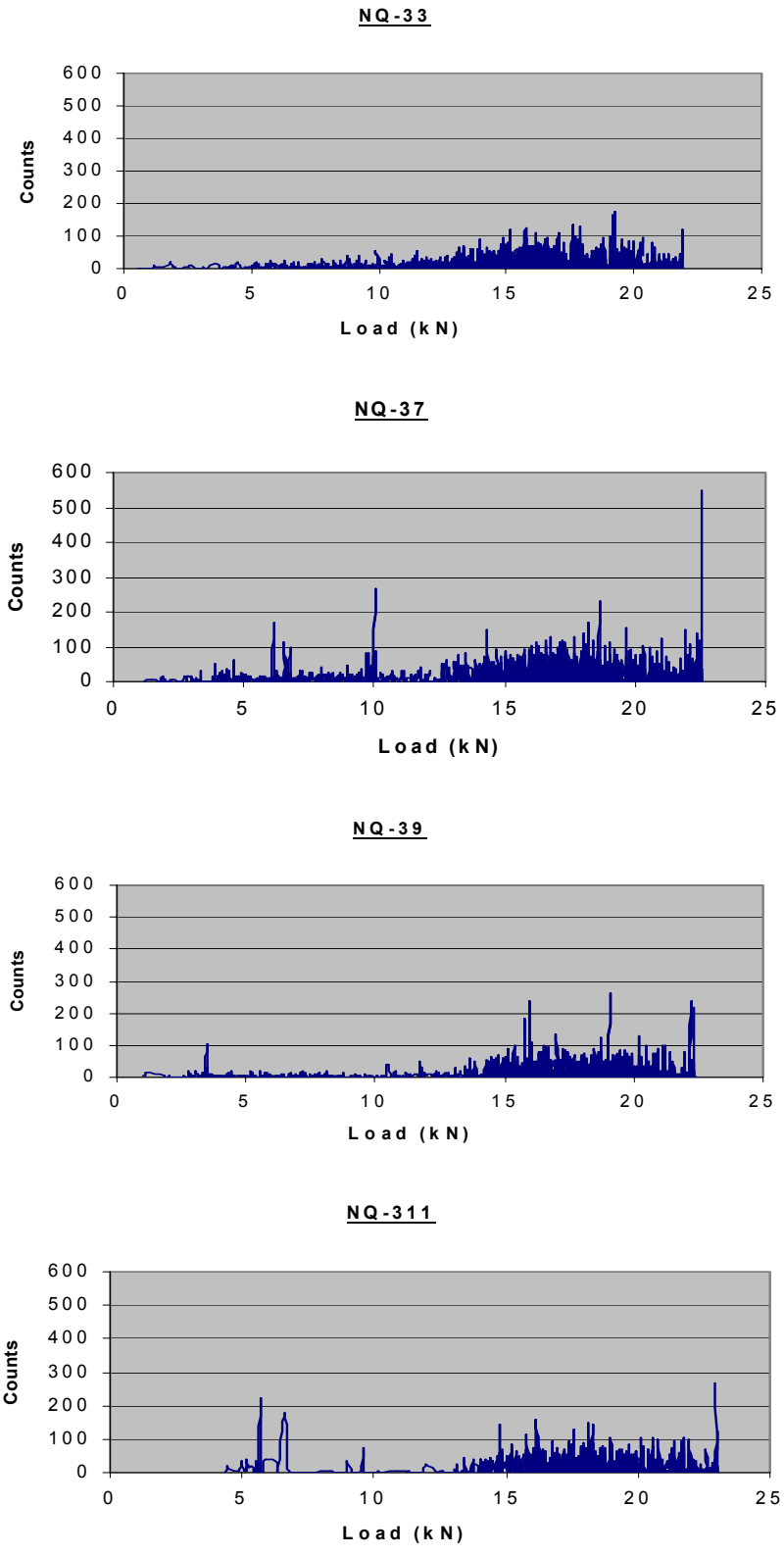

Figure 7.7 Overall AE counts vs. load for NQ joint specimens.

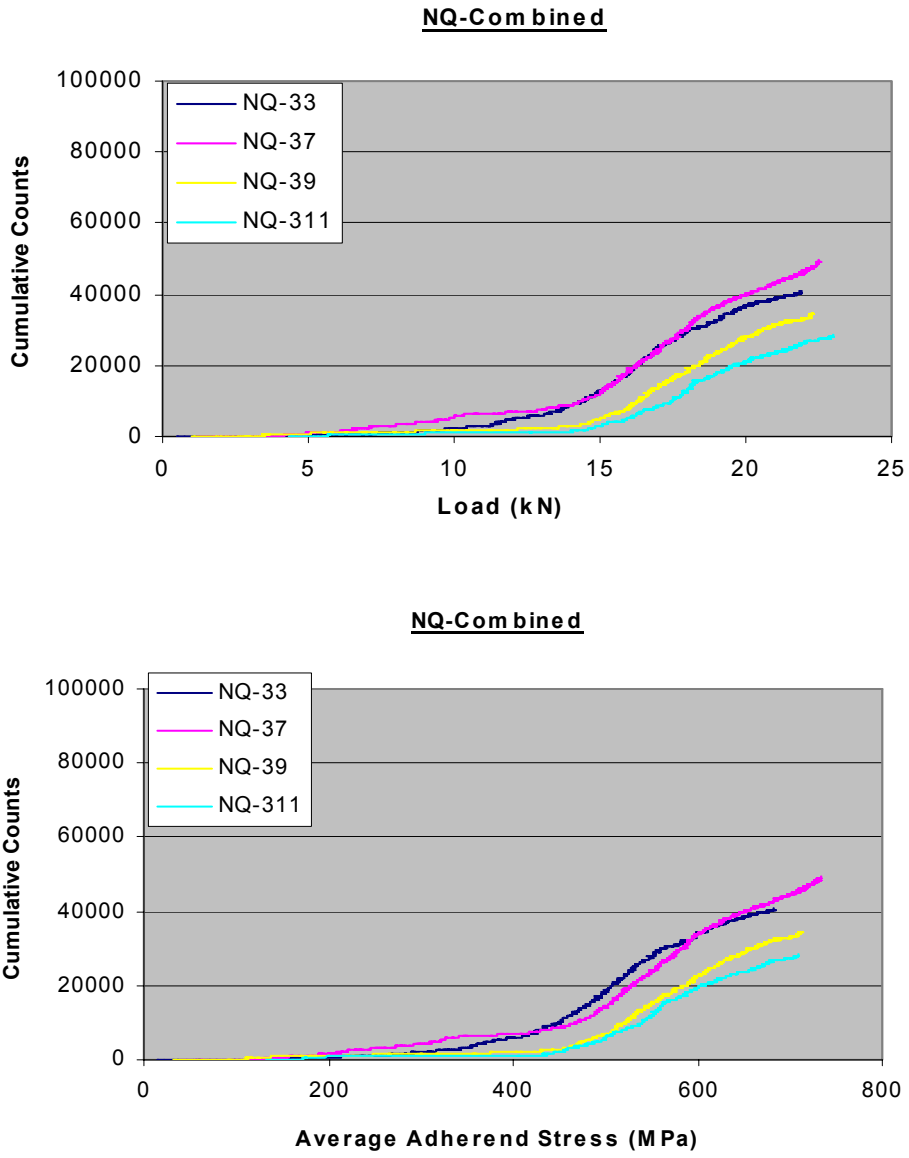

Figure 7.8 Combined cumulative AE counts vs. load or average adherend stress for NQ joint specimens.

SQ, as a reference for both LQ and NQ joints, represents a straight laminate specimen with quasi-isotropic lay-up. During monotonic loading, AE signals in SQ caused by the intensive damage activities give it a very noisy character (Figures 7.9 and 7-10). Before 13 kN, very low-counts events occur and it is assumed to be attributed to some micro damage mechanisms as aforementioned and AE increases rapidly thereafter. Similarly to LQ and NQ, a knee exists as well for SQ at around 14 kN which could relate to the initiation of macro matrix cracking, though some medium-sized matrix cracks were already counted from 13 kN for SQ (Table 6.3 and Figures 6.23 and 6.24). The most intense activities are also observed between 15 kN and the final failure for all SQ specimens. The distributed counts and the total counts numbers of four SQ specimens are much higher than those of LQ and NQ which implies SQ has more internal energy for these high-energy AE activities.

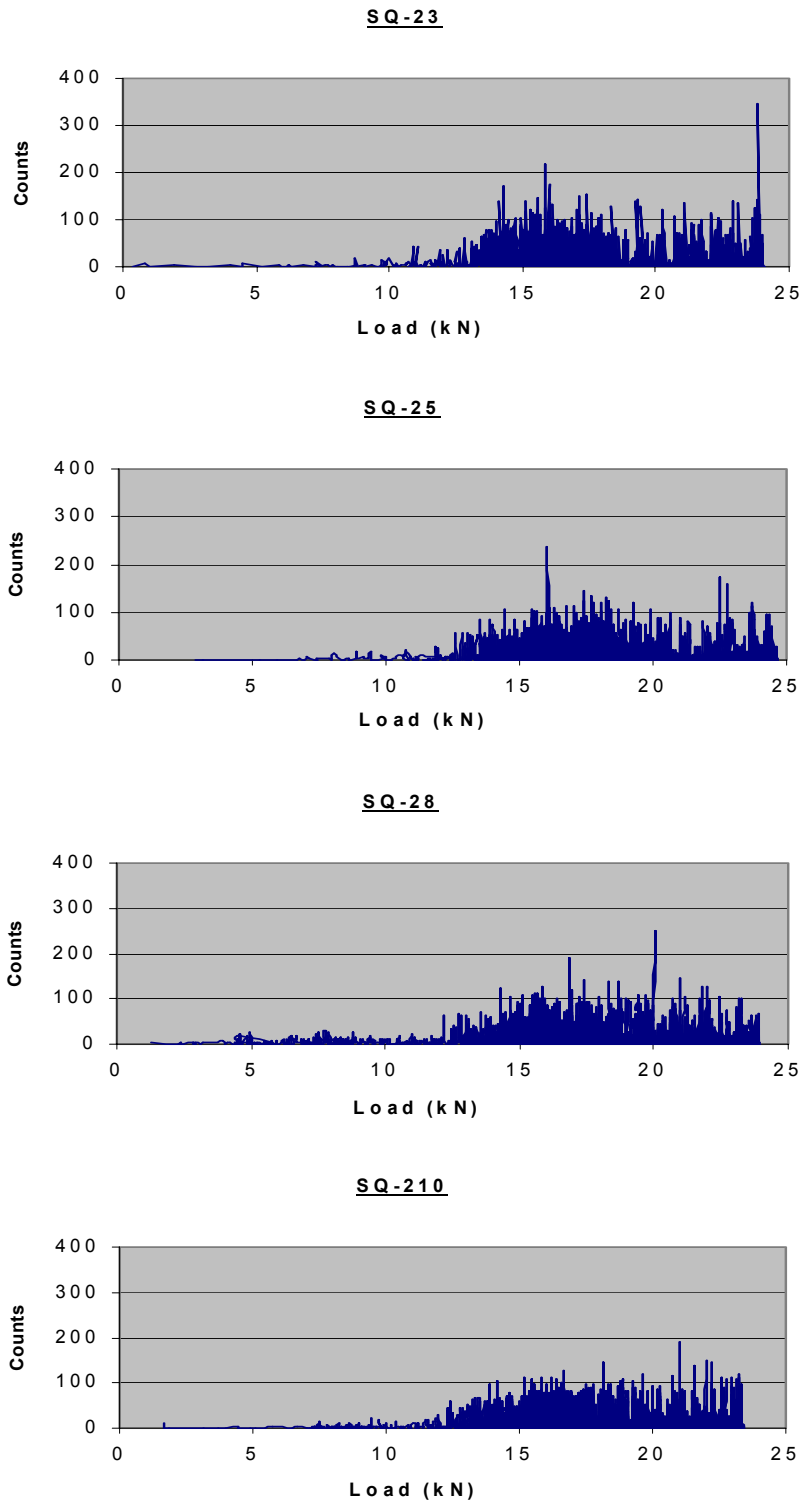

Figure 7.9 Overall AE counts vs. load for SQ laminates.

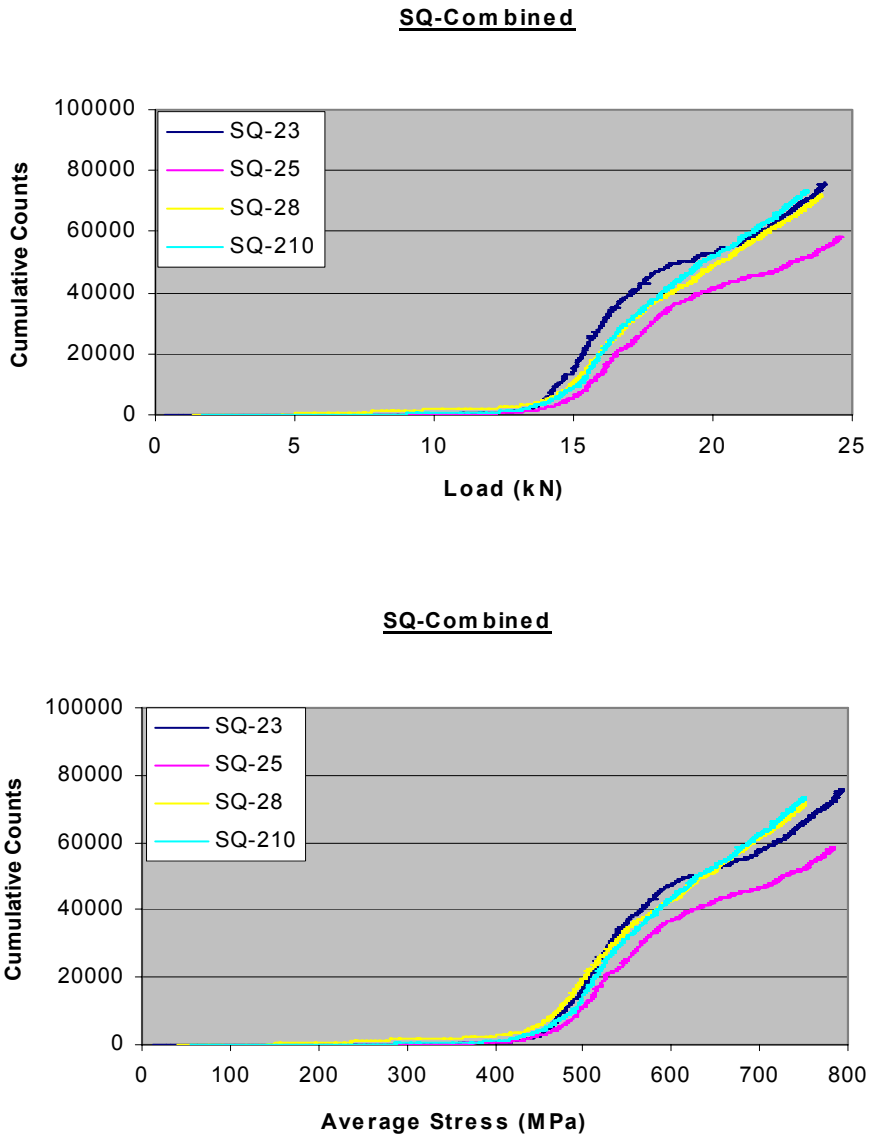

Figure 7.10 Combined cumulative AE counts vs. load or average stress for SQ laminates.

7.1.2 Parametric Distributions and Correlations

As stated in Chapter 4, acoustic emission signals can be described in terms of parameters such as ringdown counts, amplitude, duration, risetime, etc. Parametric AE analysis is based on the correlation plots among those parameters and is used to gain further insights of overall damage development and accumulation in composite joints and laminate from other AE parameters instead of from counts and load only. Parametric distribution and correlation graphs of a typical joint or laminate from each case including LU, NU, LQ, NQ and SQ respectively are plotted and compared. Basically, three types of plots of those highly correlated parameters are drawn for comparison purpose including ringdown counts vs. amplitude, duration vs. load and duration vs. amplitude. The counts vs. load plot could be found in the previous section. These plots are produced by Microsoft Excel based on the recorded acoustic emission data which is then transformed to ASCII format by the software installed in the DiSP Acoustic Emission Workstation.

With a preset 45 dB threshold and 40 dB preamplifier gains as well as with the available sensitivity of the system, all recorded AE signals fall between 45 dB and 99 dB for the amplitude distribution. Counts number increases with amplitude and the same for duration with amplitude. Comparing LU with NU joints in "U" group (Figures 7.11-7.13), the AE signals of LU are mostly located within 45 dB and 79 dB in amplitude plots and there are no events between 79 dB and 98 dB. The most events have the counts number lower than 40 and duration mostly lower than 200 μs except for some signals with series of high durations at the final failure. The NU joint has more widely distributed AE signals in amplitude and duration plots with some events with amplitude

between 79 dB and 98 dB. It also has more events with higher duration than 200 μs compared to LU. From these parametric plots, it could not tell much difference between the studied LU and NU joints.

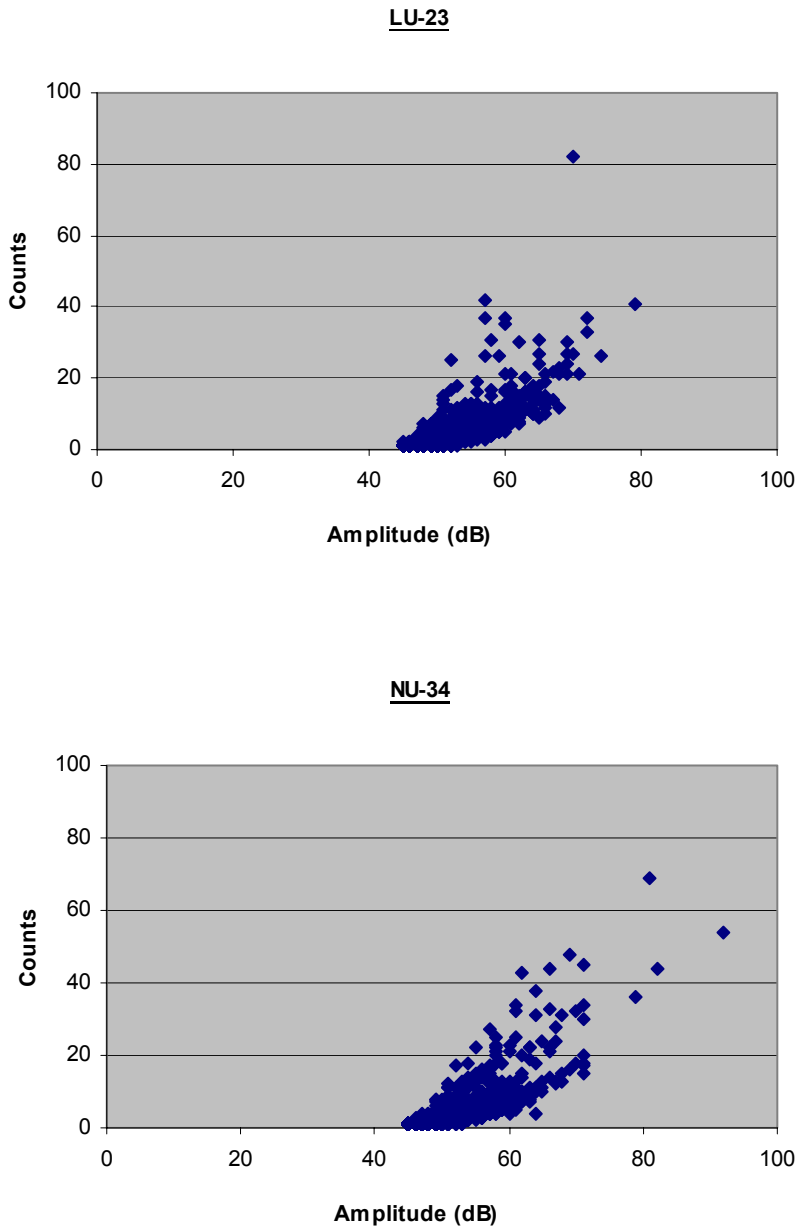

Figure 7.11 AE counts vs. amplitude for a LU and NU joint specimen.

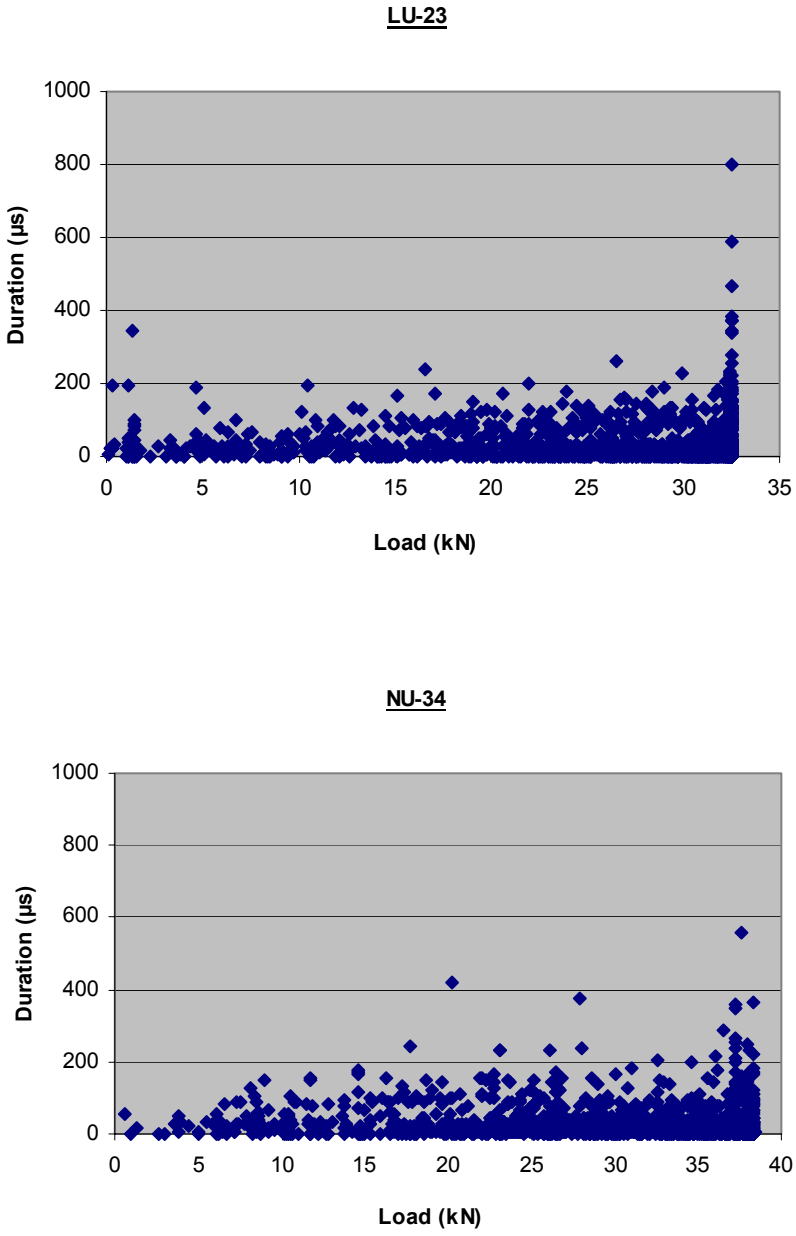

Figure 7.12 AE duration vs. load for a LU and NU joint specimen.

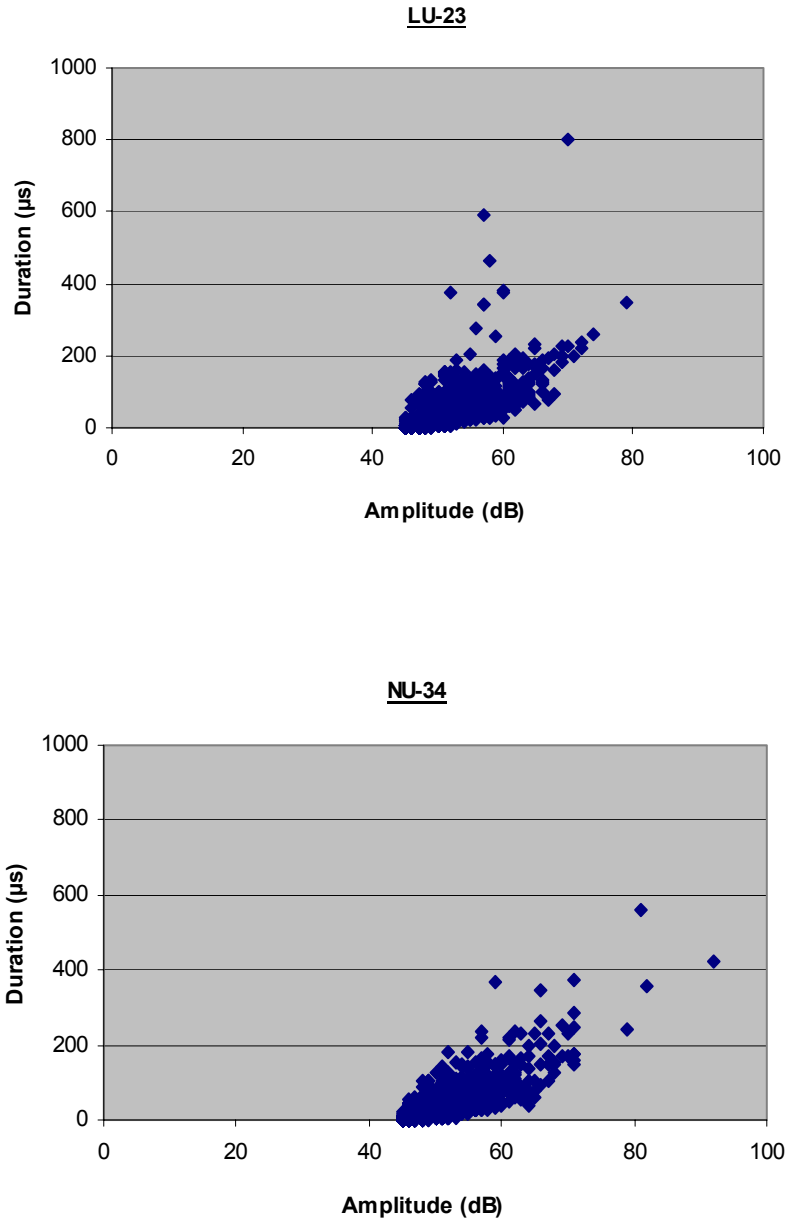

Figure 7.13 AE amplitude vs. duration for a LU and NU joint specimen.

The “Q” group (joints or laminate), especially those NQ and SQ specimens, show progressive damage development characteristics and thus more distributed AE data are recorded through the entire monotonically quasi-static loading process. Similarly to the “U” group, three types of plots are sketched for LQ, NQ and SQ (Figures 7.14-16). From the overview of those plots, it is found that AE events with higher counts number or higher duration also have higher amplitude (counts number or duration increases with amplitude); AE events with higher duration occur in the later loading stage (i.e., duration shows an increase trend with respect to load).

Compared to NQ joint, LQ produces mostly short duration signals (< 824 μs) in duration plot while NQ has longer duration events covering the range from 0 to ~1500 μs. There are more high-counts AE events (>100) in NQ. Though AE signals occupy the amplitude range from 45 dB to 99 dB for both joints, there are much fewer data between 84 dB and 99 dB for LQ.

SQ laminate, as a uniform piece through the length, shows very extensive damage progression during monotonic loading. All “Q” specimens (LQ, NQ and SQ) have the amplitude distributions that cover the amplitude range between 45 dB and 99 dB, while NQ and SQ have more alike distributions even at the final loading stage. The other plots for NQ and SQ are almost the same for duration and counts distributions. The similarity of the parametric distributions and correlations between NQ and SQ once again agrees with the previous findings of their close strengths and similar damage and failure mechanisms observed within the materials.

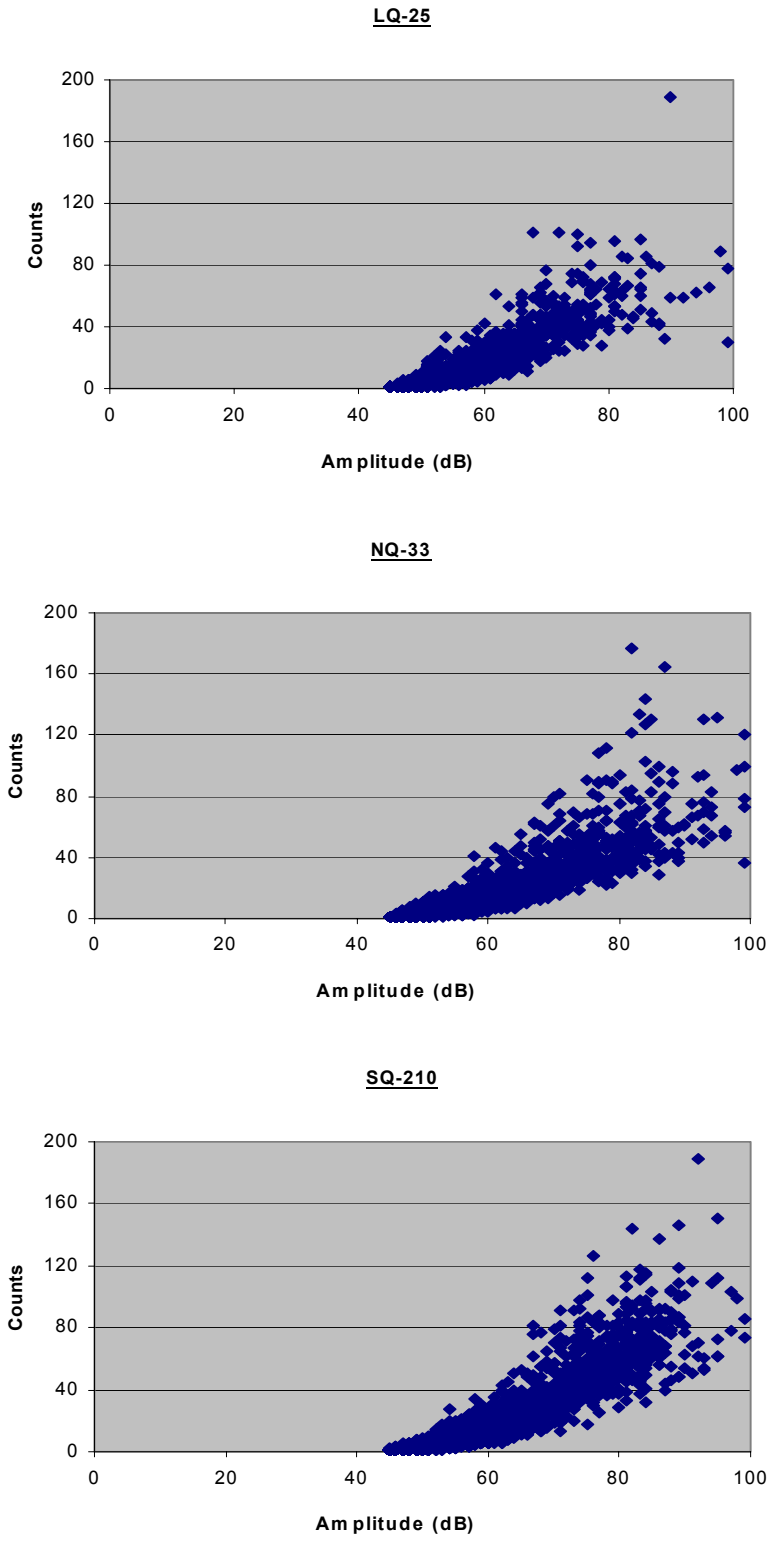

Figure 7.14 AE counts vs. amplitude for a LQ, NQ and SQ specimen.

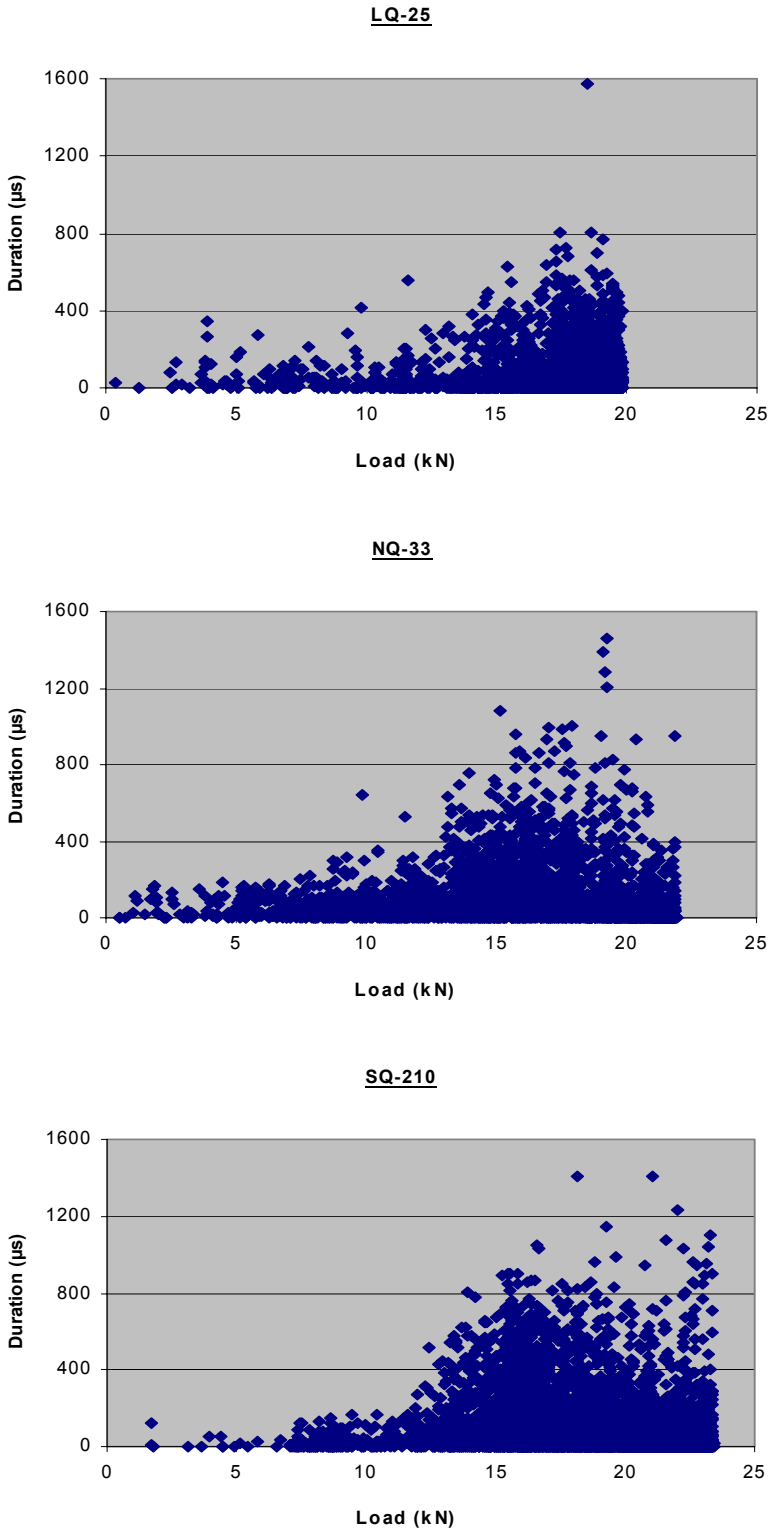

Figure 7.15 AE duration vs. load for a LQ, NQ and SQ specimen.

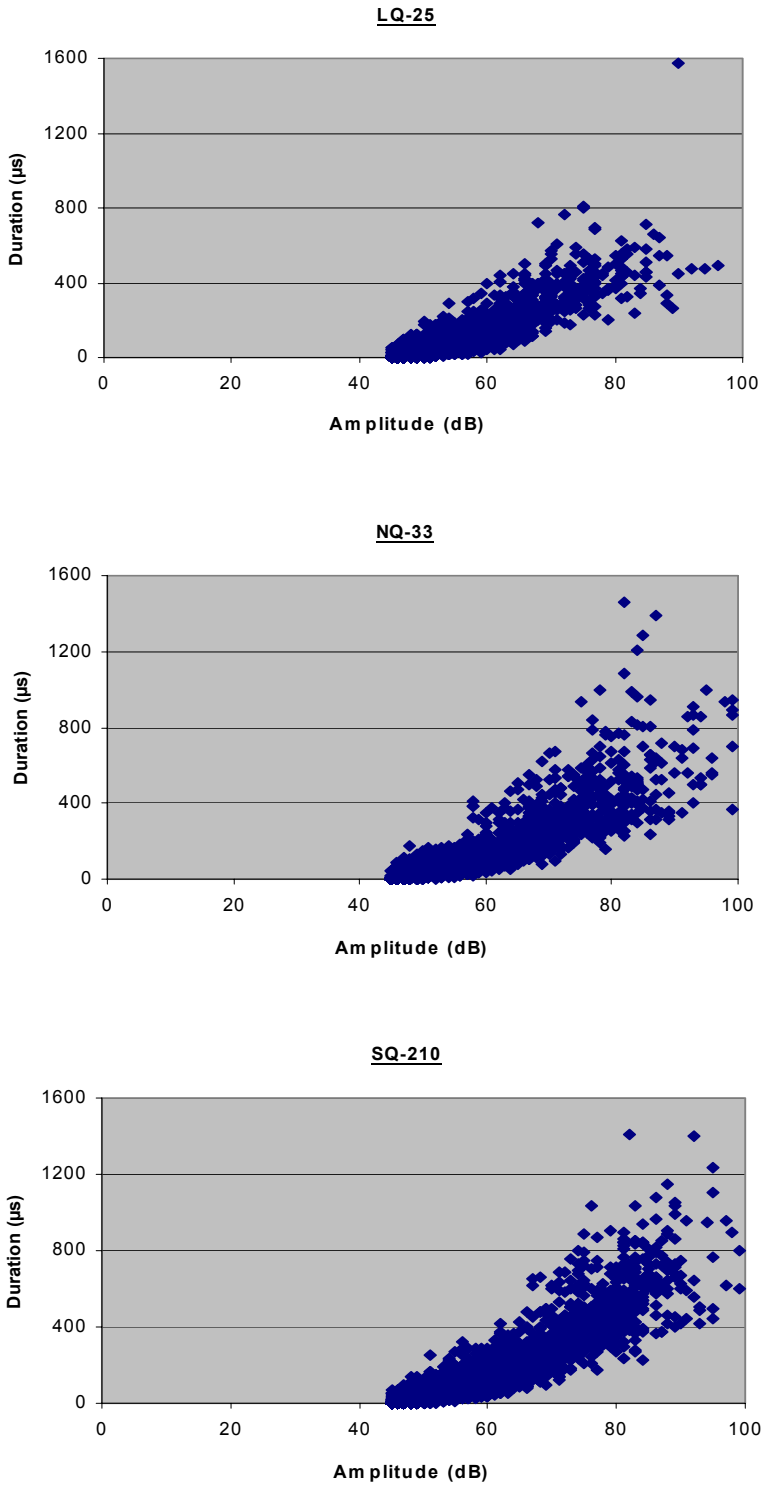

Figure 7.16 AE duration vs. amplitude for a LQ, NQ and SQ specimen.

The above parametric AE analysis provides an overall view of AE parameter distributions and correlations among several AE parameters. In addition, it demonstrates damage development and accumulations within the specimens during monotonic loading accompanied by various types of AE signals in terms of ringdown counts, amplitude and duration. However, it is difficult if not impossible to discriminate those AE data into several groups and tell which group of AE signals is from matrix cracking or delamination, except when a-priori knowledge is available for those AE parameters of a specific damage mechanism and a filtering method is used. In the next section, a hybrid clustering method combining unsupervised pattern recognition algorithm (K-means) with the k-NNC supervised method will be used to improve the AE analysis results and give a possible answer to that question.

7.2 Clustering of AE Signals

As seen from the above parametric AE analyses, it is still not possible to discriminate the acquired AE data into corresponding damage and failure mechanisms within the co-cured composite joints and laminate tested. The NOESIS software package, which has both unsupervised and supervised pattern recognition capabilities is used in this section for the differentiation purpose.

Clustering of AE data acquired during test could be achieved by the application of unsupervised pattern recognition algorithms. The unsupervised algorithms are numerical methods for the partition (grouping) of N patterns (hits/signals) to M classes/categories, without *a-priori* information on the number of classes and class characteristics. Unsupervised algorithms are used to overcome the difficulties arising from the human's inability to visualize the geometrical properties of the data in a multidimensional space and to help the analyst discover the structure of the data by identifying families of patterns (and the respective hits/signals) with similar characteristics. There are seven unsupervised pattern recognition algorithms that use similarity criteria to perform a partition of the AE data into classes (also called clusters): K-means, Max-Min Distance, Forgy, Cluster Seeking, Isodata, CAM and L.V.Q. Net. In addition, there are three supervised pattern recognition methods including k-Nearest Neighbor Classifier (k-NNC), Linear Classifier (Linear) and the BP Multi-Layer Neural Network (Back Propagation).

The K-means clustering method is selected after obtaining comparable clustering results as with the other methods but with less effort. K-means is a simple iterative algorithm, aiming to minimize the square error for a given number of clusters. The algorithm, starting with the initial clusters specified, assigns the remaining points to one

of the predefined clusters by nearest neighbor classification. The cluster centers are updated and the process continues until none of the patterns changes class membership. In K-means, the resulting number of clusters is equal to the specified number of initial clusters; this number may differ from the specified number of initial clusters for other unsupervised methods.

One set of AE data (PAC .dta file) of a specimen tested is loaded into NOESIS v3.3 and opened as Working Copy of the Main Data Set. The obviously invalid data points, such as those acquired after the specimen has broken or introduced by electromagnetic noise are deleted. Such data points would disrupt the legitimate classification of valid data. Before clustering this set of data, preprocessing by carefully selecting the acquired features to be used to separate the data into clusters is necessary and critical. The correlation hierarchy of all recorded features is examined and nine highly correlated features/parameters are selected: load, counts, counts to peak, duration, amplitude, energy, risetime, signal strength and absolute energy. Some features that are uniformly distributed, such as channel number and ASL, or calculated from other features, or without any cluster tendency, are excluded. Also, frequency-related features are not considered for all AE data sets since it is out of the scope of this research. Through an iterative selection of the number of initial clusters, a desired clustering scheme of K-means unsupervised algorithms could finally be achieved.

Upon acceptance and validation of clustering results, the Main Data Set which includes the resulting partitioning can be used as the training and/or testing set and to find similar classes on new AE data of other specimens. This process is called supervised pattern recognition and involves the training of a classification method. To do this,

supervised pattern recognition algorithms need to be trained to recognize the original classes and, once the training is completed within satisfactory error margins, be applied to classify new data. This allows the user to discover if classes of particular interest (found in the original data) also exist in any new data set. Three types of supervised algorithms are included in NOESIS: k-NNC, Linear and BP net. The k-Nearest Neighbor Classifier (k-NNC) is selected, which is a simple distance-based algorithm and its performance depends mainly on the completeness and accuracy of the training set. This algorithm classifies the unknown pattern to the class label most frequently occurring among the k-nearest samples. NOESIS implements several strategies for the dynamic creation of training/testing sets and the Interlaced Half method, where odd Main set items are used to train, while even ones are used to test the method, is employed here. The user then can train the method and evaluate its classification efficiency. The outcome k-NNC classifier is then ready for subsequent use with unknown data sets, called Usage Sets. It is then possible to compare those clustered data sets from similar-in-nature AE testing and inspect the repeatability of the test results and also the accuracy of the clustering method adopted (NOESIS v3.3 REFERNCE MANUAL, 2001).

Before analyzing and clustering the AE data from the studied five co-cured composite joints or laminate, two narrow zero-degree unidirectional laminates $[0]_8$ (called SU) were tested following the same testing procedures as for other specimens and also following the same clustering process as stated above. Due to capacity limitation of the load cell of the MTS machines used, the 8-ply standard-sized straight laminate SU with one-inch width could not be loaded to failure and it is impossible to see some critical damage and failure modes in this particular case. The dimensions of the two narrow specimens are:

1.20mm x 11.44mm x 25.4mm; 1.21mm x 11.50mm x 25.4mmm. Both tests were interrupted by the occurrence of longitudinal splitting and the MTS machine was stopped. No fracture of specimens was observed even for these specimens with smaller cross-sectional areas. However, these testing results are still useful in testing the clustering method adopted. The AE data from the first test was used to train an unsupervised classifier which was then applied to classify the second test data (supervised) of the same type of specimen.

Altogether, eight sets of unsupervised and supervised clustered plots of parametric distributions and correlations are originally made for these two tests:

1. Counts vs. Load
2. Cumulative Counts vs. Load
3. Amplitude vs. Load
4. Duration vs. Amplitude
5. Counts vs. Amplitude
6. Risetime vs. Load
7. Duration vs. Load
8. Counts vs. Duration

As a reference for clustered data, one set of plots of original data between Counts and Load are also included. During the process of training the unsupervised K-means classifier, it was found that some features/parameters like counts and duration are highly correlated. Finally, five sets of plots are chosen in order to show the most useful information and to avoid the repetition:

1. Counts vs. Load (original)
2. Counts vs. Load (clustered)
3. Cumulative Counts vs. Load (clustered)
4. Amplitude vs. Load (clustered)
5. Duration vs. Amplitude (clustered)

These five sets of plots of the tested two zero-degree unidirectional laminates (SU) are shown in Figures 7.17-21 with the top plot for test 1 and the bottom one for test 2 in each figure. Due to the longitudinal splitting, the first test was interrupted before 18 kN and the second test interrupted even earlier before 6 kN. This phenomenon has already been reported by others when testing this type of laminate. It is known that the shearing strength in $[0]_8$ laminate is much lower than its longitudinal strength and also the fibers near the specimen edge have free boundary therefore with less constraint. The reason for the earlier interruption of the second test is assumed to attribute to the improper preparation of that specimen in tabbing and the possible misalignment in the grips.

Figure 7.17 displays the original AE data of counts vs. load before clustering and the similar test data could be found in Figure 6.1 where four counts vs. load plots of one-inch wide SU laminates are listed. Figure 7.18 shows the same data but being clustered into four groups by the selected clustering method. From the clustered plot of test 1, the most interesting data are those three strips in purple which correspond to loads of around 12 kN, 14 kN and 17 kN respectively. Only one strip in purple is observed on the plot of test 2 nearby the final stage. These burst-type of data are believed generated by the longitudinal splitting, since it was observed by naked eye during the test that a piece of

specimen about 2 mm wide split from the tab region and the split propagated along the longitudinal or loading direction. The remaining data includes the majority in red with counts lower than 50 and few low-counts data in green and blue. The cumulative plots of these clustered data are shown in Figure 7.19 for both tests and it seems they share the similar distribution trend for those clustered data though with different loading duration. As reported in the literature by other researchers, loading this $[0]_8$ laminate monotonically will lead to some micro damage mechanisms such as micro matrix cracking within matrix between fibers and also fiber/matrix debonding before the final macro damage mechanisms like longitudinal splitting and fiber fracture happen. According to this, the red and green curves in the cumulative plot may represent those micro activities while the purple curve may represent longitudinal splitting. The few blue data may correspond to some noise which can not be identified here.

Figure 7.20 gives the plots of amplitude vs. load which discriminate the data according to amplitude level. It is seen that the majority data in red occupies the amplitude from 45 dB to 75 dB; the green cluster has amplitude below 61 dB and the purple cluster from splitting occupies the range of amplitude from 45 dB to 99 dB. This implies that one AE feature/parameter may have different values for the same damage mechanism at the same or different loading. It depends on the type of damage mechanism and its stage when this happens. Comparing data in Figures 7.20 and 7.21, it can be seen that the high-amplitude data also has high duration and most data has short duration below 320 μs. The data from the red cluster and the most data from the purple cluster overlap each other at low-duration range for both test results.

Overall, the selected classifier is efficient and successful. It on one hand discriminates the data of test 1 into several meaningful sets; on the other hand, it shows longitudinal splitting also occurs in test 2 of the same type of specimen with the trained clustering method.

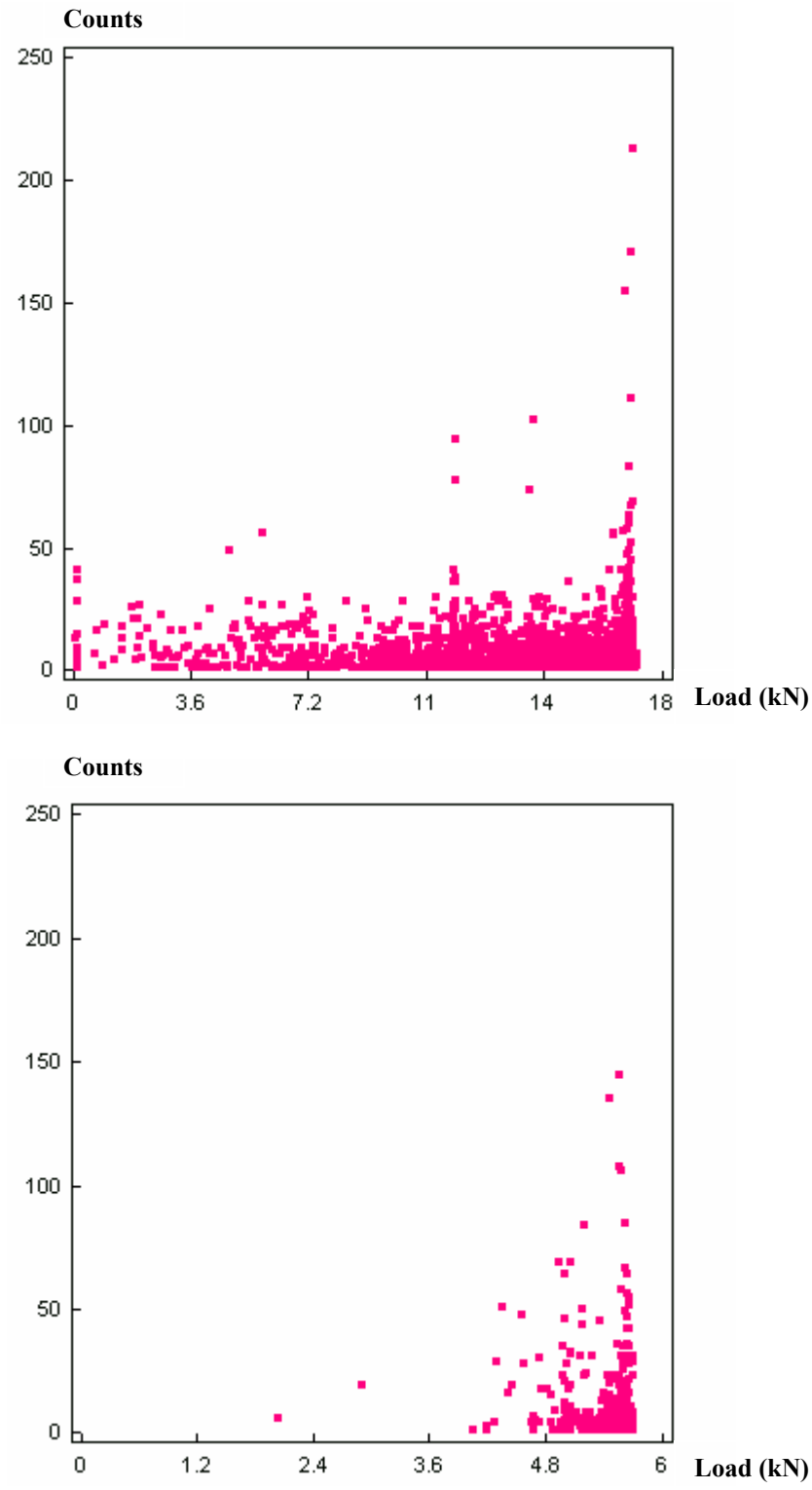

Figure 7.17 Original data of SU laminates – counts vs. load.
(top: test 1; bottom: test 2)

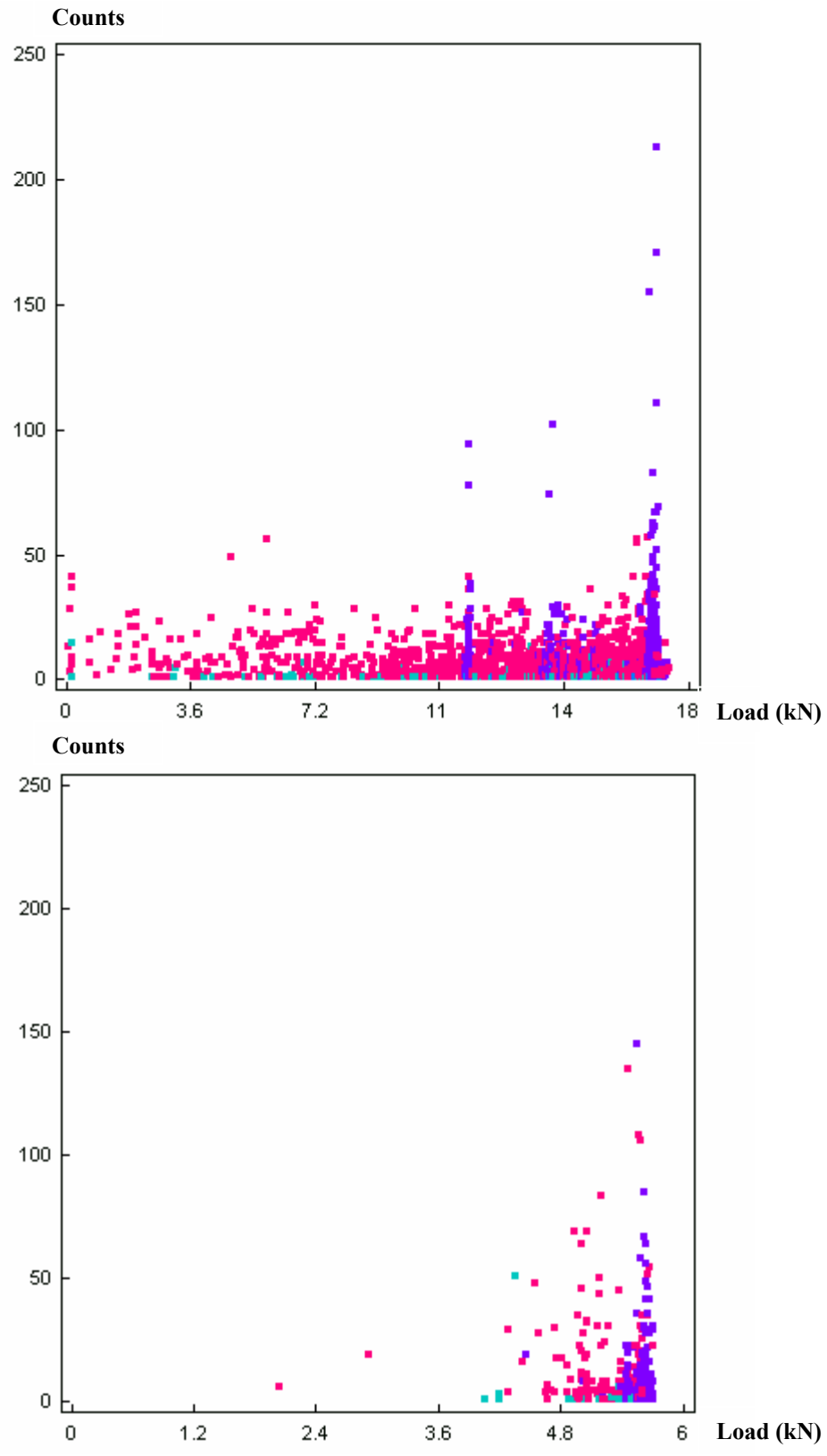

Figure 7.18 Clustered data of SU laminates – counts vs. load.
(top: unsupervised; bottom: supervised)

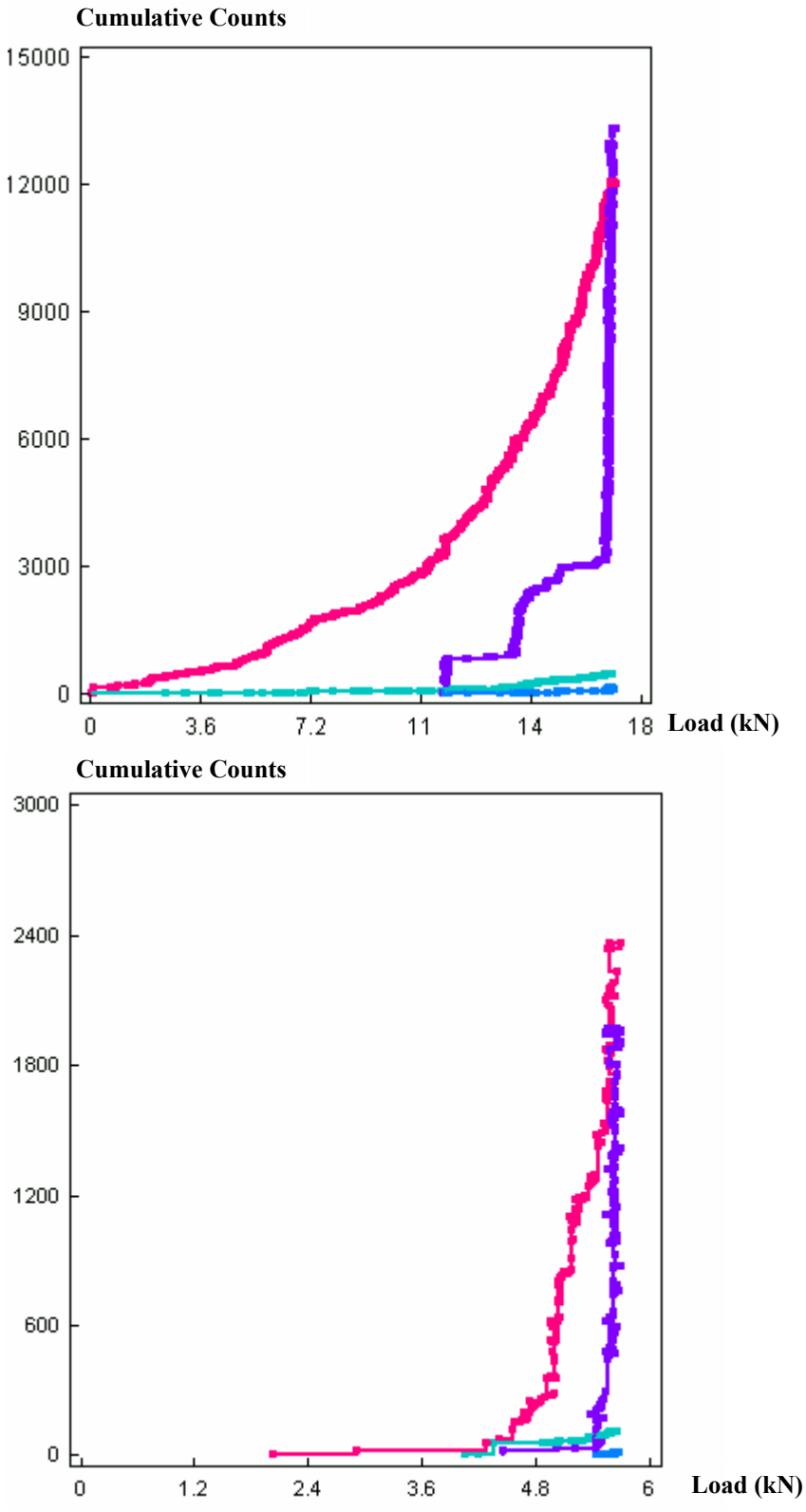

Figure 7.19 Clustered data of SU laminates – cumulative counts vs. load.
(top: unsupervised; bottom: supervised)

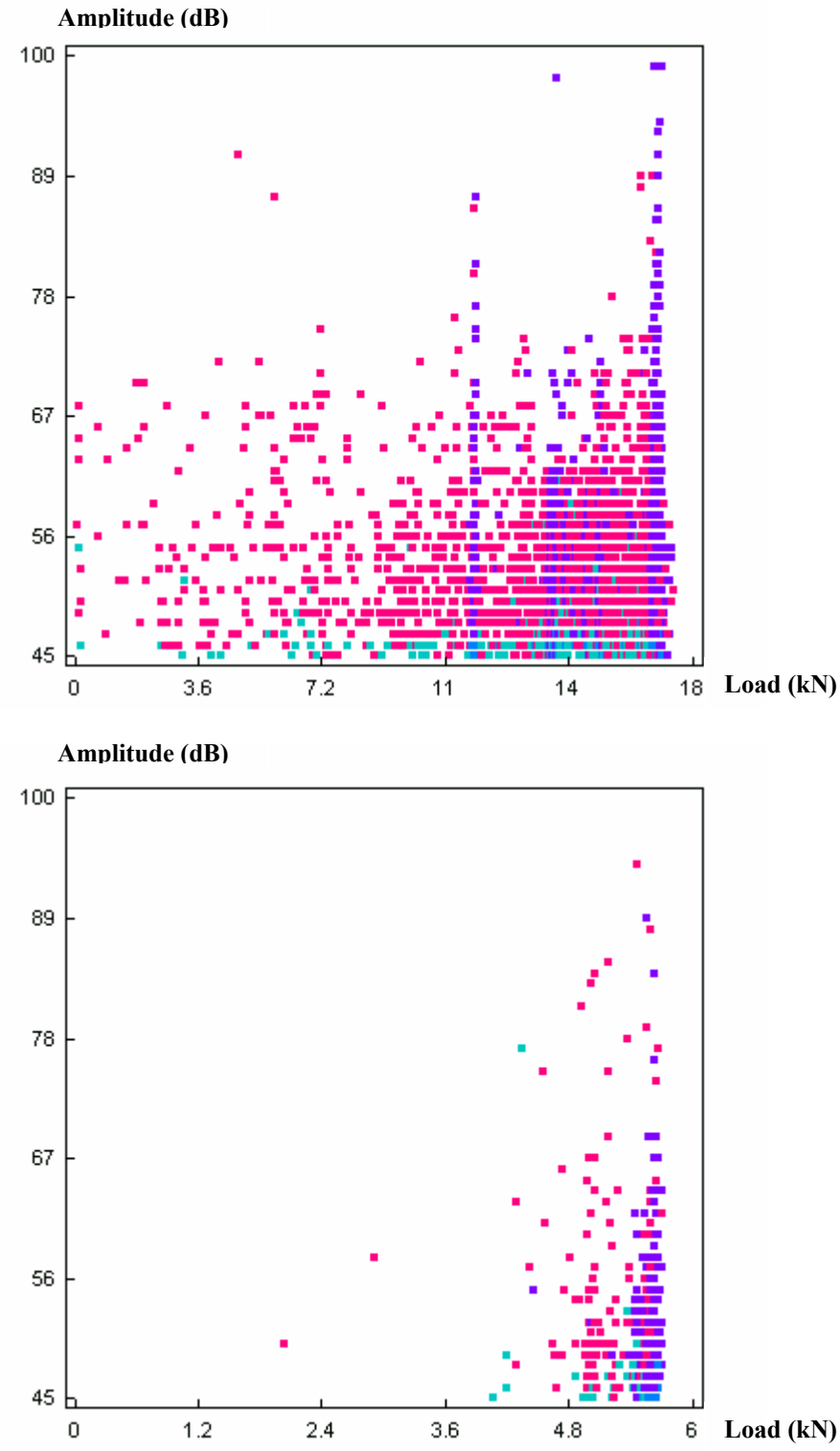

Figure 7.20 Clustered data of SU laminates – amplitude vs. load.
(top: unsupervised; bottom: supervised)

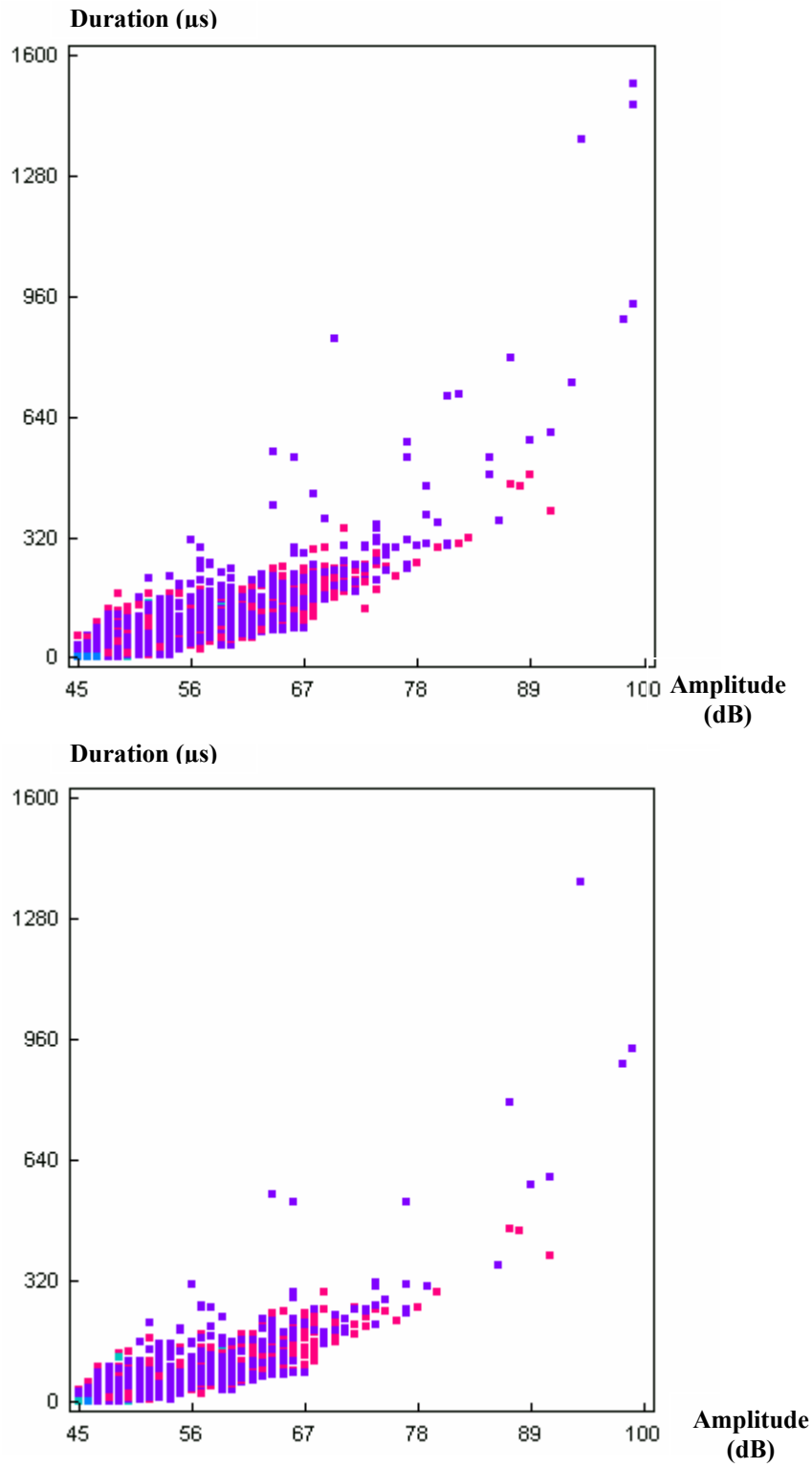

Figure 7.21 Clustered data of SU laminates – duration vs. amplitude.
(top: unsupervised; bottom: supervised)

The following part will further analyze the acquired AE data from a different point of view by using the selected clustering procedure tested for the SU laminate. The goal is to establish correlations of the respective AE clusters with particular damage and failure mechanisms by combining the physical damage observations obtained using alternate techniques (X-ray Radiography and Optical Microscopy).

As mentioned before, four specimens were tested for each case (SQ, NQ, LQ, LU and NU) and three sets of AE data are selected and studied. One data set will be used to train and test the k-NNC classifier and the other two data sets as usage sets will be clustered using that classifier. Similar to the SU laminate, five sets of plots of parametric distributions and correlations are made for each case including one set before clustering and four being clustered. All these plots will be analyzed and also compared among the same group like "U" group and "Q" group. Interpretations of the results will be included at the end of this chapter.

As a reference case, SQ exhibits the most extensive and progressive damage events with almost all types of major failure mechanisms including micro/macro matrix cracking, delamination initiation and propagation and fiber breakage as observed using Optical Microscopy and X-ray Radiography in Chapter 6. Since there is no joint part in SQ, it may be easier to start with this simpler configuration in the effort to differentiate the mechanisms by the adopted AE clustering method.

Three original data plots of counts vs. load from selected three SQ specimens are depicted in Figure 7.22 with very similar data distribution shape. The maximum counts number is lower than 200 and more intense data start from around 13 kN as also observed in the previous section of this chapter. Figure 7.23 shows the same data sets but being

clustered into four groups by the selected clustering method. From these plots, it can be seen that the green cluster with counts lower than 40 covers the whole loading history, while the data of other clusters in red, blue and orange with higher counts only appear after 13 kN. As it can be seen this is true for all three tested specimens; it once again proves the good repeatability of test results and also the success of the clustering method.

From the clustered plots of cumulative counts vs. load, the data distribution is even clearer (Figure 7.24). Four colored curves represent four clusters; the percentage of the data within each cluster is also included on each plot. They have very close percentages for each cluster for those three sets of data. For the total counts, more than 93% is from the green cluster, about 5% from the red cluster, less than 2% from both the blue and orange clusters. It is very clear that data in the green cluster starts almost from the beginning of loading, while data in red starts from around 13 kN and data in blue stating from 14 kN and 18 kN. This could be correlated very well to the damage mechanisms observed before (Figures 6.23 and 6.24). The green cluster could be related to micro matrix cracking and other small damage activities accompanying those macro damage developments through the whole loading process; the red cluster is for macro matrix cracking especially between 13 kN and 20 kN and the blue cluster for delamination which starts from 15 kN as shown in the microscopic photos (Figure 6.24). The few data in orange may come from fiber fracture.

Figure 7.25 shows the plots of amplitude vs. load. The low amplitude AE signals in the green cluster (between 45 dB and 79 dB) dominate the AE activities in SQ laminates which correspond to micro matrix cracking and other accompanying small damage events like fiber/matrix debonding. The medium-amplitude AE hits in red between 65 dB and

92 dB starting from around 13 kN should belong to the initiation/evolution of macro matrix cracking. The blue cluster with amplitude from 79 dB to 95 dB is assumed for free edge delamination initiation from matrix crack tip and propagation as mentioned in last paragraph. The high-amplitude events (between 92 dB and 99 dB) in the orange cluster are related to the fiber breakage. Some of these results could be confirmed by Hill *et al.* (1996).

Duration is defined as the time from the first to the last threshold crossing for each hit. It is already mentioned before that a high correlation exists between AE parameters counts and duration; in other words, the higher counts the higher duration. Sometimes, this is also true: the higher amplitude the higher duration. Three good examples of correlation of duration and amplitude are found in Figure 7.26. Each cluster occupies a zone with a specific amplitude and duration band. Once again, the low-duration green cluster is for micro matrix cracking, the medium-duration red cluster is for macro matrix cracking, the high-duration blue cluster is for delamination and the orange cluster for fiber breakage.

Overall, those AE data in SQ are differentiated and could be related to four damage mechanisms as follows:

Green cluster - micro matrix cracking, from zero loads to failure, 45-79 dB;

Red cluster - macro matrix cracking, from 13 kN to failure, 65-92 dB;

Blue cluster - delamination, from ~15 kN to failure, 79-95 dB;

Orange cluster - fiber fracture, mainly from 15 kN to failure, 92-99 dB.

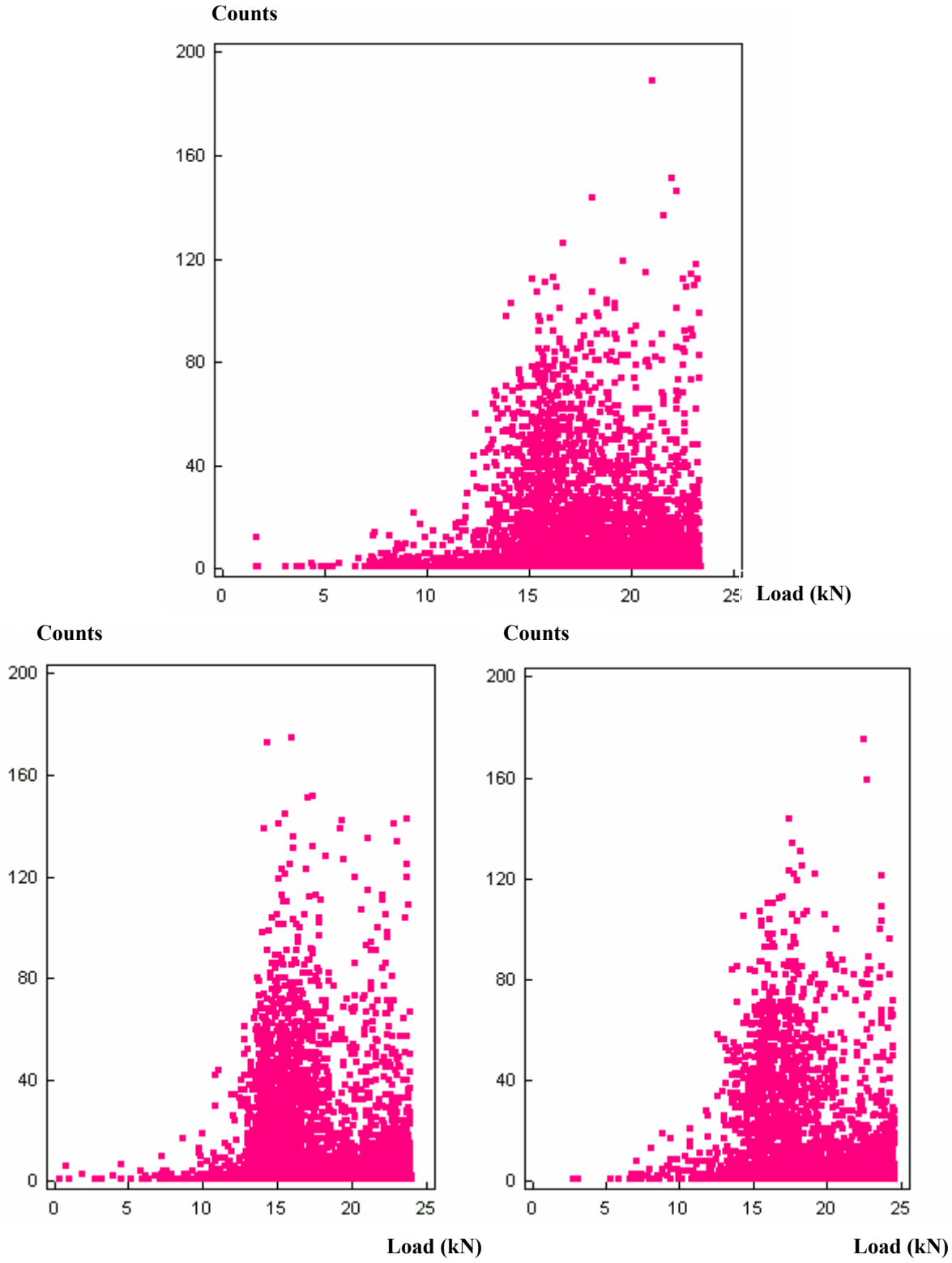

Figure 7.22 Original data of SQ laminates – counts vs. load.
(top: test 1; bottom: test 2 and 3)

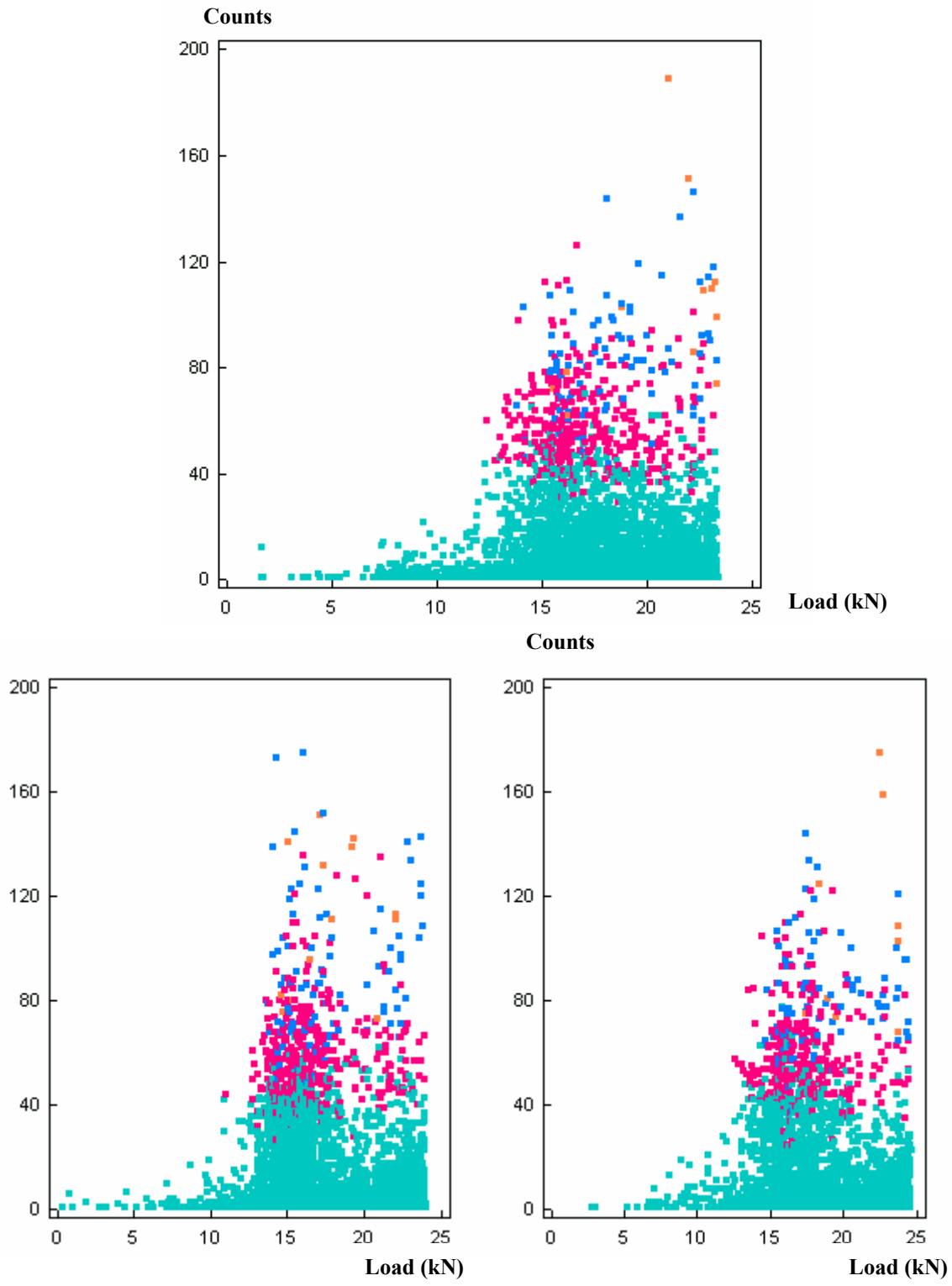

Figure 7.23 Clustered data of SQ laminates – counts vs. load.
(top: unsupervised; bottom: supervised)

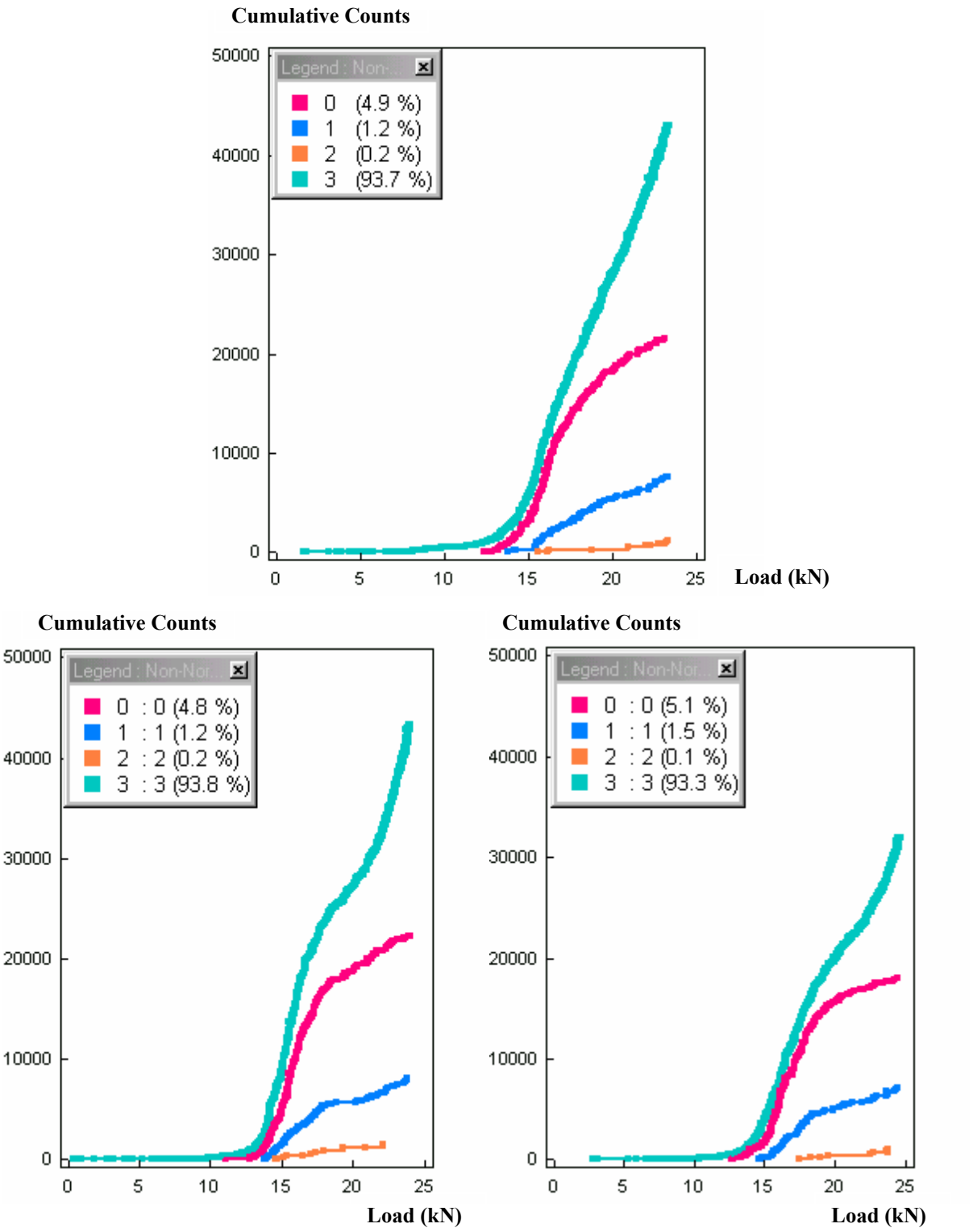

Figure 7.24 Clustered data of SQ laminates – cumulative counts vs. load.
(top: unsupervised; bottom: supervised)

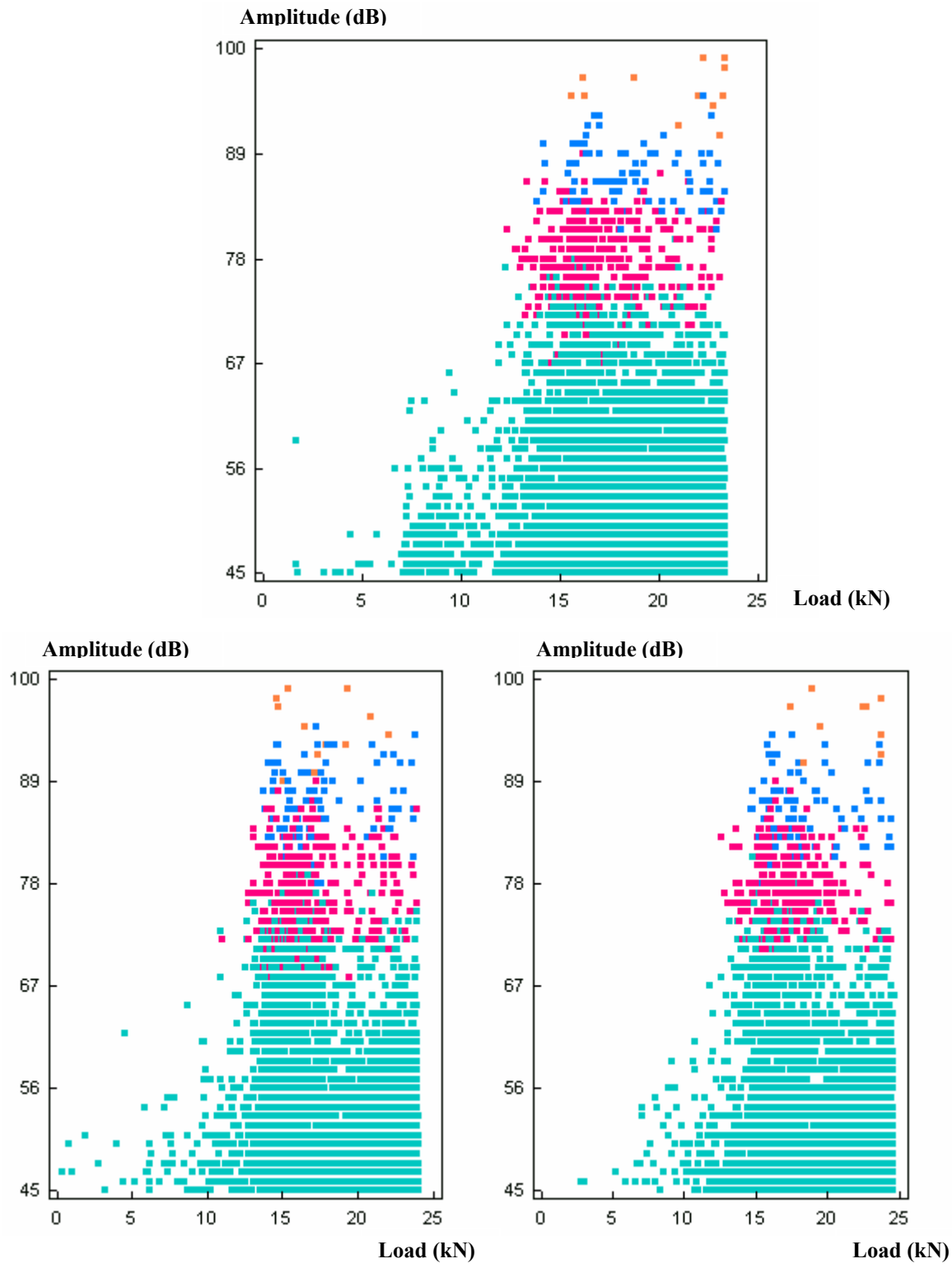

Figure 7.25 Clustered data of SQ laminates – amplitude vs. load.
(top: unsupervised; bottom: supervised)

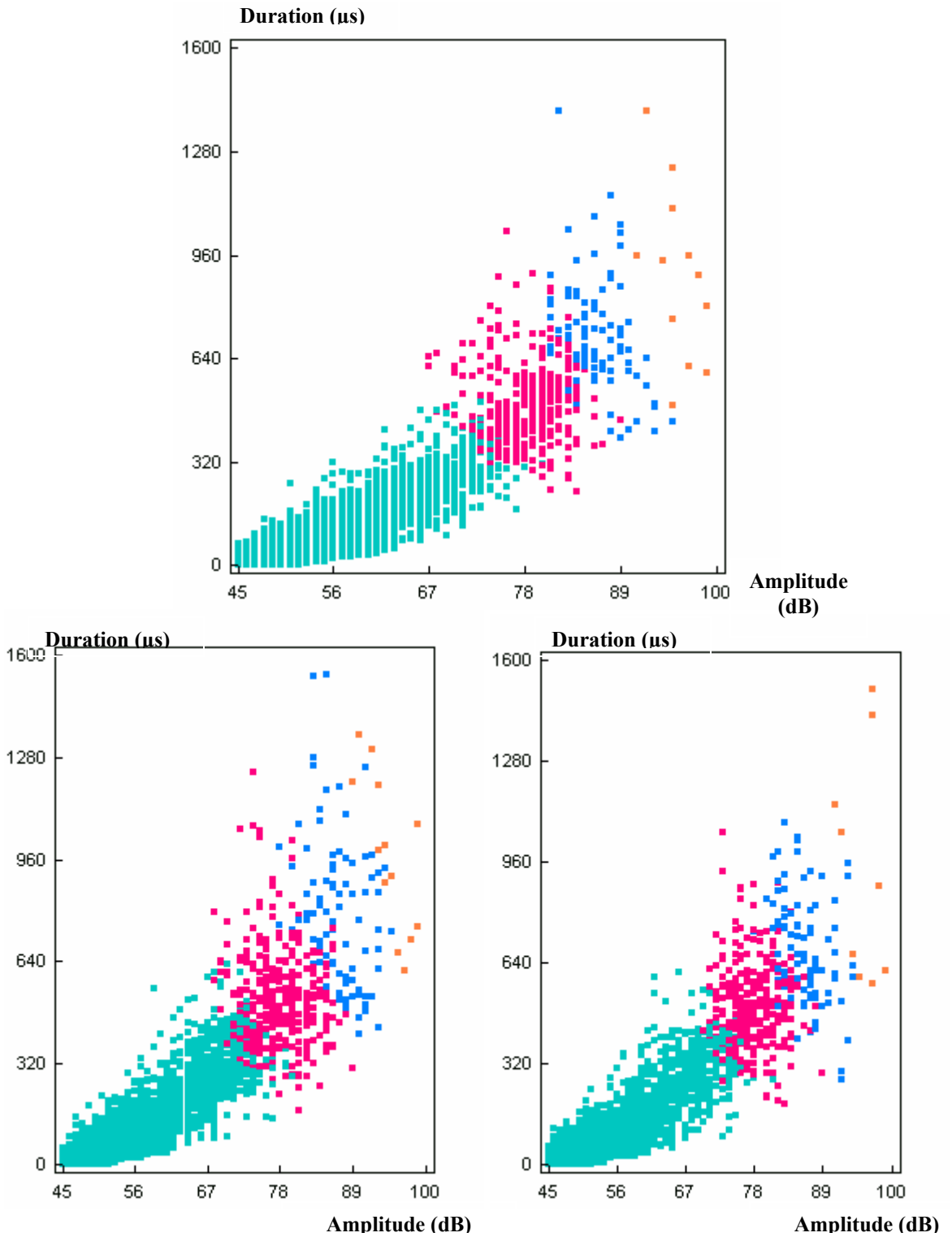

Figure 7.26 Clustered data of SQ laminates – duration vs. amplitude.
(top: unsupervised; bottom: supervised)

An NQ joint, modified from LQ by a single nested overlap within joint region shares the same quasi-isotropic lay-up as SQ. Besides, as observed before, NQ fails outside joint region and thus possesses the similar strength as SQ. Therefore, it is not surprising that AE data plots, both unclustered and clustered of three NQ specimens look very similar to those of SQ (Figures 7.27 to 7.31). It seems that the clustering scheme selected works very well for all NQ data sets. Due to the inclusion of a joint part, the progression of damage mechanisms at the same loading stage in NQ is not as extensive as for SQ (compare Figure 6.27 with Figure 6.23 in Chapter 6). High-counts, high-amplitude and high-duration events in NQ from those extensive macro damage mechanisms like matrix cracking and delamination are reduced (Figures 7.28, 7.30 and 7.31) and the total ringdown counts of each cluster are far lower than SQ.

Following the same analysis procedures as for SQ and in the meantime referencing the physical observations of NQ at different loads, AE signals are differentiated or classified into four clusters which could be related to four different damage mechanisms:

Orange cluster - micro matrix cracking, from zero loads to failure, 45-79 dB;

Blue cluster - macro matrix cracking, from 13 kN to failure, 69-90 dB;

Red cluster - delamination, from ~15 kN to 20 kN, 82-95 dB;

Green cluster - fiber fracture, mainly from 15 kN to failure, 92-99 dB.

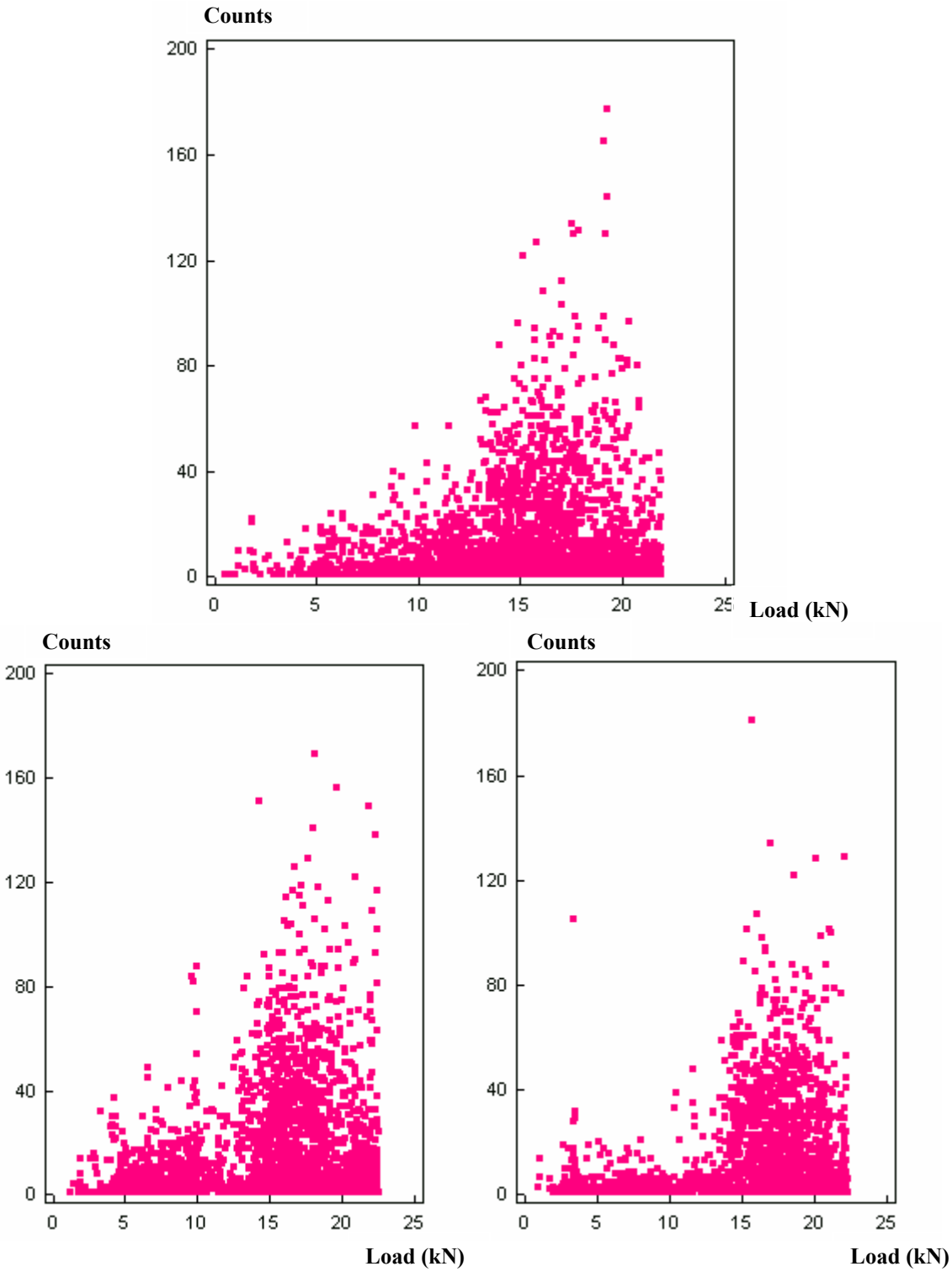

Figure 7.27 Original data of NQ joint specimens – counts vs. load.
(top: test 1; bottom: test 2 and 3)

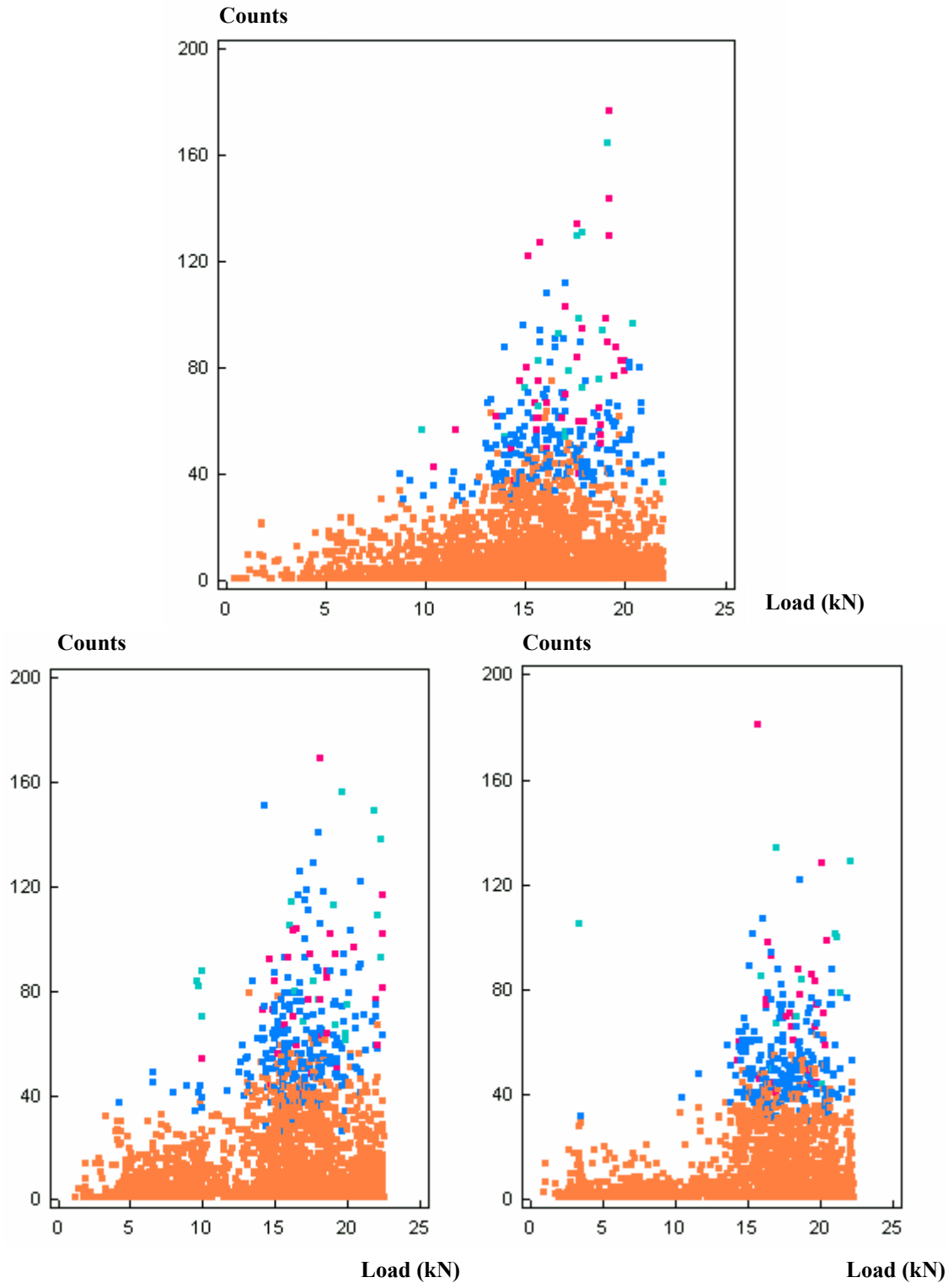

Figure 7.28 Clustered data of NQ joint specimens – counts vs. load.
(top: unsupervised; bottom: supervised)

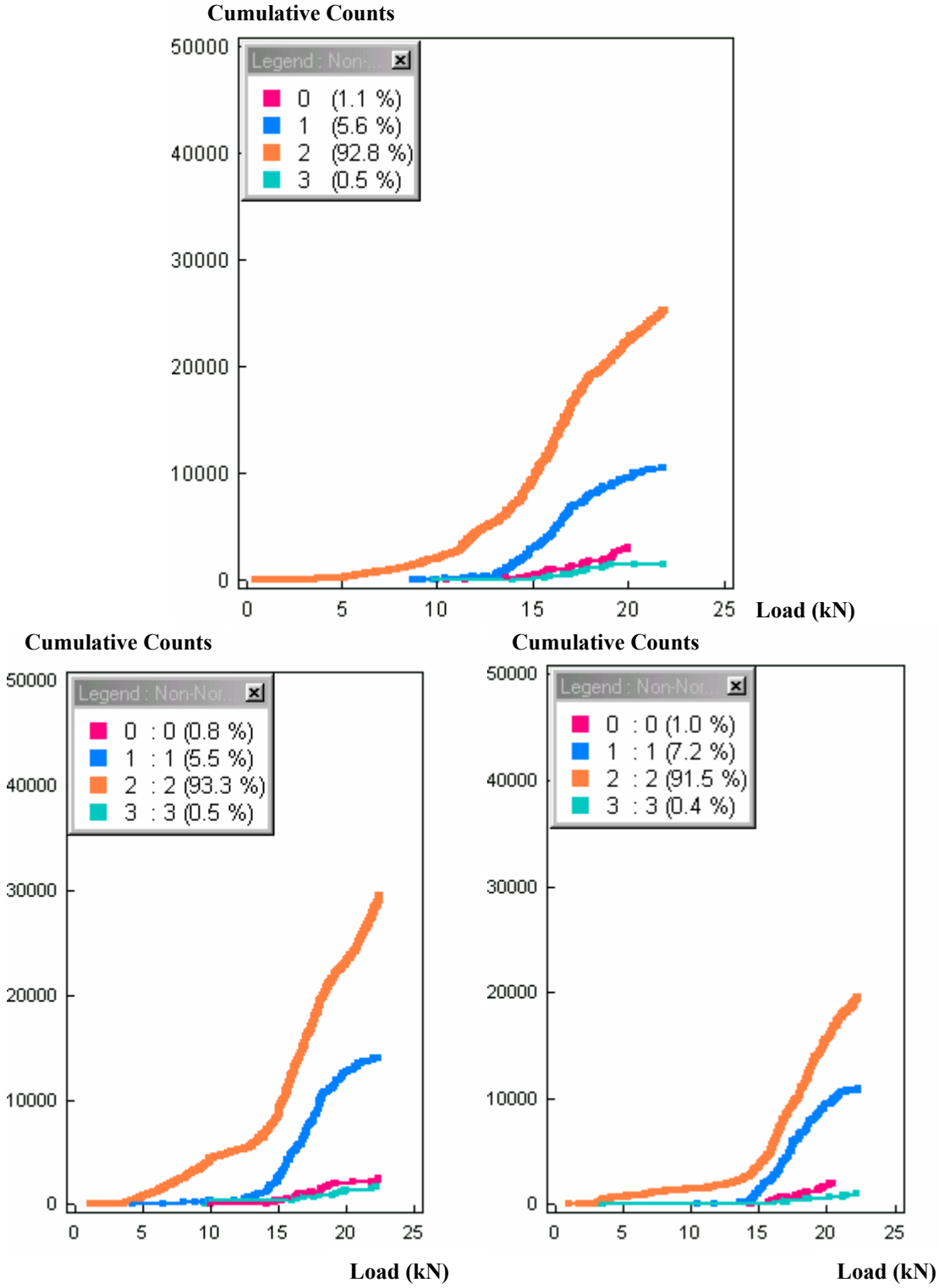

Figure 7.29 Clustered data of NQ joint specimens – cumulative counts vs. load. (top: unsupervised; bottom: supervised)

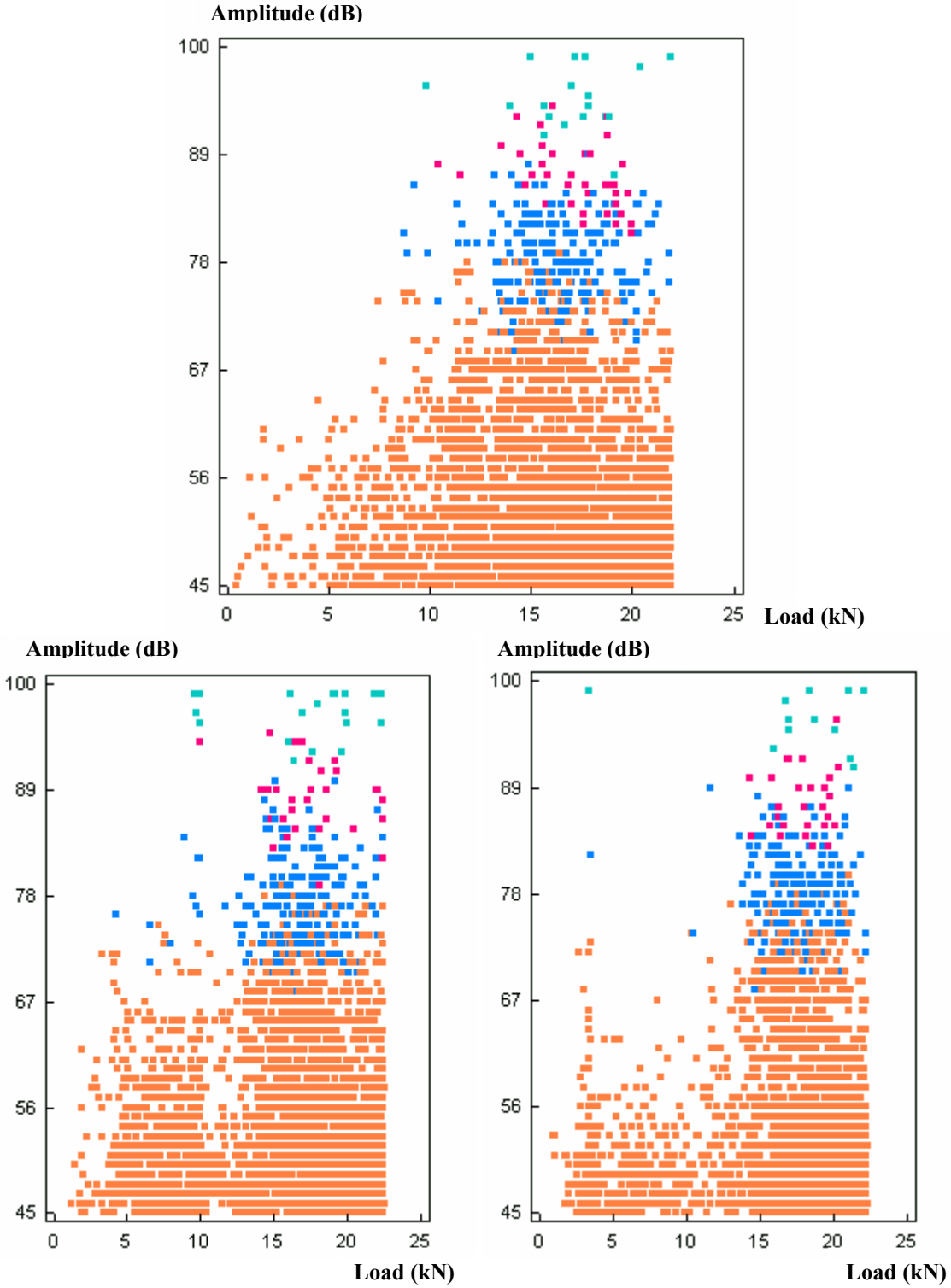

Figure 7.30 Clustered data of NQ joint specimens – amplitude vs. load.
(top: unsupervised; bottom: supervised)

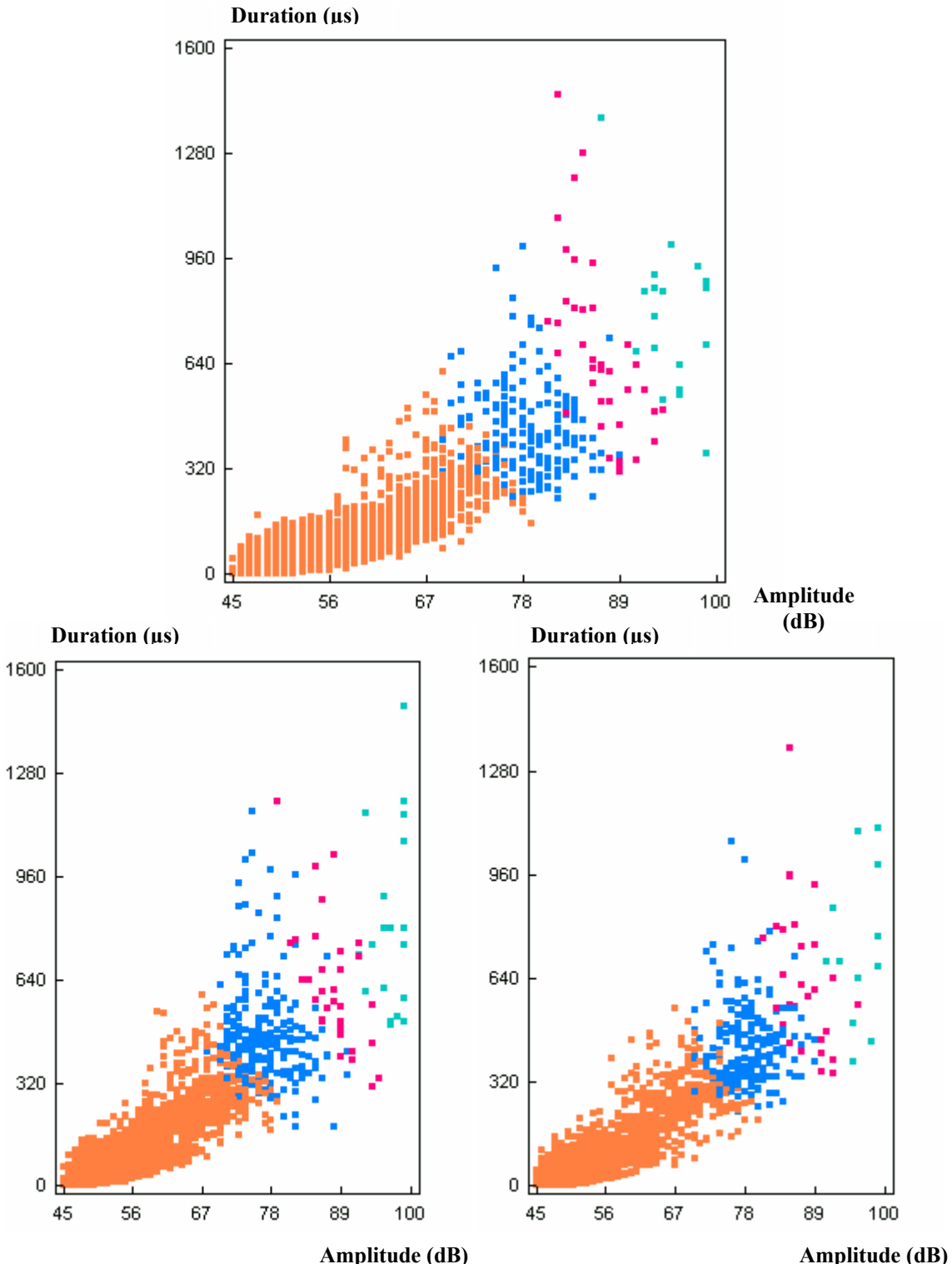

Figure 7.31 Clustered data of NQ joint specimens – duration vs. amplitude.
(top: unsupervised; bottom: supervised)

After analyzing both SQ and NQ, it is much more straightforward to differentiate the AE data from single lap joints LQ because fewer damage mechanisms are involved. It is known from the previous study that the LQ joint fails mostly in shear separation of two joint parts. The extensiveness of damage is very low; for example the crack density is smaller than both NQ and SQ at the same loading stage (Table 6.3). Not many macro matrix cracks or delaminations were observed from the specimen edges (Figure 6.25). This is confirmed by the AE data in Figures 7.33, 7.35 and 7.36 since there are very few high-counts, high-amplitude and high-duration events produced by those extensive damage mechanisms such as macro matrix cracking and delamination. LQ finally fails at the smallest load among "Q" group with almost no fiber fracture.

Though the same clustering procedure as for SQ and NQ is followed, LQ shows only three main clusters; Red, Orange and Green (Figures 7.32-7.36). The fourth cluster actually does not exist in this LQ joint and those few AE hits in blue could not be related to any type of damage mechanism.

Red cluster - micro matrix cracking, from zero loads to failure, 45-72 dB;

Orange cluster - macro matrix cracking, from 13 kN to failure, 62-81 dB;

Green cluster - delamination, from ~15 kN to failure, 72-91 dB.

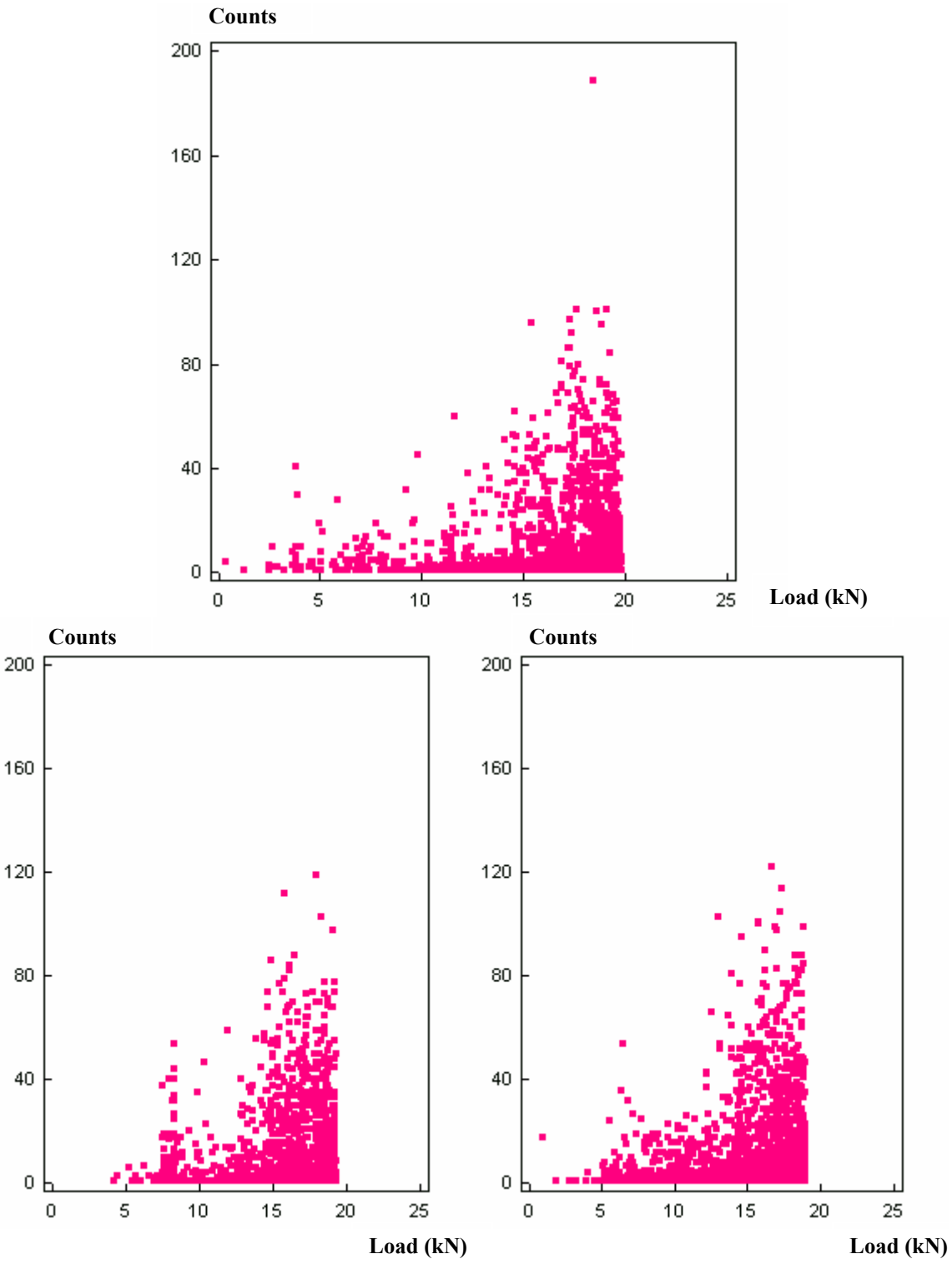

Figure 7.32 Original data of LQ joint specimens – counts vs. load.
(top: test 1; bottom: test 2 and 3)

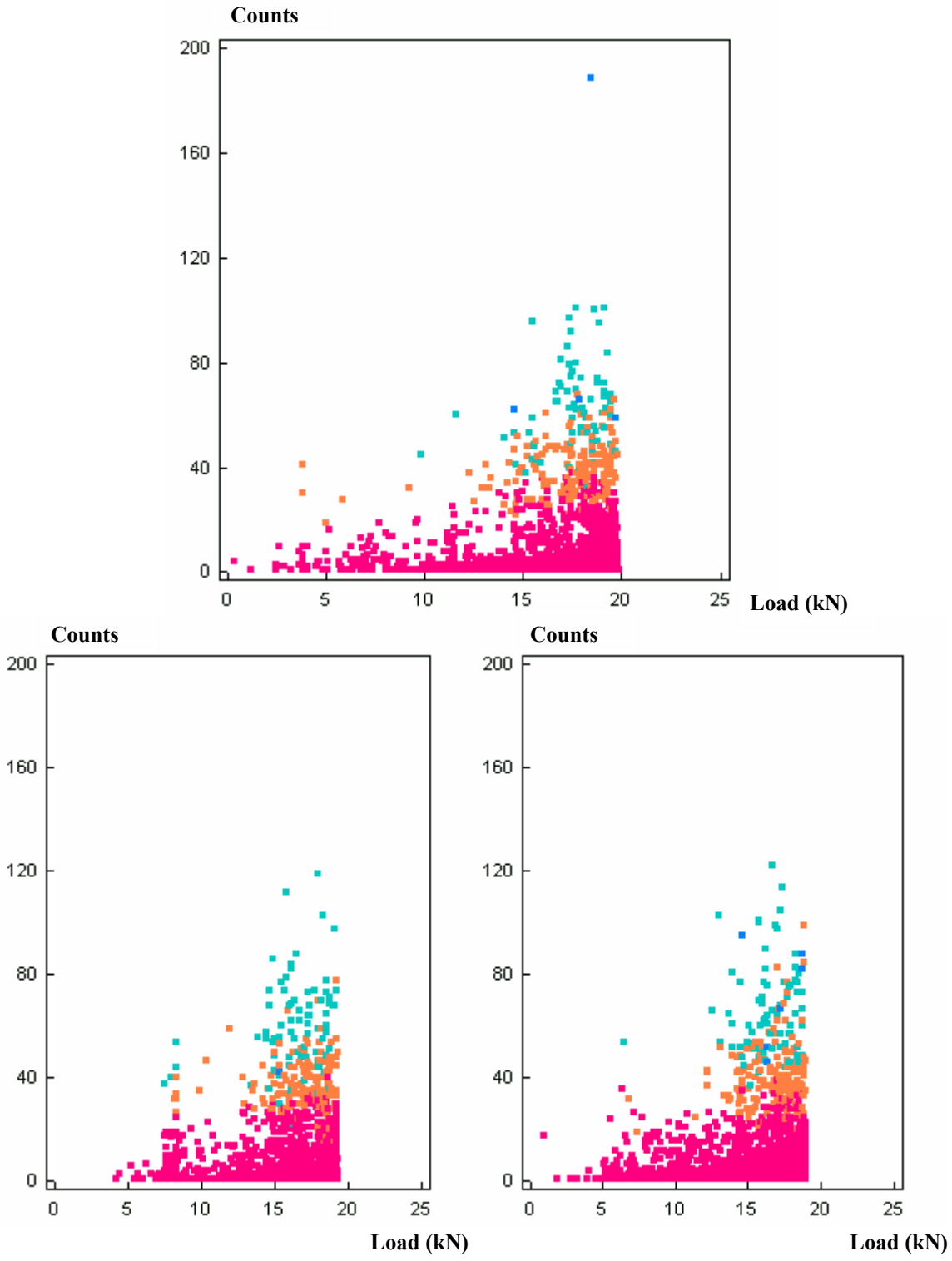

Figure 7.33 Clustered data of LQ joint specimens – counts vs. load.
(top: unsupervised; bottom: supervised)

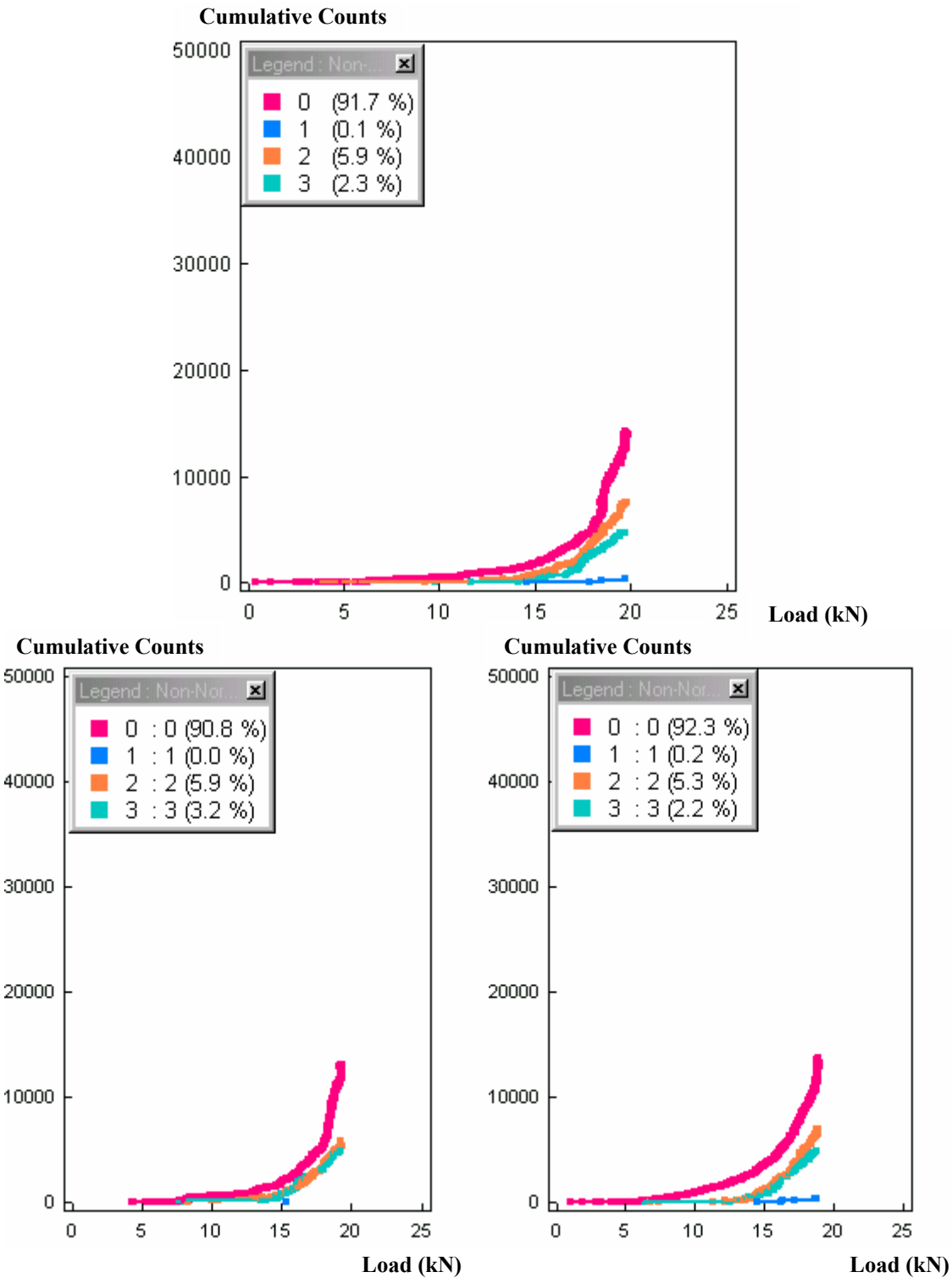

Figure 7.34 Clustered data of LQ joint specimens – cumulative counts vs. load.
(top: unsupervised; bottom: supervised)

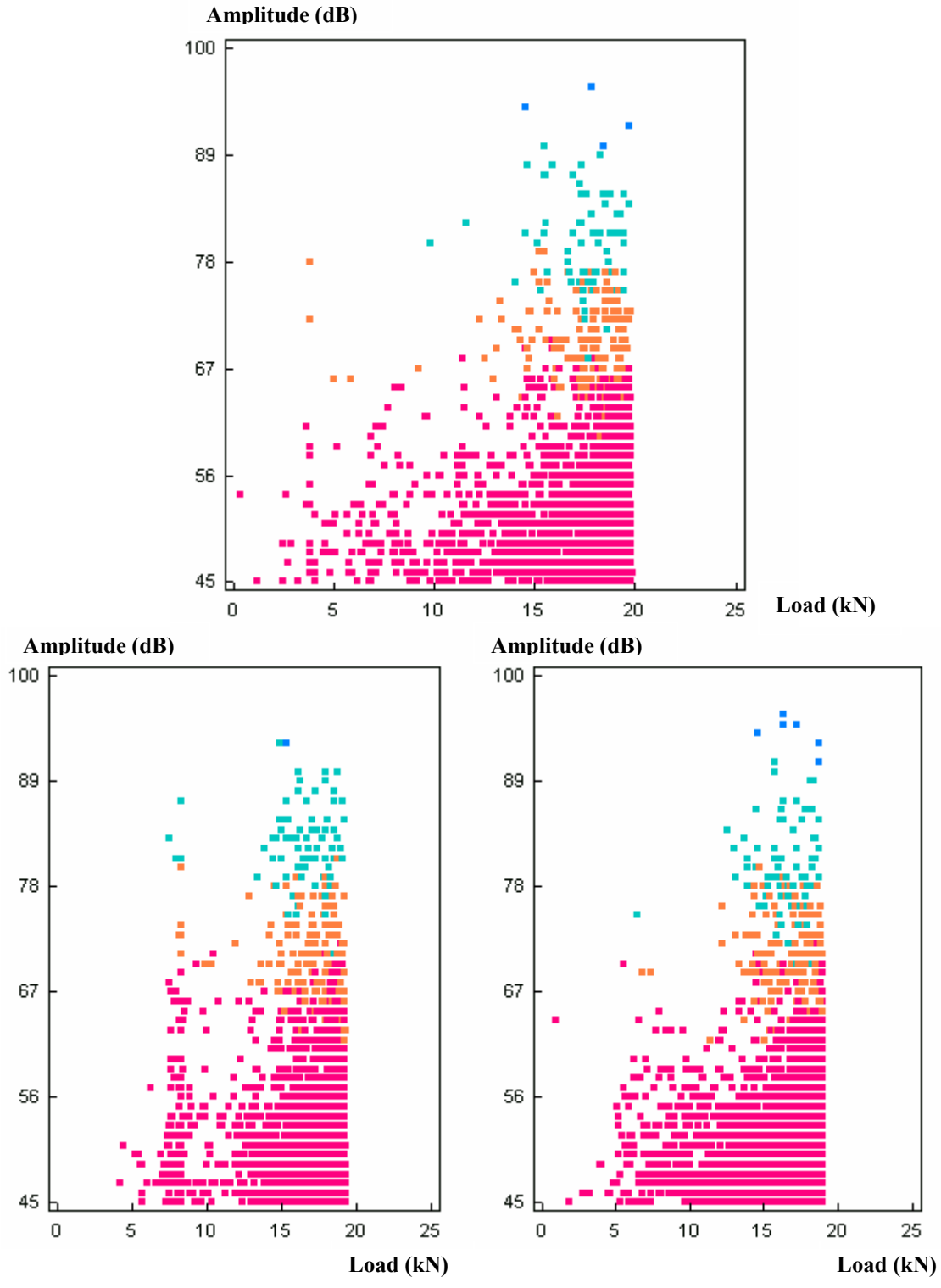

Figure 7.35 Clustered data of LQ joint specimens – amplitude vs. load.
(top: unsupervised; bottom: supervised)

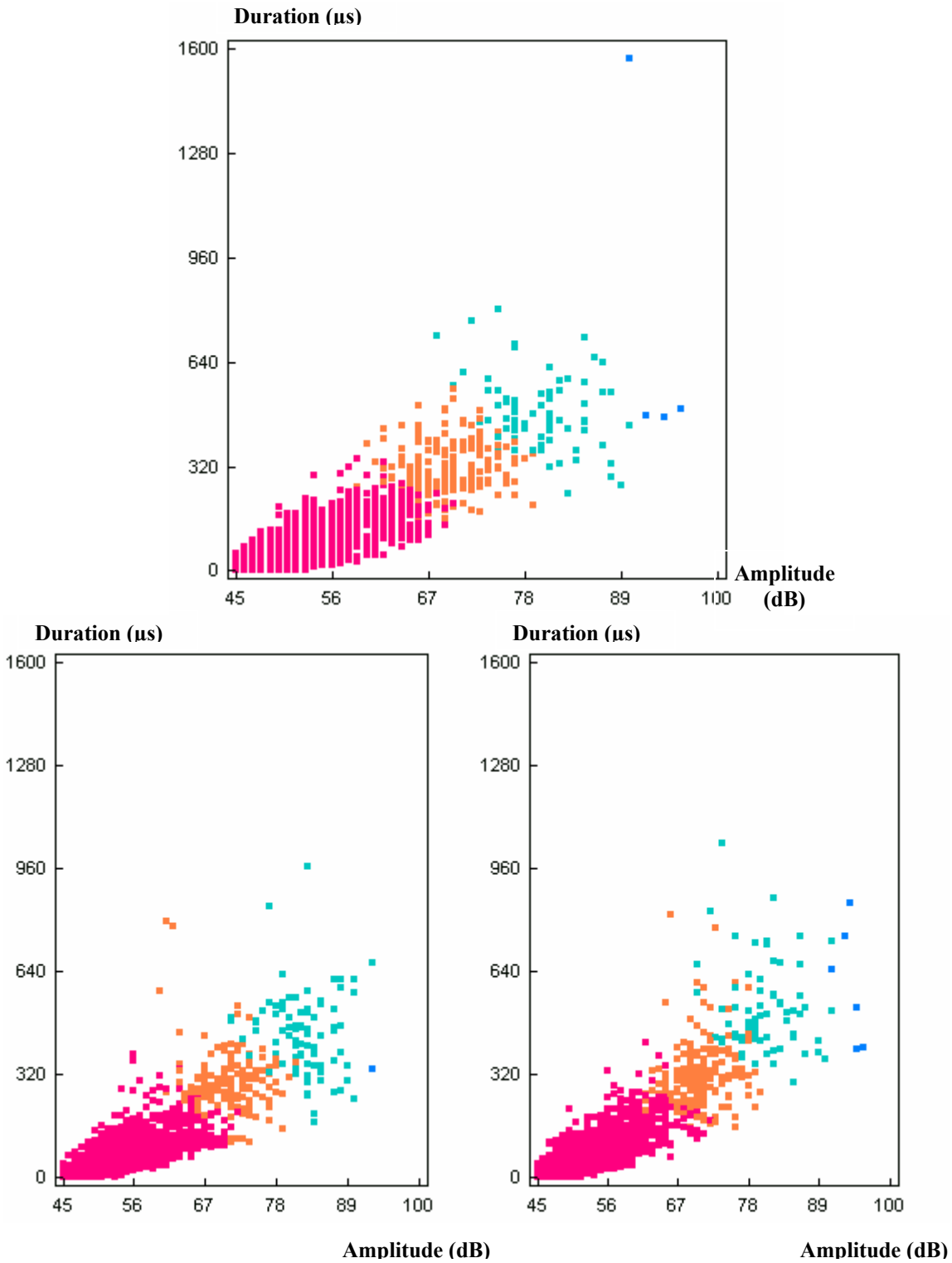

Figure 7.36 Clustered data of LQ joint specimens – duration vs. amplitude.
(top: unsupervised; bottom: supervised)

The joints made of zero-degree unidirectional fibers show very distinct damage mechanisms compared to those with quasi-isotropic lay-up as discussed in Chapter 6 for LU and NU. At early stages of loading, only micro matrix cracking and fiber/matrix debonding contribute to the low-counts acoustic emissions; the final failure of LU is more abrupt than NU while both with longitudinal splitting. This splitting event can be observed as a strip in Figures 7.37 and 7.38, which is already recognized in SU laminates (Figure 7.20).

From Figures 7.37 to 7.41, it can be seen that the scales of plots are all much smaller than those for "Q" group, which means the values of AE parameters are small like low-counts, low amplitude and low duration. Though the same clustering method is used, only three initial clusters are selected for unsupervised K-means before training the k-NNC supervised classifier. Finally, three clusters are resulted for each set of data of LU specimens and could be linked to three damage mechanisms:

Orange cluster - micro matrix cracking, from zero loads to failure, 45-61 dB;

Red cluster - fiber/matrix debonding, mostly from 9 kN to failure, 50-68 dB;

Blue cluster - longitudinal splitting, mostly at failure, 56-90 dB.

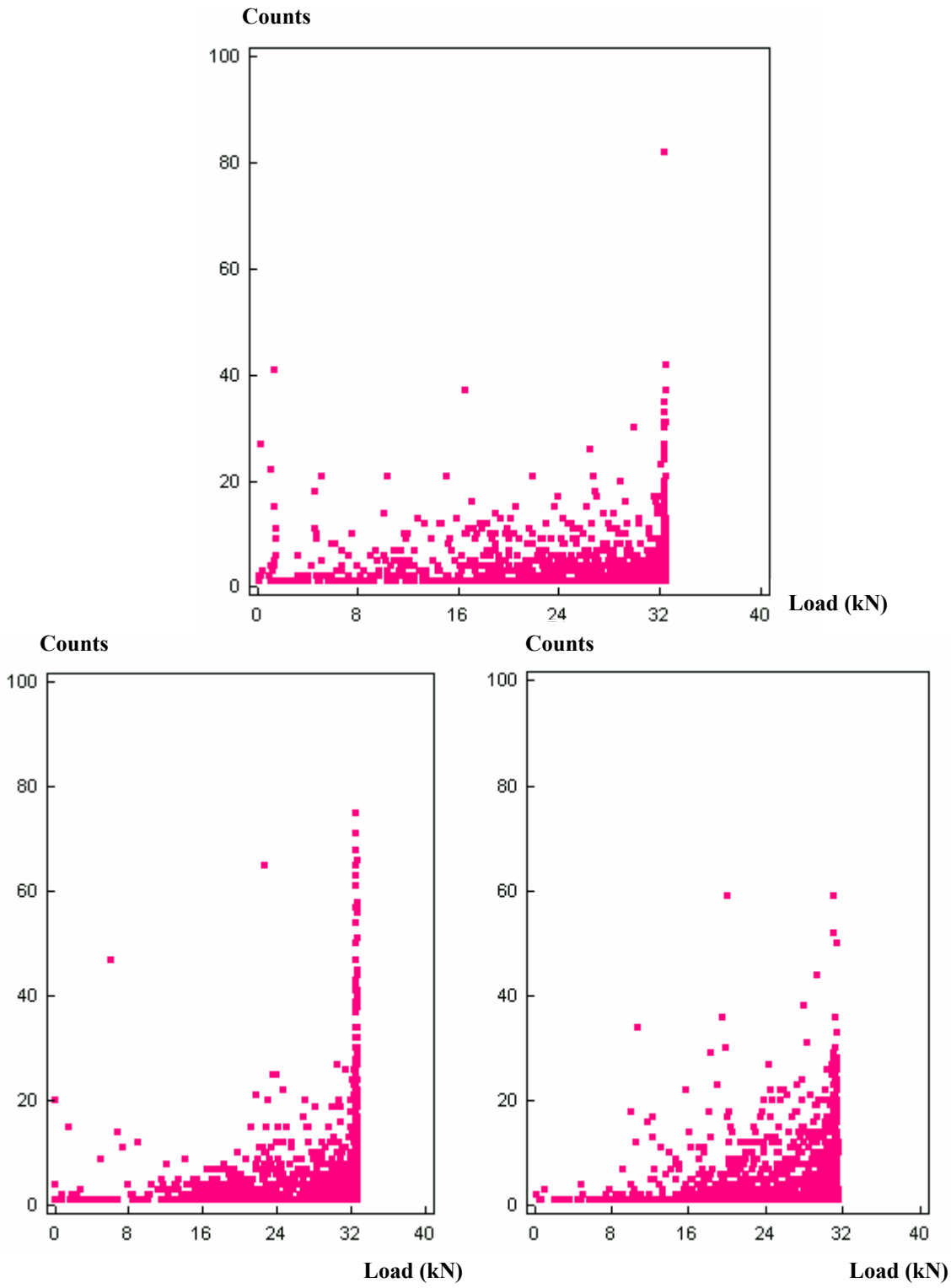

Figure 7.37 Original data of LU joint specimens – counts vs. load.
(top: test 1; bottom: test 2 and 3)

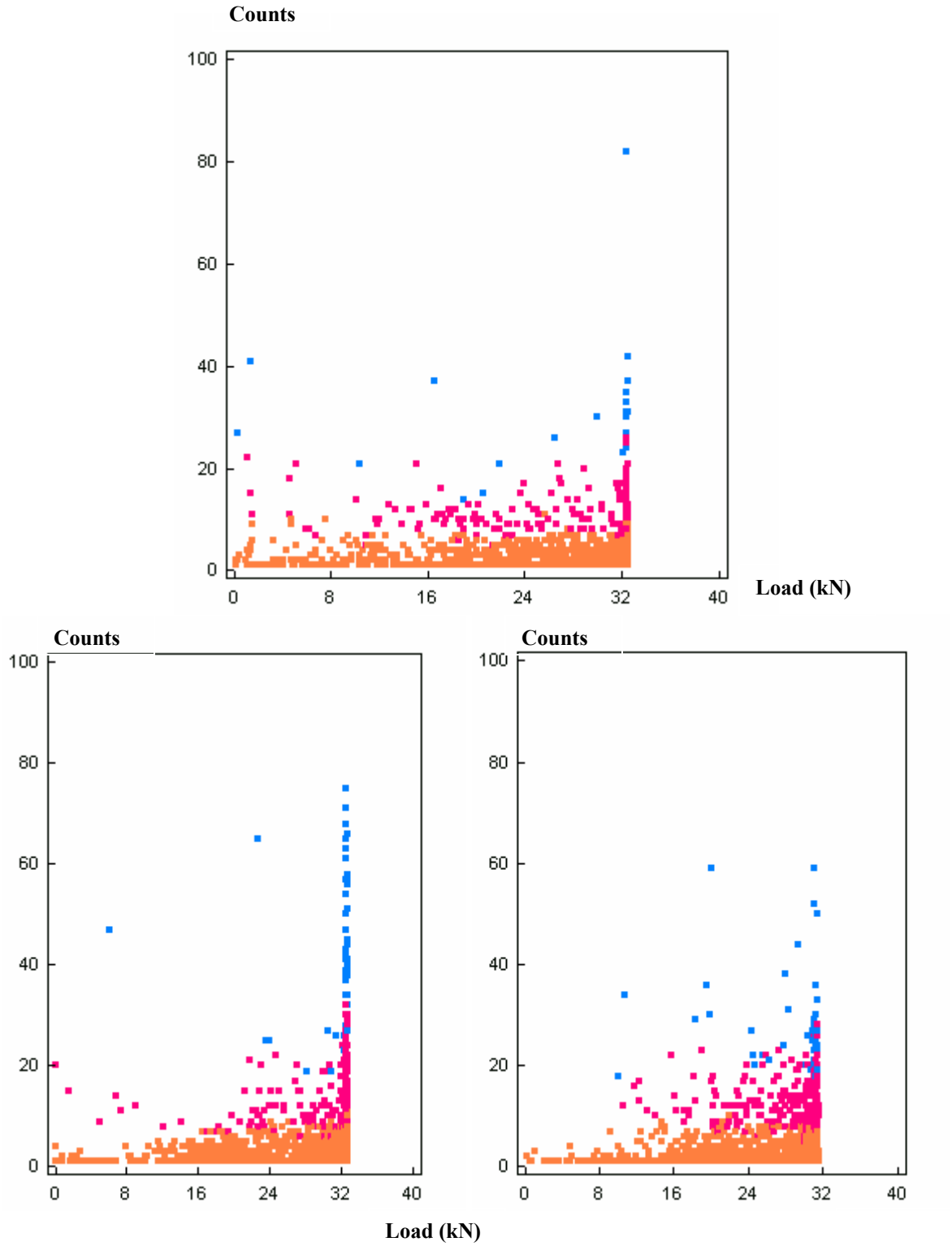

Figure 7.38 Clustered data of LU joint specimens – counts vs. load.
(top: unsupervised; bottom: supervised)

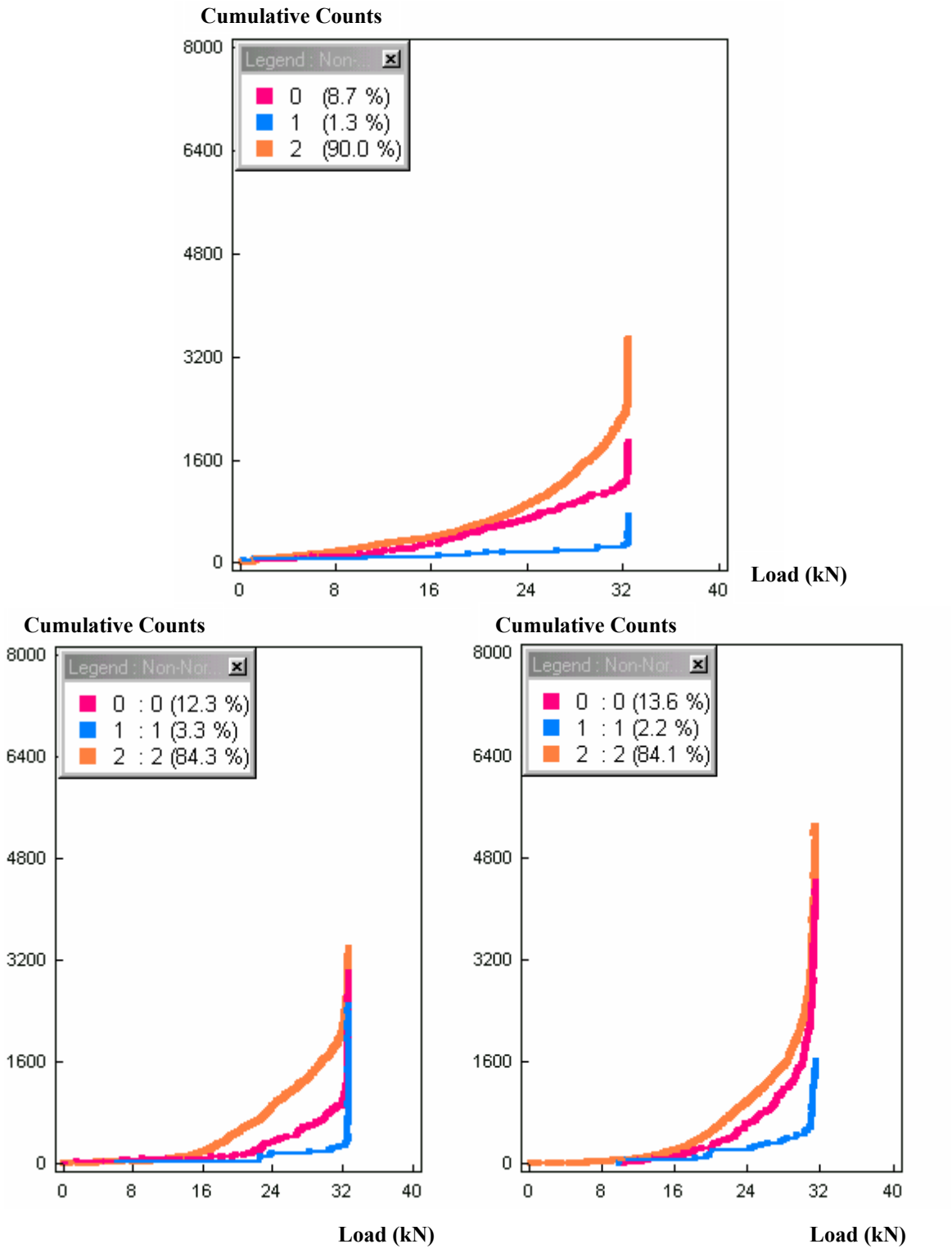

Figure 7.39 Clustered data of LU joint specimens – cumulative counts vs. load. (top: unsupervised; bottom: supervised)

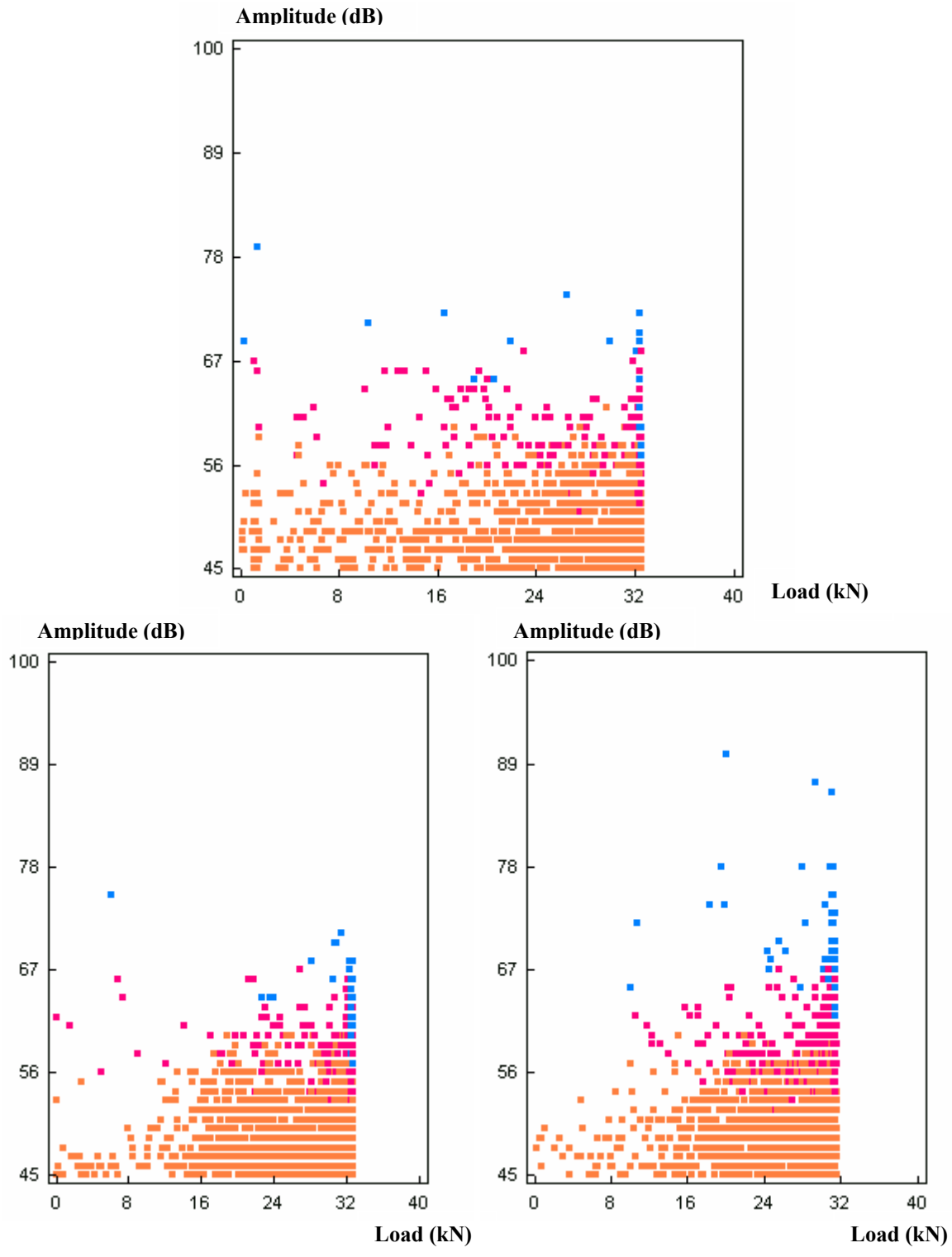

Figure 7.40 Clustered data of LU joint specimens – amplitude vs. load.
(top: unsupervised; bottom: supervised)

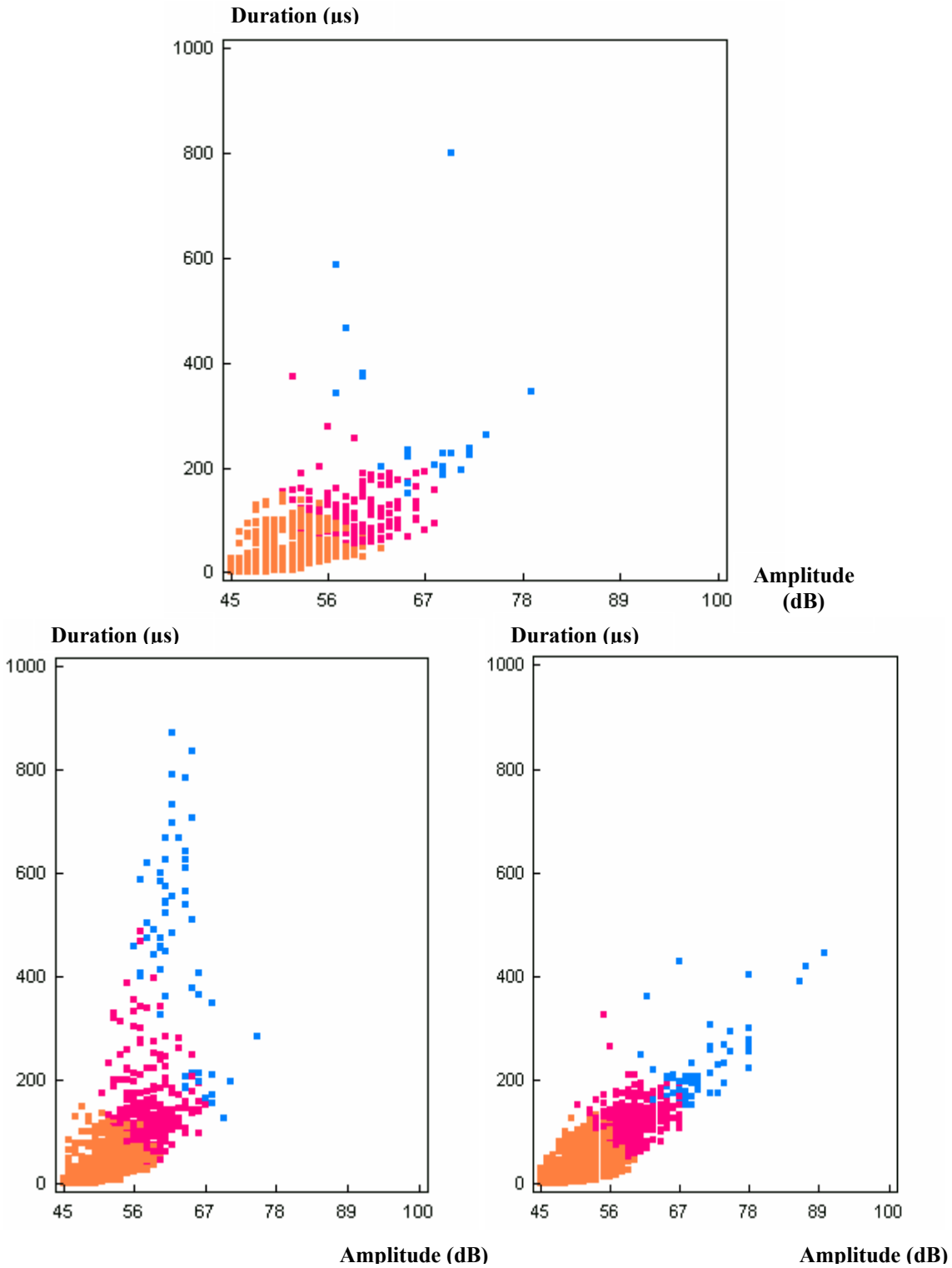

Figure 7.41 Clustered data of LU joint specimens – duration vs. amplitude.
(top: unsupervised; bottom: supervised)

Compared to LU, there is not much difference in the acquired AE data of NU during monotonic loading until failure. The only difference observed is in the failure modes. For NU, due to the existence of a nested overlap between two joints parts, there are more types of damage/failure mechanisms introduced including fiber breakage, fiber pull-out, mixed interlaminar/intralaminar shear failures within joint overlap region besides those observed in LU. However, those additional damage mechanisms mostly happen at the final failure. Before failure, the acoustic emissions are mainly produced from the joint parts other than from the joint overlap region since this region has a doubly sized cross-sectional area; the average stress is only half of that in joint part (Figures 7.42-7.46). The failure of NU still belongs to shear type though some fiber breakage accompanied by longitudinal splitting is observed within the joint overlap region. Angle-ply matrix cracking and delamination could not be observed in LU and NU joint specimens.

As before, the AE data sets of three NU specimens are clustered by the selected and proved clustering method and three clusters are created. These clusters have the similar AE characteristics as those of LU listed below:

Orange cluster - micro matrix cracking, from zero loads to failure, 45-61 dB;

Red cluster – fiber/matrix debonding, mostly from 9 kN to failure, 50-70 dB;

Green cluster - longitudinal splitting, mostly at failure, 56-92 dB.

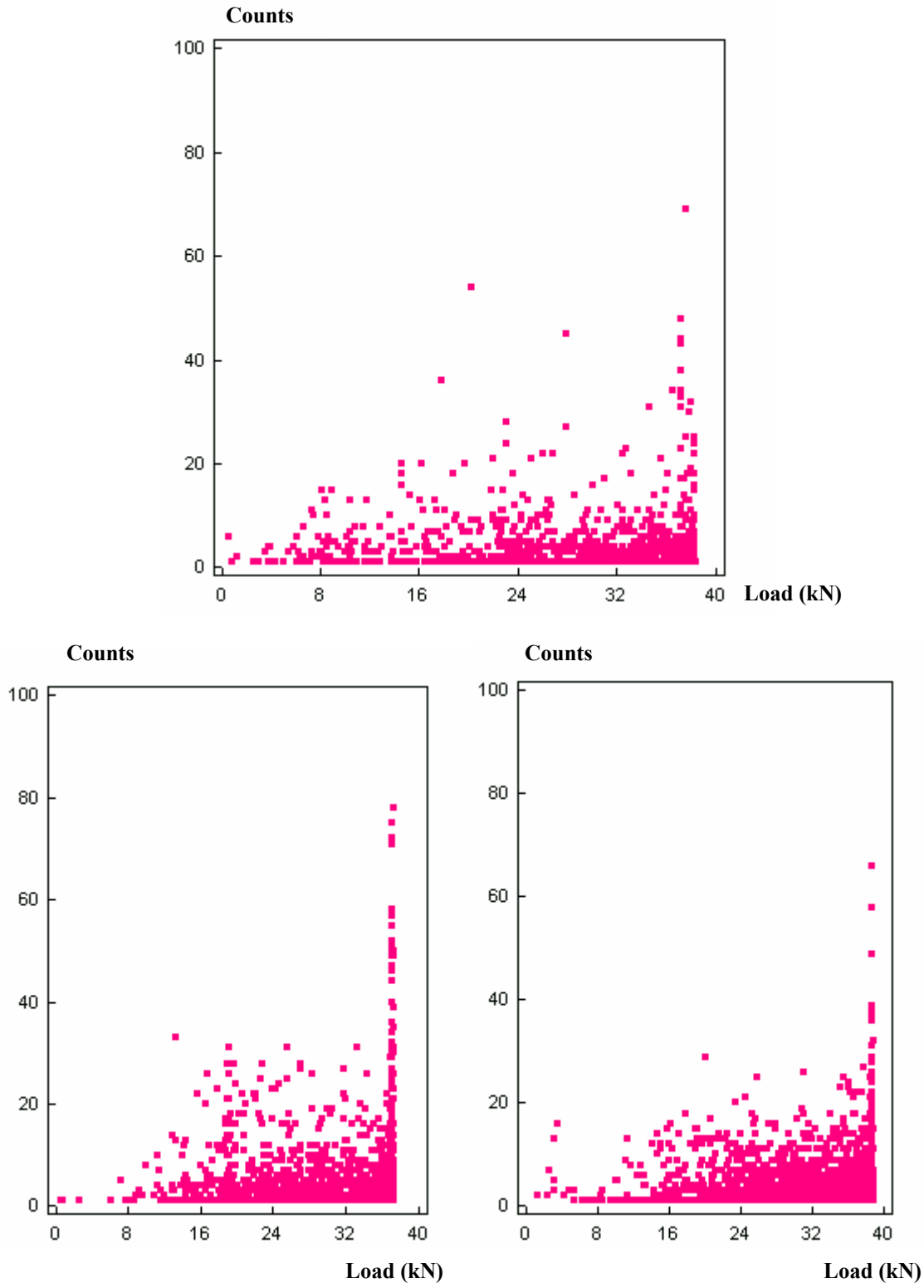

Figure 7.42 Original data of NU joint specimens – counts vs. load.
(top: test 1; bottom: test 2 and 3)

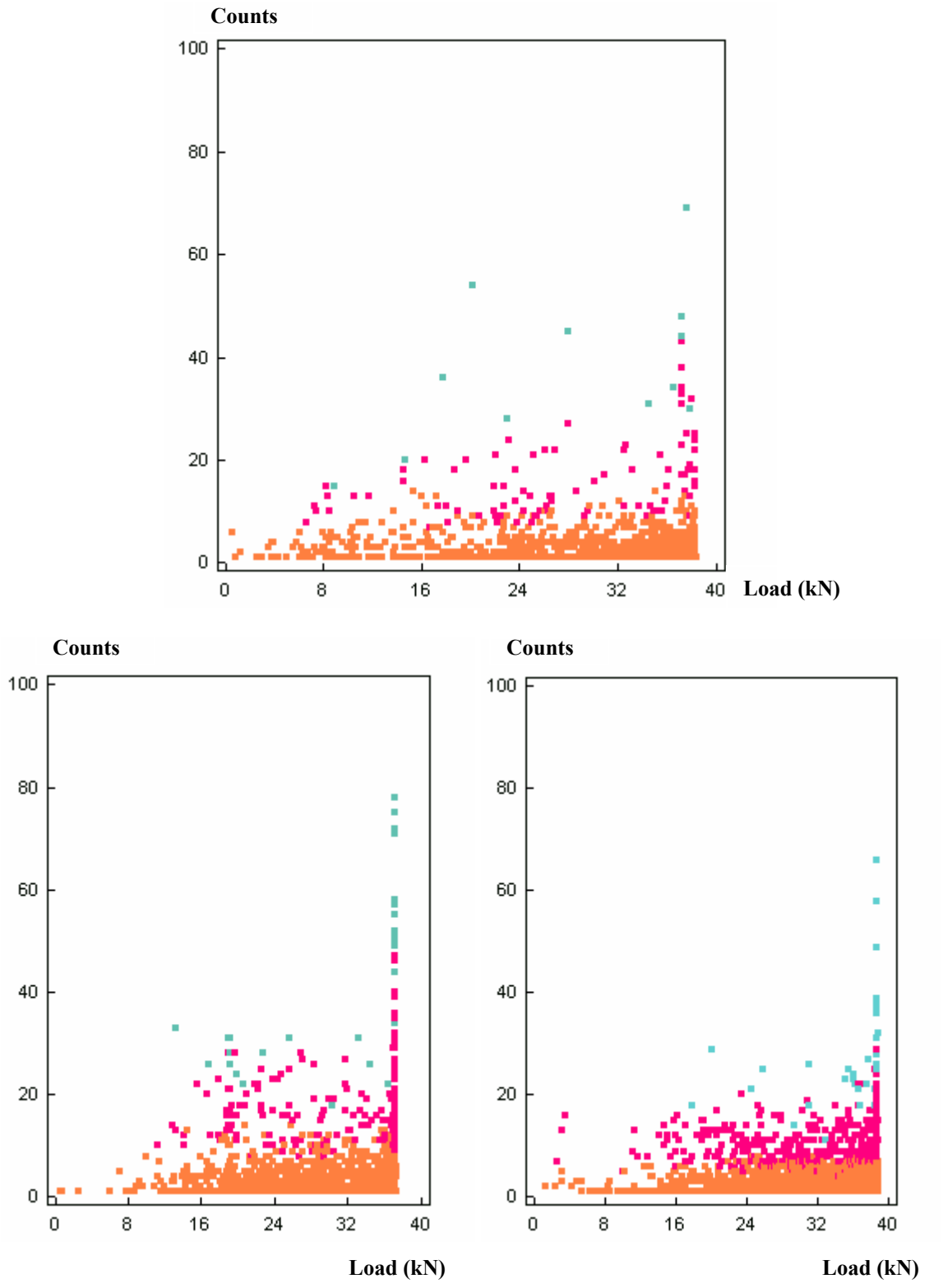

Figure 7.43 Clustered data of NU joint specimens – counts vs. load.
(top: unsupervised; bottom: supervised)

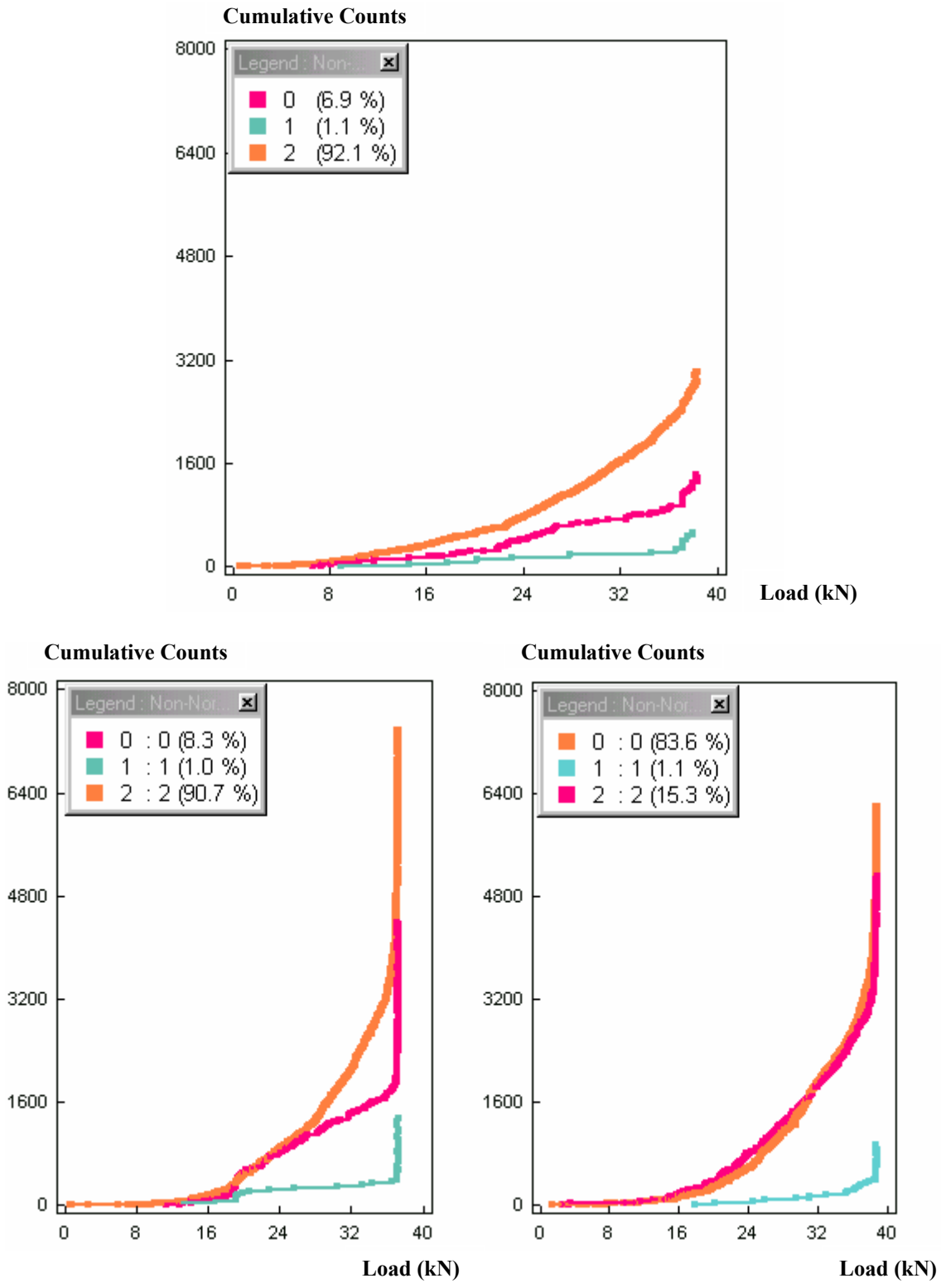

Figure 7.44 Clustered data of NU joint specimens – cumulative counts vs. load.
(top: unsupervised; bottom: supervised)

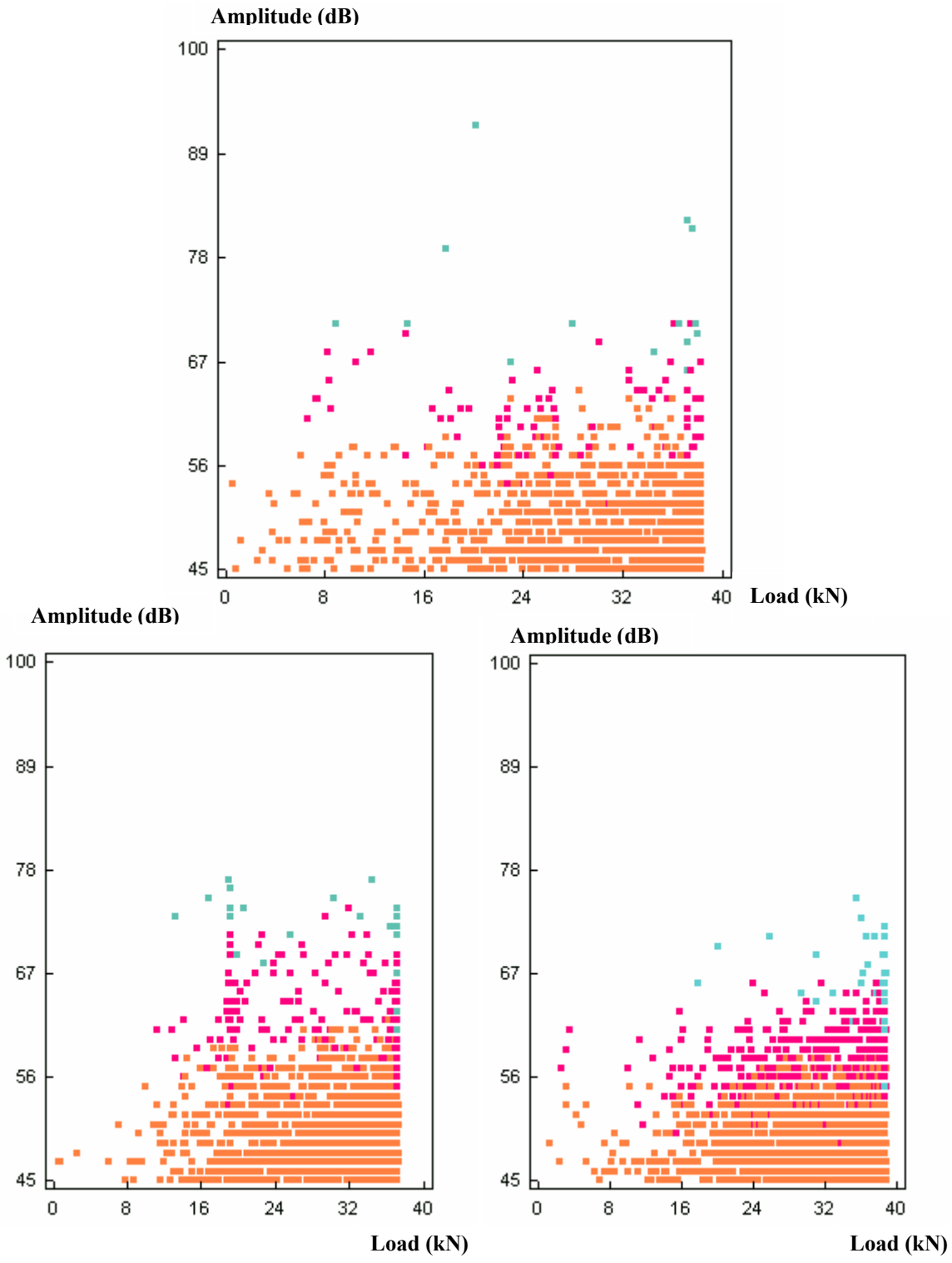

Figure 7.45 Clustered data of NU joint specimens – amplitude vs. load.
(top: unsupervised; bottom: supervised)

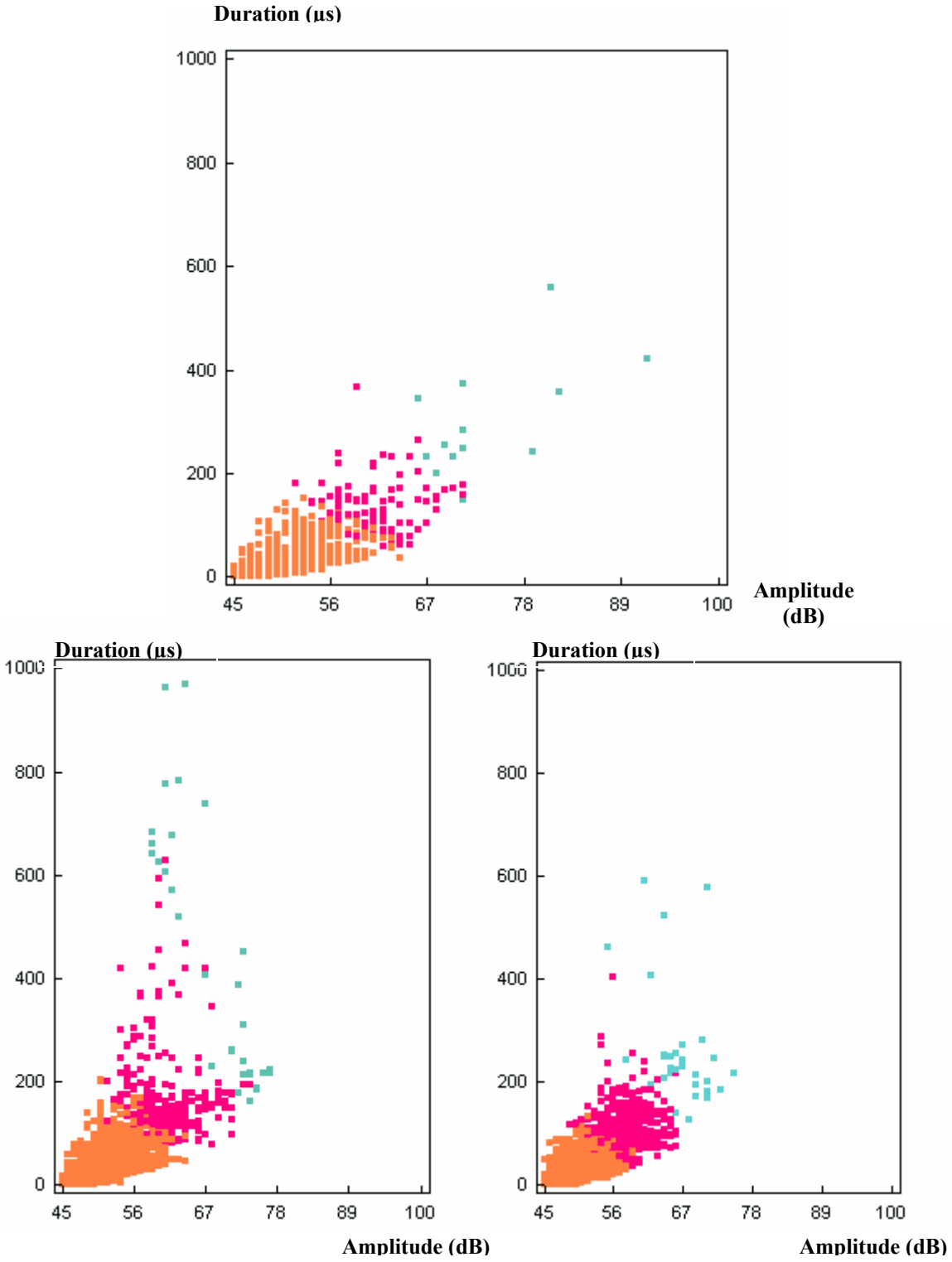

Figure 7.46 Clustered data of NU joint specimens – duration vs. amplitude.
(top: unsupervised; bottom: supervised)

7.3 Interpretations of Data and Results

The clustered AE data of five different types of specimen configurations are presented and analyzed. For comparison purpose, it is necessary to combine the results together, especially for two important AE parameters amplitude and duration, which are also extensively studied by other researchers. The acoustic emission Amplitude parameter (dB) is a logarithmic representation of the peak signal voltage of the acoustic emission waveform (Figure 4. 2). It is seen from the AE data discussed earlier, different damage mechanisms occupy different amplitude bands and usually the macro damage events such as delamination produce high-amplitude AE signals. Duration (μs) is the time covering the appearance of the first counts to the last in one hit and this parameter is usually proportional to counts - higher counts higher duration. This explains why they show high correlation for most studied cases.

The following is a list of amplitude and duration ranges which correspond to the related damage mechanisms both in the "U" and "Q" groups.

LU joint:

Micro matrix cracking – 45-61 dB; 0~150 μs

Fiber/matrix debonding – 50-68 dB; 70~250 μs

Longitudinal splitting – 56-90 dB, 150~900 μs

NU joint:

Micro matrix cracking – 45-61 dB; 0~150 μs

Fiber/matrix debonding – 50-70 dB; 70~620 μs

Longitudinal splitting – 56-92 dB; 120~1000 μs

SU laminate:

Micro matrix cracking – 45-61 dB; 0~100 μs

Fiber/matrix debonding – 45-75 dB; 0~500 μs

Longitudinal splitting – 45-99 dB; 0~1500 μs

LQ joint:

Micro matrix cracking – 45-72 dB; 0~320 μs

Macro matrix cracking – 62-81 dB; 150~640 μs

Delamination – 72-91 dB; 180~1000 μs

NQ joint:

Micro matrix cracking – 45-79 dB; 0~640 μs

Macro matrix cracking – 69-90 dB; 160~1100 μs

Delamination – 82-95 dB; 320~1400 μs

Fiber breakage – 92-99 dB; 350~1500 μs

SQ laminate:

Micro matrix cracking – 45-79 dB; 0~640 μs

Macro matrix cracking – 65-92 dB; 160~1250 μs

Delamination – 79-95 dB; 320~1520 μs

Fiber breakage – 92-99 dB; 500~1500 μs

To get more insight into these data in the above lists, it is more meaningful to list the amplitude and duration ranges which cover the minimum and maximum values for each dominant mode of damage in all the specimens from the same group (Tables 7.1-7.2).

Table 7.1 Correspondence between the dominant modes of damage and AE amplitude and duration in "U" group

Damage/Failure Mechanism	**Amplitude Range (dB)**	**Duration Range (μs)**
Micro matrix cracking	45-61	0-150
Fiber/matrix debonding	45-75	0-620
Longitudinal splitting	45-99	0-1500

Table 7.2 Correspondence between the dominant modes of damage and AE amplitude and duration in "Q" group

Damage/Failure Mechanism	**Amplitude Range (dB)**	**Duration Range (μs)**
Micro matrix cracking	45-79	0-640
Macro matrix cracking	62-92	150-1250
Delamination	79-95	180-1520
Fiber breakage	92-99	350-1500

Since micro matrix cracking is the common damage mechanism found in both U and Q specimens, these parameter ranges should be comparable. From the above list, the amplitude ranges of micro matrix cracking for the "U" and "Q" groups are from 45 to 61 dB and from 45-79 dB respectively. However, due to the different surroundings in U and Q specimens generated by different lay-ups, the scale of this AE activity is therefore varied. For the "U" group, matrix only exists between fibers and the resulted micro cracks can not be observed using Optical Microscopy in this study. For the "Q" group, the situation is totally different since matrix cracks can occur in any of those angle plies ($\pm 45^{o}$, 90^{o}) besides two 0^{o} plies. It is believed that AE data from some medium-sized cracks between micro and macro could be clustered either into micro matrix cracking or macro matrix cracking group. This is the reason for a narrower range of amplitude in the "U" group and for the overlap of amplitude ranges between neighboring mechanisms. Similar explanation could be made for the difference in duration range of this common micro matrix cracking mechanism in both the "U" and "Q" groups.

The k-NNC supervised classifier shows the power in clustering the AE signals into several groups and the action is proved to be repeatable. When combining the previous observations by other means such as X-ray Radiography and Optical Microscopy, these clusters could be correlated to the damage and failure mechanisms observed in co-cured composite joints and laminate. However, due to the complex AE activities of wave propagation and reflection as well as mode conversion inside the material, the resulted clusters have certain amount of overlap. In addition, the clustering method will not work in discriminating AE signals from some damage mechanism like longitudinal splitting since its AE data can cover all ranges of AE parameters such as counts, amplitude and

duration. A complementary method is needed to be able to recognize the particular failure mechanism by looking at the waveforms recorded and also could tell when this failure mechanism takes place.

CHAPTER 8

CONCLUSIONS AND RECOMMENDATIONS

8.1 Conclusions

The single nested overlap joint configuration proposed by Coates and Armanios is further investigated and its joint strength improvement over the conventional single lap joint under monotonic loading condition is confirmed. In this study, six specimen configurations including LU, NU, SU, LQ, NQ and SQ are fabricated by autoclave curing or co-curing method and then tested. With a minor alteration of the basic single lap joint during manufacturing, the SNO joint has 29.2% and 27.4% higher average ultimate joint strengths for 0^o unidirectional and quasi-isotropic lay-ups, respectively.

Several nondestructive evaluation techniques are used to characterize the physical damage and failure mechanisms of the studied specimens and to monitor their mechanical responses. Using X-ray Radiography and Optical Microscopy techniques at varied load intervals, the different mechanisms of damage initiation, progression and accumulation in joint counterparts, like LU vs. NU or LQ vs. NQ, are obtained and recorded, which from one aspect explains the resulting different joint strengths. Basically, only micro matrix cracking and fiber/matrix cracking are observed in LU with additional complex mechanisms like fiber breakage, fiber pull-out and longitudinal splitting involved in NU.

SQ and NQ exhibit multiple modes of damage such as micro/macro matrix cracking, delamination and fiber breakage except for their different extensiveness in progression or propagation (for example, different matrix crack density at the same load intervals). No fiber breakage is observed in LQ due to the premature shear separation failure with the lowest failure load among "Q" specimens. X-ray radiographs supply important information regarding internal damage with good quality for delaminations.

The Acoustic Emission data acquired during monotonic loading shows the overall picture of AE parameter distributions and correlations as well as of damage development and accumulation via parametric analysis. Further AE analysis via a selected supervised clustering method from NOESIS v3.3 is carried out and proved to be successful in differentiating the AE data and separating them into clusters which, when correlated with the physical observations from other techniques, appear to correspond to specific damage and failure mechanisms.

The SNO joint configuration has enhanced joint strength over its counterpart (single lap joint) of the same lay-up.

Based upon physical observations, co-cured SNO joints show that more material participated, more complex fracture surfaces are generated, and more damage mechanisms are involved. The premature failure of LU and LQ is caused by the failure of the weak link with only one interface between the two joint parts. However, the single nested overlap manipulation makes the link stronger by introducing three interfaces between the two adherends and permits more material to be involved for load-carrying in NU or a good joint design for NQ. Therefore, SNO joints have higher joint efficiency with more material utilized compared to single lap joints.

AE activities of SNO joints are more intense. There are more total AE counts as well as more high-counts, high-duration, and high-amplitude events in SNO joints, which suggest more fracture energy stored and dissipated. From the clustered AE data combined with physical observations, it shows that each specific damage and failure mechanism occupies a distinct band of AE amplitude and duration; different types of damage can interact and occur simultaneously; one type of damage mechanism could cover a wide range of AE amplitude values like longitudinal splitting.

The co-cured single nested overlap joint with quasi-isotropic lay-up NQ is an example of good joint design. It fails in the 8-ply base material outside the joint region. The damage progression procedures of this case are as follows:

1. Micro/macro matrix cracking initiated within 90^{o} plies

2. Free edge delamination initiated from matrix crack tips within adherends

3. Delamination propagating towards and reaching nearby joint end

4. Geometric discontinuity between disintegrated adherend and 16-ply joint portion, results in fracture of the NQ joint specimen.

From the above analysis, it can be seen that free edge delaminations reduce the integrity of the base material of NQ. For any future practical applications, it suggests suppressing delaminations along the free edges of the joint structures either by adding caps or by introducing stitches along edges.

8.2 Recommendations for Future Work

1. Fatigue Test

Joint response under fatigue loading is of primary importance for structural applications. Therefore, an extension of this work for the case of fatigue loading is necessary in order to provide an understanding of damage initiation, progression and of failure mechanisms for this loading case, which will further form the basis for a structural durability and reliability assessment.

2. Wideband Transducers

Narrowband resonant sensors are used for threshold-based acoustic emission systems and usually have an operating frequency range from 100 kHz to 300 kHz, while wideband displacement sensors are used for waveform-based AE systems and their operating frequency can reach 150 MHz or beyond. There are two significant difficulties with the narrowband approach. First, distinguishing between real, crack-based AE and extraneous AE (for example, due to friction and fretting) is difficult. Second, accuracy of source location is poor or even non-existent for narrowband, threshold-based systems. Due to these limitations of resonant transducer, the acquired AE data in this study may distort the real source-wave properties. In addition, since only one transducer is used for this study, many overlaps of AE signals resulting from wave propagation and reflection within inhomogeneous materials could be present. In order to record more precisely AE data, especially from near joint taper ends, wideband sensors are recommended.

3. Test on Model Specimens

It is necessary to manufacture model composite laminates, like 0-degree unidirectional, 90-degree unidirectional, 45-angle ply and cross-ply laminates and characterize the dominant damage and failure mechanisms in these model specimens under loading. Then, the recorded AE data could be correlated with these mechanisms.

4. Transient AE Analysis

With data acquired by wideband transducers it is possible to perform a transient AE analysis and a database of signature waveforms for each damage mechanism could be established. This could further help discriminate AE activities detected during testing of alternate joint configurations.

REFERENCES

Adams, R. D. and Wake, W. C., 1984, "*Structural adhesive joints in engineering*," Elsevier Applied Science Publishers LTD 1984.

Armanios, E. A., Sriram, P. and Badir, A. M., 1991, "Fracture analysis of transverse crack-tip and free-edge delamination in laminated composites," *Composite Materials: Fatigue and Fracture (Third Volume), ASTM STP 1110*, O'Brien, T. K., Ed., 269-286.

Ashcroft, I. A., Abdel Wahab, M. M., Crocombe, A. D., Hughes, D. J. and Shaw, S. J., 2001, "The effect of environment on the fatigue of bonded composite joints, Part 1: testing and fractography," *Composites: Part A*, 32:45-58.

ASTM Standards D3039/D3039M-00, "Standard test method for tensile properties of polymer matrix composite materials."

Awerbuch, J., Gorman, M. R. and Madhukar, M., 1985, "Monitoring Acoustic Emission during quasi-static loading-unloading cycles of filament-wound graphite-epoxy laminate coupons," *Materials Evaluation*, 43:754-764.

Awerbuch, J., Madhukar, M. and Gorman, M. R., 1984, "Monitoring damage accumulation in filament-wound graphite/epoxy laminate coupons during fatigue loading through acoustic emission," *J. Reinforced Plastics and Composites*, 3:2-39.

ASTM Standards D3518/D3518M-94, "Standard test method for in-plane shear response of polymer matrix composite materials by tensile test of a $\pm 45^{o}$ laminate."

Bai, W. and Wong, B. S., 2000, "Non-destructive evaluation of aircraft structure using lock-in thermography," *Nondestructive Evaluation of Aging Aircraft, Airports and Aerospace Hardware IV*, Mal, A. K., Ed., 37-46.

Bakuckas, J. G., Jr., Prosser, W. H. and Johnson, W. S., 1994, "Monitoring damage growth in titanium matrix composites using acoustic emission," *J. Composite Materials*, 28(4):305-328.

Bar-Cohen, Y. and Mal, A. K., 1987, "End product nondestructive evaluation of adhesive-bonded composite joints," *Engineered Materials Handbook--Volume 1 "Composites"*, Reinhart, T. J., Ed., ASM International, OH, 777-784.

Barsoum, R. S., 1989, "Finite element application in the fracture analysis of composite materials-delamination," *Key Engineering Materials*, 37:35-58.

Birt, E. A., 2000, "The application of X-radiography to the inspection of composites," *INSIGHT*, 42(3):152-157.

Briskham, P. and Smith, G., 2000, "Cyclic stress durability testing of lap shear joints exposed to hot-wet conditions," *Int. J. Adhesion and Adhesives*, 20:33-38.

Cao, C. and Dancila, D. S., 2003 (a), "Damage and Failure Analysis of Co-cured Composite Joints with Unidirectional Lay-up", *44th AIAA/ASME/ASCE/AHS Structures, Structural Dynamics, and Materials Conference*, Norfolk, VA, April 2003.

Cao, C. and Dancila, D. S., 2003 (b), "Damage and Failure Analysis of Co-cured Composite Joints with Quasi-Isotropic Lay-up", *AHS International 59th Annual Forum & Technology Display*, Phoenix, AZ, May 2003.

Cho, D. H., Lee, D. G. and Choi, J. H., 1997, "Manufacture of one-piece automotive drive shafts with aluminum and composite materials," *Composite Structures*, 38(1-4):309-319.

Cho, D. H. and Lee, D. G., 2000, "Optimum design of co-cured steel-composite tubular single lap joint under axial load," *J. Adhesion of Science and Technology*, 14(7):939-963.

Coates, C.W. and Armanios, E. A., 2000, "Monotonic and fatigue response of co-cured composite lap joints with modified interfaces," *Proceedings of American Helicopter Society 56th Annual Forum*, Virginia Beach, VA May 2-4, 2000.

Coates, C. W., 2001, "New concepts for strength enhancement of co-cured composite single lap joints," *Ph.D. Dissertation*, School of Aerospace Engineering, Georgia Institute of Technology, GA.

Cope, R. D. and Pipes, R. B., 1982, "Design of the composite spar-wingskin joint," *Composites*, January:47-53.

Crews, *Jr.*, J. H., 1981, "Bolt-bearing fatigue of a graphite/epoxy laminate," *Joining of Composite Materials, ASTM STP 749*, Kedward, K. T., Ed., American Society for Testing and materials, 131-144.

Dzenis, Y. A. and Qian, J., 2001, "Analysis of microdamage evolution histories in composites," *International Journal of Solids and Structures*, 38:1831-1854.

Gao, Z., 1996, 'Numerical modeling of damage, property degradation and life prediction in fatigue of composite laminates," *Numerical Analysis and Modeling of Composite Materials*, Bull, J. W., Ed., 247-286.

Georgeson, G. E., 2000, "Ultrasonic evaluation of co-cured composite structures," Nondestructive E*valuation of Aging Aircraft, Airports and Aerospace Hardware IV*, Mal, A. K., Ed., 164-173.

Gustafson, C. G. and Selden R. B., 1985, "Monitoring fatigue damage in CFRP using acoustic emission and radiographic techniques," *Delamination and Debonding of Materials, ASTM STP 876*, Johnson, W. S., Ed., American Society for Testing and Materials, Philadelphia, 448-464.

Guyott, C. C. H., Cawley, P. and Adams, R. D., 1986, "The nondestructive testing of adhesively bonded structures; a review," *Journal of Adhesion*, 20:129-159.

Hamstad, M. A., 1986, "A review: acoustic emission, a tool for composite materials studies," *Experimental Mechanics*, 26(1):7-13.

Hart-Smith, L. J., 1981, "Further developments in the design and analysis of adhesively-bonded structural joints," *Joining of Composite Materials, ASTM STP 749*, Kedward, K. T., Ed., 1981:3-31.

Hart-Smith, L. J., 1987, "Joints," *Engineered Materials Handbook--Volume 1 "Composites"*, Reinhart, T. J., Ed., ASM International, OH, 479-495.

Hart-Smith, L. J., 1993, "Some observations on the analysis of in-plane matrix failures in fibrous composite laminates," *Composite Materials: Fatigue and Fracture, Fourth Volume, ASTM STP 1156*, Stinchcomb, W. W., Ed., 363-380.

Hashin, Z., 1976, 'Fatigue failure of angle ply laminates,' *AIAA JOURNAL*, 14(7):868-872.

Hashin, Z., 1981, 'Fatigue failure criteria for unidirectional fiber composites," *Transactions of the ASME*, 48:846-852.

Hashin, Z., 1986, "Analysis of stiffness reduction of cracked cross-ply laminates,' Engineering Fracture Mechanics, 25(5/6):771-778.

Herakovich, C. T., 1998, "*Mechanics of Fibrous Composites*," Wiley, New York.

Herrera-Franco, P. J. and Cloud, G. L., 1992, "Strain-relief inserts for composite fasteners—an experimental study," *J. Composite Materials*, 26(5):751-768.

Highsmith, A. L. and Reifsnider, K. L., 1982, 'Stiffness-reduction mechanisms in composite laminates,' *Damage in Composite Materials, ASTM STP 775*, Reifsnider, K. L., Ed., 103-117.

Highsmith, A. L. and Reifsnider, K. L., 1986, 'Internal load distribution effects during fatigue loading of composite laminates," *Composite Materials: Fatigue and Fracture, ASTM STP 907*, Hahn, H. T., Ed., 233-251.

Hillman, D. J. and Hillman, R. L., 1985, "Thermographic inspection of carbon epoxy structures," *Delamination and Debonding of Materials, ASTM STP 876*, Johnson, W. S., Ed., 481-493.

Hill, E. v. K., Walker II, J. L. and Rowell, G. H., 1996, "Burst pressure prediction in graphite/epoxy pressure vessels using neural networks and acoustic emission amplitude data," *Materials Evaluation*, June:744-748.

Hyer, M. W., 1998, *Stress Analysis of Fiber-Reinforced Composite Materials*, McGraw-Hill.

Ireman, T., 1998, "Three-dimensional stress analysis of bolted single-lap composite," *Composite Structures*, 43:195-216.

Johnson, W. S. and Mall, S., 1985, "A fracture mechanics approach for designing adhesivelt bonded joints," *Delamination and Debonding of Materials, ASTM STP 876*, Johnson, W. S., Ed., 189-199.

Kellas, S., Morton, J. and Kackson, K. E., 1993, "Damage and failure mechanisms in scaled angle-ply laminates," *Composite Materials: Fatigue and Fracture, Fourth Volume, ASTM STP 1156*, Stinchcomb, W. W., and Ashbaugh, N. E., 2557-280.

Kenner, V. H., Staab, G. H. and Jing, H.-S., 1985, "Quantification of the 'tapping' technique for the detection of edge defects in laminated plates," *Delamination and Debonding of Materials, ASTM STP 876*, Johnson, W. S., Ed., 465-480.

Kim, H. S., Lee, S. J. and Lee, D. G., 1995, "Development of a strength model for the co-cured stepped-lap joints under tensile loading," *Composite Structures*, 32:593-600.

Kim, J. K., Lee, D. G. and Cho, D. H., 2001, "Investigation of adhesively bonded joints for composite propeller shafts," *J. Composite Materials*, 35(11):999-1021.

Komai, K., Minoshima, K. and Shibutani, T, 1991, "Investigation of the fracture mechanism of carbon/epoxy composites by AE signal analyses," *JSME International Journal*, 34 (3):381-388.

Kradinov, V., Barut, A., Madenci, E. and Ambur, D. R., 2001, "Bolted double-lap composite joints under mechanical and thermal loading," *International Journal of Solids and Structures*, 38:7801-7837.

Krause, H-J, Hohmann, R. and Maus, M., 2000, "Aircraft wheel and fuselage testing with eddy current and SQUID," *INSIGHT*, 42(3):148-151.

Lagace, P. A., 1992, "On delamination failures in composite materials," *Composite Structures: testing, Analysis and Design*, Reddy, J. N. and Murty, A. V. K., Eds, 111-132.

Lagace, P. A. and Allen, M. W., 1985, "Evaluation of the alternative manufacturing methods for bonding graphite/epoxy composites," *30th National SAMPE Symposium*, March 19-21, 1985.

Lee, D. G. and Cho, D. H., 2000, "Prediction of the tensile load capability of co-cured steel-composite tubular single lap joints considering thermal degradation," *J. Composite Materials*, 34(8):689-722.

Lee, S. W., Lee, D. G. and Jeong, K. S., 1997, "Static and dynamic torque characteristics of composite co-cured single lap joint," *J. Composite Materials*, 31(21):2188-2201.

Li, G., Pang, S., Woldesenbet, E. and Stubblefield, M. A., 2001, "Investigation of prepreg bonded composite single lap joint," *Composites: Part B*, 32:651-658.

Masters, J. E., 1989, "Improved impact and delamination resistance through interleafing," *Key Engineering Materials*, 37:317-348.

McCarty, J. E., 1987, "Full-scale tests," *Engineered Materials Handbook--Volume 1 "Composites"*, Reinhart, T. J., Ed., ASM International, OH, 346-351.

Messler, R. W., Jr., 1993, "*Joining of advanced materials*," Butterworth-Heinemann, MA.

MIL-HDBK-17-3E, 1997.

Mizutani, Y., Morino, Y. and Hiromu, T., 2003, "Acoustic emission monitoring of CFRP tank at ambient and cryogenic temperature," *44th AIAA/ASME/ASCE/AHS Structures, Structural Dynamics, and Materials Conference*, Norfolk, VA, April 2003.

Moffatt, J. G. and Markov, V. B., 2002, "On-wing inspection techniques using laser technology," *AHS International 58th Annual Forum and Technology Display*, June 11-13, 2002, Montreal, Quebec, Canada.

NOESIS v3.3 REFERENCE MANUAL (Rev. 4), Professional Edition, February 2001, ENVIROCOUSTICS S.A., Athens, Greece.

O'Brien, T. K., 1982, 'Characterization of delamination onset and growth in a composite laminate," *Damage in Composite Materials, ASTM STP 775*, Reifsnider, K. L., Ed., 140-167.

O'Brien, T. K., 1985, "Analysis of local delaminations and their influence on composite laminate behavior," *Delamination and debonding of Materials, ASTM STP 876*, Johnson, W. S., Ed., 282-297.

O'Brien, T. K., 1988, 'Fatigue delamination behavior of PEEK thermoplastic composite laminates," *J. Reinforced plastics and Composites*, 7:341-359.

O'Brien, T. K. and Reifsnider, K. L., 1977, "Fatigue damage: stiffness/strength comparisons for composite materials,' *Journal of Testing and Evaluation*, JTEVA, 5:384-393.

Oliva, P. V., 1991, "Integral wing/fuel box," *23rd International SAMPE Technical Conference, October 21-24*, 1047-1059.

Oplinger, D. W., 1996, "Bolted joints in composite structures—an overview," *The 83rd Meeting of the AGARD SMP on "Bolted/Bonded Joints in Polymeric Composites"*, Florence, Italy, September 2-3, 1996.

Prassinanakis, I. N., 2000, "Non-destructive testing of adhesively bonded materials," *INSIGHT*, 42(3):158-161.

Prosser, W. H., Jackson, K. E., Kellas, S., Smith, B. T., McKeon, J. and Friedman, A., 1995, "Advanced waveform based acoustic emission detection of matrix cracking in composites," *Material Evaluation*, 53 (9):1052-1058.

Reifsnider, K. L., Schulte, K. and Duke, J. C., 1983, "Long-term fatigue behavior of composite materials," *Long-Term Behavior of Composites, ASTM STP 813*, O"Brien, T. K., Ed., 136-159.

Schmidt, H-J, Schmidt-Brandecker B. and Tober G., 2000, "Design of modern aircraft structure and the role of NDI," *INSIGHT*, 42(6):141-147.

Schwartz, M. M., 1994, "*Joining of composite matrix materials*," ASM International Materials Park, OH.

Shin, K. C., Lee, J. J. and Lee, D. G., 2000, "A study on the lap shear strength of a co-cured single lap joint," *J. Adhesion Science and Technology*, 14 (1):123-139.

Shin, K. C. and Lee, J. J., 2000a, "Prediction of the tensile load-bearing capacity of a co-cured single lap joint considering residual thermal stresses," *J. Adhesion Science and Technology*, 14 (13):1691-1704.

Shin, K. C. and Lee, J. J., 2000b, "Tensile load-bearing capacity of co-cured double lap joints," *J. Adhesion Science and Technology*, 14 (12):1539-1556.

Soni, S. R., 1981, "Failure analysis of composite laminates with a fastener hole," *Joining of Composite Materials, ASTM STP 749*, Kedward, K. T., Ed., American Society for Testing and materials, 145-164.

Sriram, P. and Armanios, E. A., 1993, "A shear deformation model for transverse cracking in composite laminates,*' International Journal of Damage Mechanics*, 2:73-91.

Steiner, K. V., 1992, "Defect classification in composites using ultrasonic nondestructive evaluation techniques," *Damage Detection in Composite Materials, ASTM STP 1128*, Masters, J. E., Ed., 72-84.

Stinchcomb, W. W. and Reifsnider, K. L., 1979, "Fatigue damage mechanisms in composite materials: a review," *Fatigue Mechanisms, Proceedings of an ASTM-NBS-NSF Symposium, ASTM STP 675*, Fong, J. T., Ed., 762-787.

Suresh, S., 1991, "*Fatigue of materials*," Cambridge University Press 1991.

Surgeon, M. and Wevers, M., 1998, "Quantifying the damage state of quasi-isotropic CFRP with embedded optical fibers during fatigue testing using acoustic emission and

microfocus radiography," *The e-Journal of Nondestructive Testing*, http://www.ndt.net/article/ecndt98/aero/027/027.htm.

Surgeon, M. and Wevers, M., 1999, "Modal analysis of acoustic emission signals from CFRP laminates," *NDT & E International*, 32:311-322.

Talreja, R., 1985, "Transverse cracking and stiffness reduction in composite laminates," J. *Composite Materials*, 19:355-375.

Talreja, R., 1987, *Fatigue of composite materials*, Technomic Publishing Company, Inc.

Tanary, S., Haddad, Y. M., Fahr, A. and Lee, S., 1992, "Nondestructive evaluation of adhesively bonded joints in graphite/epoxy composites using acousto-ultrasonics," *Transactions of the ASME Journal of Pressure Vessel Technology*, 114:344-352.

Tsai, M. Y., Oplinger, D. W. and Morton, J., 1998, "Improved theoretical solutions for adhesive lap joints," *Int. J. Solids and Structures*, 35(2):1163-1185.

Tsamtsakis, D. and Wevers, M., 1999, "Acoustic emission to model the fatigue behavior of quasi-isotropic carbon-epoxy laminate composites," *INSIGHT*, 41(8):513-516.

Tsamtsakis, D., Wevers, M. and Meester, P. De, 1996, "Damage monitoring during monotonic tensile loading of quasi-isotropic carbon epoxy laminates," *Materials Science Forum 210*, 125-132.

Tsamtsakis, D., Wevers, M. and Meester, P. De, 1998, "Acoustic emission from CFRP laminates during fatigue loading," *Journal of Reinforced Plastics and Composites*, 17(13):1185-1201.

Wang, A. S. D., 1989, "An overview of the delamination problem in structural composites," *Key Engineering Materials*, 37:1-20.

Wevers, M., 1997, "Listening to the sound of materials: acoustic emission for the analysis of material behaviors," *NDT & E International*, 30 (2):99-106.

Whitworth, H. A., 1990, "Cumulative damage in composites,' *Transactions of ASME*, 112:358-361.

Youssef, Y., Roy, C., and Fahr, A., 1992, "Pattern recognition applied to NDE of single-lap bonded joints," *Composite Structures and Materials*, Hoa, S. V. and Gauvin, R., Eds., 364-371.

VITA

Caihua Cao was born on August 24th, 1968 in Wuxi County, now Xishan City, China. Before the age of fourteen she enrolled in the Meicun Junior and Senior Middle School and was selected for the Amateur Track and Field Team of Wuxi County. While studying there between 1982 and 1987 she also received formal training as an athlete. Upon graduation Ms. Cao enrolled in the School of Civil Engineering of Hohai University, Nanjing, China, graduating with Bachelor of Science and Master of Science degrees in 1991 and 1994, respectively. In September 1996, Ms. Cao joined the Department of Aerospace Engineering and Engineering Mechanics of the University of Cincinnati, receiving a Master of Science in Aerospace Engineering degree in August 1997. In September 1997, she was admitted to the Ph.D. program in the School of Aerospace Engineering of the Georgia Institute of Technology, performing research on post-impact fatigue of woven composite materials and subsequently on the topic of this dissertation.

As coeditor-in-chief, Ms. Cao collaborated with Professor Wei Zhongming on a "Chinese-English Dictionary for Sporting Terms," published in 1999 in China. This dictionary collects most sporting terms of the Olympic Games and other sports around the world. Currently she has plans to translate two English language books into Chinese, for subsequent publication.